UNIVERSIDADE
BEIRA INTERIOR

Development of aptamer nanoparticles for treatment of retinal diseases

David Nabais Moreira

Dissertação para obtenção do Grau de Mestre em
Ciências Biomédicas
(2º ciclo de estudos)

Orientadora: Prof. Doutora Cândida Ascensão Teixeira Tomaz
Co-orientadora: Prof. Doutora Carla Patrícia Alves Freire Madeira Cruz
Co-orientadora: Doutora Fátima Raquel Milhano dos Santos

novembro de 2022

Declaração de Integridade

Eu, David Nabais Moreira, que abaixo assino, estudante com o número de inscrição M10773 de Ciências Biomédicas da Faculdade Ciências da Saúde, declaro ter desenvolvido o presente trabalho e elaborado o presente texto em total consonância com o **Código de Integridades da Universidade da Beira Interior.**

Mais concretamente afirmo não ter incorrido em qualquer das variedades de Fraude Académica, e que aqui declaro conhecer, que em particular atendi à exigida referenciação de frases, extratos, imagens e outras formas de trabalho intelectual, e assumindo assim na íntegra as responsabilidades da autoria.

Universidade da Beira Interior, Covilhã 30/11/2022

Assinado por: **David Nabais Moreira**
Num. de Identificação: 14456307
Data: 2022.11.30 09:52:31+00'00'

CHAVE MÓVEL

(assinatura conforme Cartão de Cidadão ou preferencialmente
assinatura digital no documento original se naquele mesmo formato)

Acknowledgements

To start, I would like to thank my supervisor, Professor Cândida Tomaz and my co-supervisors, Professor Carla Cruz, and Fátima Santos for all the scientific support they gave me in this work. It was a great pleasure to work under your supervision and to be treated not just as a student but also as a scientist. Thank you, a lot, for bringing me into the amazing world of science. I would like to deeply thank Professor Carla Cruz for the opportunity to work in the G4 team lab and for all the material and equipment provided during this last year.

I would also to thank all the G4 team for the help they give me and for all the friendly environment that they created at the lab. Thank you all, for guiding me in CICS facilities, in this work and in all the daily routines of our convivence. I'm especially grateful for the help that Jéssica Nunes gave me during the development of this work but especially in my first steps on the G4 team. Thanks a lot for all the patience you all had during this time.

To Health Sciences Research Centre (CICS-UBI) to provide all facilities and equipment to perform my experiments developed and presented in this dissertation.

To all the funding supported by the European Regional Development Fund through the "Programa Operacional Regional do Centro (Centro 2020)—Sistema de Apoio à Investigação Científica e Tecnológica—Programas Integrados de IC&DT" (Project Centro-01-0145-FEDER-000019—C4—Centro de Competências em Cloud Computing), CICS-UBI projects UIDB/00709/2020 and UIDP/00709/2020, financed by national funds through FCT/MCTES and by Bolsa de Inovação da SR Sul e Regiões Autónomas da Ordem dos Farmacêuticos 2021 (BInov).

To my family for all the support on the worst days and all the happiness on the good moments. Thanks for investing in my formation and for all you made for giving me the best future possible.

Finally, thanks to all the friends and important people that in these last 5 years shared their life with me and that in one way or another helped me to reach my personal and academic objectives.

Resumo

Em estágios mais avançados, as doenças da retina como a retinopatia diabética, degeneração macular associada à idade e oclusões da retina são caracterizadas por neovascularização, que pode ser desencadeada por um episódio de hipoxia que envolve a sobre expressão do fator de crescimento endotelial vascular (VEGF) e da nucleolina (NCL). Os tratamentos disponíveis são principalmente corticosteroides e/ou anticorpos específicos para algumas moléculas angiogénicas. Para ultrapassar a baixa eficácia destas terapias e os seus efeitos secundários, os aptameros surgiram como uma ferramenta emergente que, de modo semelhante aos anticorpos, visam estas proteínas com elevada especificidade. Além disso, os aptameros são mais fáceis de sintetizar e apresentam maior estabilidade e menor imunogenicidade.

O AT11-L0 é um derivado do aptamero AS1411, composto por sequências ricas em G, que pode adotar estruturas em G-quadruplex e reconhecer a NCL, uma proteína que pode atuar como coreceptora de vários fatores de crescimento. Assim, este estudo visou caracterizar a estrutura do AT11-L0 e a sua interação com vários ligandos (moléculas estabilizadoras ou fármacos), para ligar de modo específico à NCL. Este complexo foi posteriormente incorporado num nanossistema, para aumentar a biodisponibilidade do fármaco e do aptamero usados na formulação.

Para alcançar estes objetivos, foram realizados estudos biofísicos, tais como ressonância magnética nuclear, dicroísmo circular e experiências de fluorescência. Após estudos de caracterização biofísica, foram sintetizadas nanopartículas de ouro e lipossomas contendo o complexo aptamero-fármaco. Finalmente, os lipossomas e os fármacos foram testados num modelo de células endoteliais de veia umbilical humana (HUVEC) para analisar a sua capacidade antiangiogénica.

Os resultados mostraram que os complexos aptamero-fármaco têm uma elevada estabilidade térmica, com temperaturas de fusão que atingem 45 ºC a 60 ºC, permitindo uma interação com a NCL com um K_D na ordem dos micromolares. O ensaio antiangiogénico mostrou que, embora os lipossomas não promovam um aumento do efeito dos fármacos testados, o C_8 apresentou um efeito antiangiogénico que nunca foi descrito, mesmo quando usado em baixa concentração. Este resultado pode permitir uma nova abordagem utilizando o C_8 associado a aptameros de G4 que visem a NCL.

Keywords

Aptameros em G-quadruplex; doenças da retina; nanossistemas; nucleolina; angiogénese.

Resumo Alargado

O olho é um dos órgãos mais importantes e sensíveis do corpo humano e é através dele que são recolhidas as imagens do mundo que nos rodeia, para posterior interpretação no cérebro. Apesar de todas as estruturas de proteção que rodeiam o olho, por vezes, este pode sofrer de doenças que afetam de forma severa a qualidade de vida dos pacientes que dela padecem. Um dos principais tipos de doença que afeta este órgão são as doenças vasculares da retina, que tal como o nome indica afetam a retina através de um processo angiogénico. A retina é uma estrutura que recolhe as imagens captadas pelo olho e as transforma em estímulos elétricos para envio ao cérebro. Quando afetada por um processo angiogénico anormal, esta capacidade pode ficar comprometida. Estas patologias são a principal causa de cegueira nos países desenvolvidos, e com o aumento da prevalência da diabetes (um fator de risco para estas doenças), prevê-se que este seja um problema com grande impacto a nível mundial.

Uma das principais razões para o aparecimento das doenças vasculares da retina são episódios de hipoxia, muitas vezes desencadeados por fatores de risco, como a diabetes ou a hipertensão que afetam a normal circulação sanguínea. Estes episódios levam a uma sobre expressão do fator de crescimento endotelial vascular (VEGF). O VEGF é o responsável por desencadear vias de sinalização que levam à proliferação celular e ao início de um processo angiogénico e inflamatório. Um importante interveniente nestas vias de sinalização é a nucleolina (NCL). A NCL é uma fosfoproteína, que durante estes episódios em que existe uma sobre expressão de VEGF, migra do núcleo para a superfície celular, onde atua como um recetor de fatores de crescimento, intervindo direta ou indiretamente no processo inflamatório e de angiogénese. Assim, a NCL pode ser considerada um importante alvo no tratamento das doenças vasculares da retina. O AS1411 é um aptamero com uma estrutura de G-quadruplex (G4) capaz de reconhecer e ligar especificamente a esta proteína, podendo ser potencialmente utilizado no tratamento destas doenças. No entanto, o elevado grau de polimorfismos deste aptamero pode reduzir a sua eficácia, uma vez que é difícil reconhecer e isolar a estrutura G4 com importância biológica.

Assim, neste trabalho é apresentada uma abordagem com o intuito de caraterizar um derivado do AS1411, conhecido como AT11-L0, e de o conjugar num nanossistema contendo um fármaco com capacidade anti-inflamatória/antiangiogénica. Para avaliar a efetividade destes nanossistemas no tratamento das doenças vasculares da retina, estes foram testados em células HUVEC, de modo a avaliar a sua capacidade antiangiogénica.

Os resultados obtidos por técnicas de caraterização biofísica, como dicroísmo circular, permitem concluir que o AT11-L0 é capaz de formar uma estrutura bem definida de G4 paralela. Esta estrutura é estabilizada quando associada a pequenas moléculas conhecidas como ligandos. O ligando com o resultado mais promissor foi uma molécula conhecida como C_8 que deriva de uma acridina. Foram também formulados nanossistemas com dexametasona, devido à sua conhecida capacidade antiangiogénica e anti-inflamatória. O principal nanossistema usado foram lipossomas, nos quais foram encapsulados os fármacos e conjugado o aptâmero à superfície. Foram também sintetizadas nanopartículas de ouro (AuNPs) com o aptamero conjugado à superfície. Neste caso o fármaco foi conjugado na estrutura G4 do aptamero. No entanto, quando testada a capacidade antiangiogénica dos lipossomas, verificou-se que esta não foi consideravelmente superior à dos fármacos isolados. Ainda assim, este estudo permitiu descrever pela primeira vez uma capacidade antiangiogénica do C_8 com potencial semelhante à da dexametasona, mas numa menor concentração.

Abstract

At more advanced states, retinal diseases such as diabetic retinopathy, age-related macular degeneration, and retinal vessel occlusions are characterized by neovascularization, which is usually triggered by a hypoxia episode leading to the overexpression of vascular endothelial growth factor (VEGF) and nucleolin (NCL). The treatments available are mainly corticosteroids or/and antibodies against some angiogenic molecules. Regarding the low efficacy of these therapies and their side effects, aptamers are an emerging tool that can target these proteins with high specificity, such as antibodies. Furthermore, aptamers are easier to synthesize and present higher stability and lower immunogenicity.

AT11-L0 is an aptamer derivative of AS1411 composed of G-rich sequences which can adopt G-quadruplex (G4) structure and target NCL, a protein that can act as a co-receptor for several growth factors. Hence, this study aimed to characterize the AT11-L0 structure and its interaction with several ligands (stabilizing molecules or drugs) for NCL targeting. The AT11-L0-drug/molecule complex was then incorporated in a nanoparticle to increase the bioavailability of the aptamer-based drug in the formulation.

To achieve these objectives, we have performed biophysical studies, such as nuclear magnetic resonance, circular dichroism, and fluorescence experiments. Following biophysical characterization studies, we synthesised gold nanoparticles and liposomes containing AT11-L0 aptamer-drug complex. Finally, liposomes and the encapsulated drugs were tested on Human umbilical vein endothelial cells (HUVEC) model to assess their antiangiogenic capacity.

The results showed that AT11-L0 aptamer-drug complex has a high stability with melting temperatures reaching 45 ºC to 60 ºC allowing an efficient targeting of NCL with a K_D in the order of micromolar. HUVEC antiangiogenic assay showed that, although liposomes did not promote an increase in the antiangiogenic effect of the tested drugs, C_8 showed an antiangiogenic effect that was not previously described, at lower concentration. This result can be a basis for the development of a new therapeutic approach using C_8 and G4 aptamers targeting NCL.

Keywords

G-quadruplex aptamers; retinal diseases; nanosystems; nucleolin; angiogenesis.

List of Figures

List of Tables

List of abbreviatures

AMD – Age-related macular degeneration
AuNPs – Gold nanoparticles
BRB – Blood-retinal barrier
CD – circular dichroism
CRVO – Central retinal vein occlusion
DLS – Dynamic light-scattering
DMSO – Dimethyl sulfoxide
DOPE – 1,2-dioleoyl-sn-glycero-3-phosphoethanolamine
DPPC – 1,2-dipalmitoyl-sn-glycero-3-phosphocholine
DPPG – 1,2-dipalmitoyl-sn-gly-cero-3-phospho-(1′-rac-glycerol)
DR – Diabetic retinopathy
DSPE-PEG – 1,2-distearoyl-sn-glycero-3-phosphoethanolamine-N-[carboxy(polyethylene glycol)-2000, NHS ester] (sodium salt)
EDTA – Ethylenediaminetetraacetic acid
EE – Encapsulation efficiency
ESI-MS – Electrospray mass spectrometry
FRET – Fluorescence resonance energy transfer
G4 – G-quadruplex
GUVs – Giant unilamellar vesicles
HPLC – High-performance liquid chromatography
HUVEC – Human Umbilical Vein Endothelial Cells
ITC – Isothermal titration calorimetry
KPi – Potassium phosphate buffer
LUVs – Large unilamellar vesicles
MLVs – Multilamellar large vesicles
MTT – 3-[4,5-dimethylthiazol-2-yl]-2,5 diphenyl tetrazolium bromide
MVVs – Multivesicular vesicles
NCL - Nucleolin
NMR – Nuclear magnetic resonance
NPs - Nanoparticles
NTA – Nanoparticle Tracking Analysis
NVG – Neovascular glaucoma
OIS – Ocular ischemic syndrome
PDGF – Platelet derived growth factor
PDI – Polydispersity dispersion index

PEG – Polyethylene glycol

PG – 1,2-distearoyl-sn-glycero-3-phospho-(1'-rac-glycerol) (sodium salt)

RPE – Retinal pigment epithelium

SELEX – Systematic evolution of ligands by exponential enrichment

SUVs – Small unilamellar vesicles

TBE – Tris/Borate/EDTA buffer

TCEP – tris-(2-carboxyethyl)-phosphine hydrochloride

TDS – Thermal difference spectra

TEM – Transmission electron microscopy

TGF-β – Transforming growth factor-beta

T_m – Melting temperatures

VEGF – Vascular endothelial growth factor

List of Publications

Published manuscripts (others)

1. Moreira, D.; Leitão, D.; Lopes-Nunes, J.; Santos, T.; Figueiredo, J.; Miranda, A.; Alexandre, D.; Tomaz, C.; Mergny, J.-L.; Cruz, C. G-Quadruplex Aptamer-Ligand Characterization. *Molecules* 2022, *27*,6781.https://doi.org/10.3390/molecules27206781.

Conferences presentations (part of the dissertation)

1. D. Moreira, J. Nunes, Fátima Santos, C. Cruz, C. Tomaz – "Development of aptamer nanoparticles for treatment of retinal diseases" – XVI Annual CICS-UBI Symposium (30th September and 1st October).

2. D. Moreira, J. Nunes, F. Santos, C. Cruz, C. Tomaz – "Characterization of a nucleolin targeting aptamer to develop nanosystems against retinal diseases" - XVII International CICS-UBI Symposium (21st and 22nd July 2022).

3. D. Moreira, J. Lopes-Nunes, F. Santos, C. Cruz, C. Tomaz – "Aptamero anti-nucleolina no tratamento de doenças neovasculares da retina" – VIII Ciclo de Conferências da Faculdade de Ciências (23rd and 24th september 2022).

4. D. Moreira, J. Lopes-Nunes, F. Santos, C. Cruz, C. Tomaz – "Aptamero anti-nucleolina para o desenvolvimento de nanopartículas para terapia do retinoblastoma" - 4º Encontro Nacional de Jovens Investigadores em Oncologia (24th september 2022).

1. Introduction

The human eye is one of the most complex organs of the human being and it is the primary organ of vision [1]. This sophisticated organ helps us to get information about our environment and it allows our brain to have enough information to process things that happen in our world. Eyes are considered the windows of the soul due to the importance they have in human relationships [2].

However, sometimes this organ may suffer from several diseases that greatly affect the life quality of individuals. Due to the population ageing, these diseases are appearing with more frequency and causing more health problems in developed countries [3]. However these pathologies have more prevalence on developing countries, regarding the lower access that populations have to basic health care [4,5].

1.1. Anatomy and physiology of the human eye

Due to its vital importance for human daily life, the eyes are protected by several structures that help to prevent possible traumas. The first is the bony orbits that surround each eyeball. This structure protects eyeballs, especially from large objects. Above each eye, the eyebrow and the eyelids help to protect the eye from sweat and from small objects that can injure the eye [2].

The eyeballs are a complex association of distinct types of tissues that form different structures with varied functions. Clinically, the eye is composed of two segments: the anterior and the posterior. The anterior segment is composed of all the structures from the lens forward and the posterior one of the structures posterior to the lens [1].

Figure 1 shows the principal eye structures that contribute to the reception of the environmental light and transform it into information that the brain can interpret.

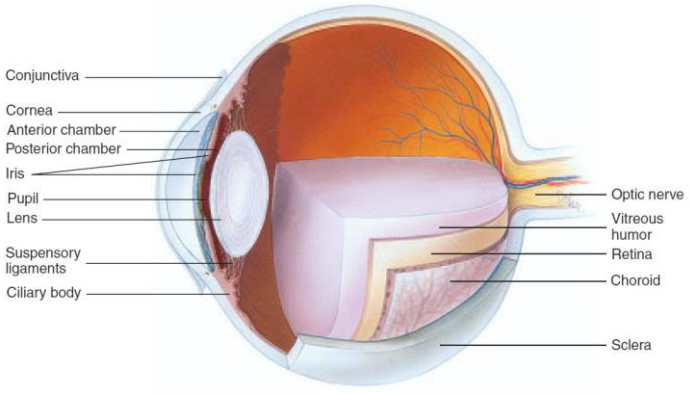

Figure 1 – Sagittal section of the eye (adapted from [6]).

The light enters the eye through the cornea and is amplified and inverted on the lens [2]. This processed image will be projected on the retina which is one of the most important tissues of the posterior segment. This tissue is the one that surrounds the vitreous cavity, lining with one of the middle layers of the eye, the choroid, which is the main responsible to provide oxygen and nutrients to the retina. The outer layer is composed by the sclera and the cornea, which provides protection to the retina and to other ocular tissues [7].

The retina can be divided into the neural retina and retinal pigment epithelium (RPE) [7]. The RPE acts as a protection system for the neural retina. Such protection functions include phagocytosis and the storage of some molecules that are essential for the normal working of the neural retina. These cells also compose the outer blood-retinal barrier (BRB) [7]. BRB is a highly specialized blood–neural barrier that selectively restricts the flux of ions, metabolites, and harmful toxins into the retina maintaining an adequate neural environment, which is essential for phototransduction [8].

The neural retina is more complex and consists of several classes of neurons: photoreceptors (rods and cones), bipolar cells, horizontal cells, amacrine cells, ganglion cells, and Müller glia. These complex tissues are responsible for receiving the projected lens image and converting it into an electric signal that will be transmitted to the brain [7].

However, sometimes this complex process that allows human beings to see the world may suffer from several issues such as retinal diseases that may lead to the progressive loss of vision and consequent loss of daily life quality.

1.2. Retinal diseases

Retinal diseases are all the processes that affect retinal homeostasis and function, which may result in loss of vision. In developed countries these diseases are the main cause of

blindness, however, the prevention of these diseases is not included in blindness prevention programmes in developing countries. It is expected that the incidence of retinal diseases will keep increasing especially due to the increased incidence of diabetes worldwide and world population ageing [9,10].

These diseases may be of two types: inherited or acquired. The first type is inherited genetically and because of that, the medical history not just of the patient but also of the family must be considered [11]. In these cases, it is important to have early diagnostics based on the genetic risk and also a regular clinical examination. On the other hand, acquired retinal diseases may be more difficult to predict and consequently to diagnose. However, these diseases may be sometimes avoided by healthy life habits.

Retinal diseases can also be classified based on different criteria that consider, the part of the retina that is damaged or the pathological process event that causes the disease. Thus, according to the first criterion, retinal diseases can be classified into the following categories: diseases of the inner retina, diseases of the outer retina, diseases that affect all retinal layers and finally diseases that affect both retina and optic nerve structures [12]. In this work the classification of pathologies based on the process that causes the disease will be considered. However, the classification of retinal diseases based on this type of classification is complicated by the fact that most of these diseases have multifactorial nature. The majority of retinal diseases are characterized by vascular changes and/or ischemia, inflammation, oxidative stress, and neurodegeneration. In this work, the focus will be on retinal diseases that involve neovascularization, neovascular retinal diseases.

1.2.1 Neovascular retinal diseases

Neovascular retinal diseases are caused by an abnormal growth of new blood vessels from the existing vasculature (neovascularization). On one hand, this process affects the normal blood supply of the retina and on the other side, it may directly damage the retinal neovascular unit, which is indispensable for the normal vision of an individual [13]. These damages are caused by haemorrhages, fibrosis, vascular leakages, and edemas. Usually, the neovascularization episode is started by an ischemia incident that triggers the production of angiogenic factors. The principal neovascular retinal diseases are diabetic retinopathy (DR), AMD, central retinal vein occlusion (CRVO), and neovascular glaucoma (NVG).

1.2.1.1 Age-related macular degeneration

AMD is a disease that affects the central retina and is the main responsible for visual loss among adults older than 65 years in developed countries, affecting about 170 million individuals all over the world [10,14,15]. At more advanced states, AMD can be neovascular (wet AMD) or atrophic (Dry AMD) but the most severe form of the disease is the neovascular one [16]. Even if Dry AMD may be considered a progressive, neurodegenerative disorder since it leads to the progressive death of photoreceptors [17], it may progress to a neovascular disease (wet AMD), in which new blood vessels start growing from the macula (macular neovascularization) into the subretinal space [18–20].

It is important to understand the mechanisms that lead to the development of this disorder and especially to the formation of the blood vessels. This is not an easy task since it is a multifactorial disease that can depend on many factors [17], such as the combination of ageing, genetic, environmental and immunological factors [16]. Despite all these factors that can contribute to AMD, the trigger that starts wet AMD is usually inflammation or an episode that causes intense oxidative stress [16,17]. Thus, the principal molecules that interfere in AMD beginning are inflammatory molecules, such as vascular endothelial growth factor (VEGF), TGF-β, inflammatory cytokines, and complement molecules [21]. Also nucleolin (NCL) has an important role in AMD since it acts as a growth factor receptor that was found to be overexpressed in the cell surface of migrating endothelial cells in the laser-induced model of wet AMD [18].

1.2.1.2 Diabetic retinopathy

DR is the most common cause of blindness in adults in the world [12,22]. However, the mechanisms that trigger this disease are still not fully understood. Usually, the first histological changes that are observed include capillary basement membrane thickening, leukostasis, loss of pericytes, endothelial proliferation, and gliosis [16]. These changes will develop and will affect the microvasculature of the retina. Based on the phenotype of the vascular changes they can be divided into non-proliferative (early stage) and proliferative (late stage) [12,22]. Microvascular alterations typically occur in the early stage including microaneurysms, intraretinal haemorrhages, intraretinal lipid exudation, irregular retinal venous diameter, and pericytes loss, which leads to retinal edema, capillary nonperfusion and, consequently, retinal ischemia [23]. Recently, it has been suggested that neuroglial degeneration and inflammation may precede these microvascular abnormalities [24], [25]. The late stage is usually characterized by the growth of abnormal new blood vessels, which

is driven by retinal ischemia and associated with some ischemia-induced factors such as VEGF (also related with chronic inflammation) and TGF-β [12]. However, it is known that this late stage can be also mediated by other angiogenic molecules [26].

1.2.1.3 Neovascular glaucoma

NVG is a potentially severe blinding secondary glaucoma, characterized by the development of rubeosis iridis and elevated intraocular pressure that is difficult to treat if it is not detected in an early stage [27]. This disease can evolve from other ocular diseases but the most common are DR, ischemic CRVO, and ocular ischemic syndrome (OIS) [28]. In addition to eye vascular diseases, NVG may be secondary to tumours, inflammatory and systemic diseases [28,29]. NVG is characterized by a chronically red, painful eye that can lead to vision loss if not treated. However, in the early stages, it can also be asymptomatic which makes this disease hard to detect [29].

Usually, NVG is triggered by an episode of retinal hypoxia that will lead to the release of angiogenic factors like VEGF, which has an important role in all neovascular retinal diseases. Other molecules, such as IL-6 (an inflammatory cytokine) and the transforming growth factor-beta (TGF-β), are also relevant players in this disease as it happens on AMD and DR. These molecules will promote increased vascular permeability, increased endothelial cell mitosis and leucocyte accumulation in the eye. These responses will cause neovascularization leading to the clinical symptoms that characterize the disease [29].

1.2.1.4 Central retinal vein occlusion

CRVO is the second most common cause of visual loss from retinal vascular disorders and the leading cause of NVG worldwide [19,20]. This disease is characterized by superficial and deep intraretinal haemorrhages that frequently cause unilateral visual loss. However, the way that this disease develops is still a mystery for science. Several hypotheses have been proposed to explain the pathological mechanisms of CRVO, highlighting the combination of several factors, such as vessel wall changes, and haemorrhagic, and thrombotic tendencies [30]. Considering that this is a vascular disease, the risk of developing CRVO may depend on the daily habits of individuals, so it can be prevented by healthy cardiovascular habits.

1.3 Targets and treatments for retinal vascular diseases

As reported previously, retinal vascular diseases have some similarities and often, share the same pathological events. Nowadays, one considerable part of the available treatments are not specific to a single disease. This lack of specificity explains why these "traditional" treatments have low efficacy. The "traditional" treatments for ocular diseases include surgery of the affected part of the eye (e.g., vitrectomy), focal laser photocoagulation, and photodynamic therapy [27,31]. However, all these therapies are not always effective. Therefore, in recent years there have been developed treatments that improve specificity by targeting VEGF, an important molecule involved in the pathological pathway of retinal diseases, and reformulated anti-inflammatory agents, such as dexamethasone or triamcinolone acetonide [32] (Figure 2).

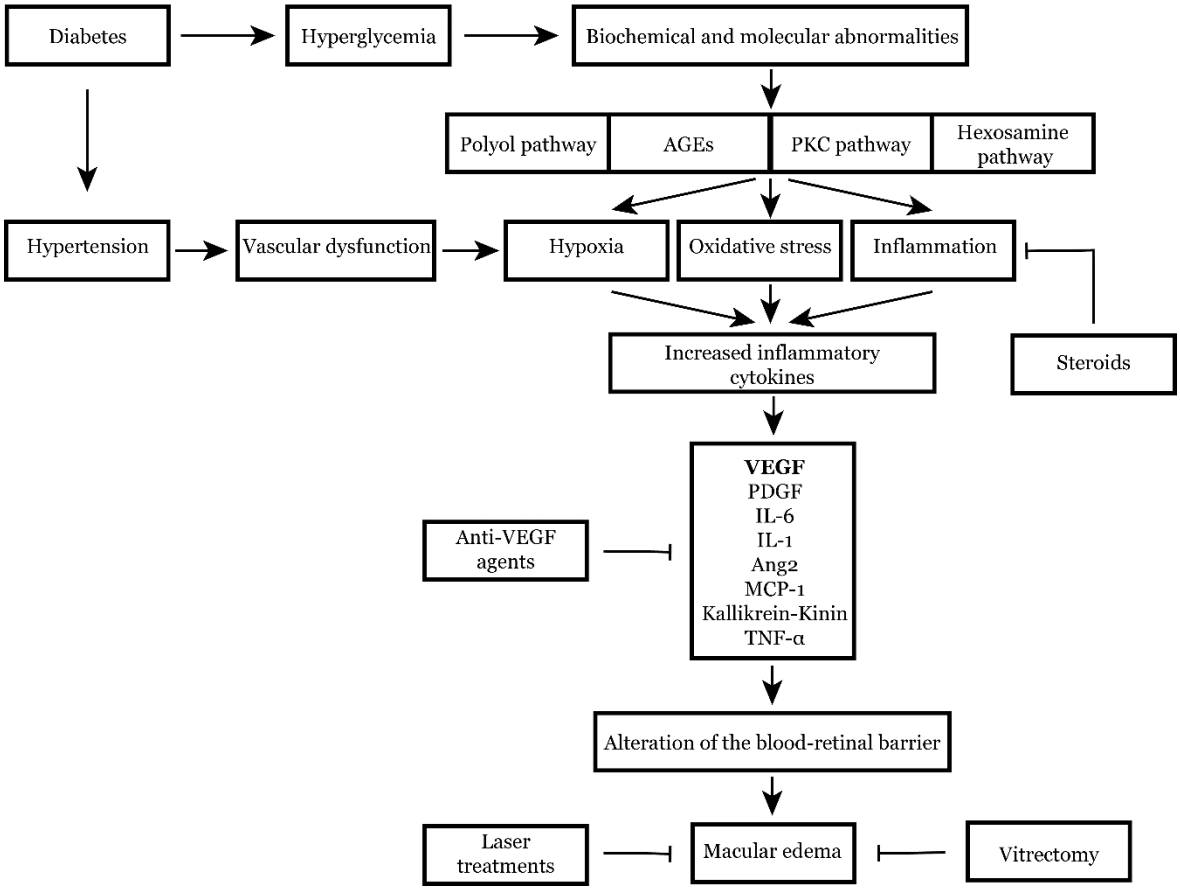

Figure 2 - Pathways involved in the development of DR (adapted from [33]).

One of the solutions that improved the management of neovascular diseases was the use of anti-VEGF antibodies. Nowadays, there are several antibodies approved for these diseases such as bevacizumab or ranibizumab [34]. Ranibizumab (commercially named Lucentis®) is the most used treatment for neovascular AMD. It consists of a humanized monoclonal antibody fragment with only one antigen-binding domain designed to bind all the isoforms

of VEGF. It is administrated by intravitreal injections preventing vision loss and improving visual acuity. The major drawbacks of intravitreal ranibizumab are side effects such as eye pain, inflammation, and conjunctival haemorrhage. Bevacizumab (Avastin) is also a monoclonal antibody that targets all isoforms of VEGF. However, it has less affinity to VEGF than ranibizumab. It has the advantages of having two antigen-binding domains and an increased half-life time, however, side effects are similar to those reported for ranibizumab. Other important drawbacks are related to the production process since these antibodies are obtained using a biological synthesis (using E. coli cells for ranibizumab and Chinese hamster ovary cells for bevacizumab), which implies a specific and costly purification process, thus making the final product very expensive and consequently the cost of the treatment [35]. Aflibercept, also known as VEGF Trap-eye (Eylea®) is one of the most recently approved antibodies for retinal diseases treatments. It consists of a fully humanized recombinant protein that acts as a soluble decoy receptor that binds to VEGF-A, VEGF-B and placental growth factor (PIGF). Since its approval by the FDA for use in neovascular AMD, intravitreal aflibercept has been approved for a variety of other retinal pathologies and it is already one of the most used therapy [36]. More recently, FDA approved a new anti-VEGF, faricimab, which showed a comparable but more durable therapeutic effect compared to the other anti-VEGF drugs, including aflibercept, which reduces the treatment burden in patients [37].

Two important tools have also emerged to help in the treatment of these diseases, aptamers, and nanoparticles (NPs).

1.3.1 Aptamers

Aptamers are small sequence-specific nucleic acids (DNA or RNA) or peptides that can recognise and interact with a specific target [38,39]. The word aptamer comes from the Latin *aptus*, to fit, and the Greek *meros*, part of a region. As the name indicates, aptamers are oligonucleotides that are selected because of their ability to bind a target with high specificity and affinity. Usually, aptamers are compared to antibodies since they both can interact with a specific target. However, aptamers have some advantages when compared with antibodies making them perfect candidates for diverse applications. They have the advantage to be easier to synthesize since the involved chemical process is more efficient than the biological synthesis used to obtain antibodies. They also have low immunogenicity and an increased shelf-life and stability, that may be further increased with nucleotide chemical modifications [39–41]. Researchers have been taking advantage of these

characteristics using them for flow cytometry staining, as drug delivery systems and to inhibit enzymes or molecular pathways [39].

One of the most important features of aptamers is their structure and some of them can adopt a G-quadruplex (G4) structure [42]. In these cases, the sequences repeated guanines form G-quartets (G-tetraplex, G-tetrads, or tetrads). These G-quartets are the basic structural motif of G4. Each G-quartet is formed by four guanines linked and stabilized via Hoogsteen bonds in a co-planar square. The stacking of G-quartets forms the G4 structure. This structure is usually stabilized by cations located on the central channel of the G-quartet.

The stabilization by a cation depends on the cation species (and its properties, such as size and charge) and also on its concentration. Several cations may stabilize G4 structures but the more studied are K^+ and Na^+ due to their biological importance in the cells [43]. However, not all the G4 have the same space arrangement. There are three major conformations that G4 can adopt: parallel, anti-parallel, and hybrid topologies. These different topologies result from different polarities of the strands [44]. In Figure 3 the G4 structure and its topologies are represented.

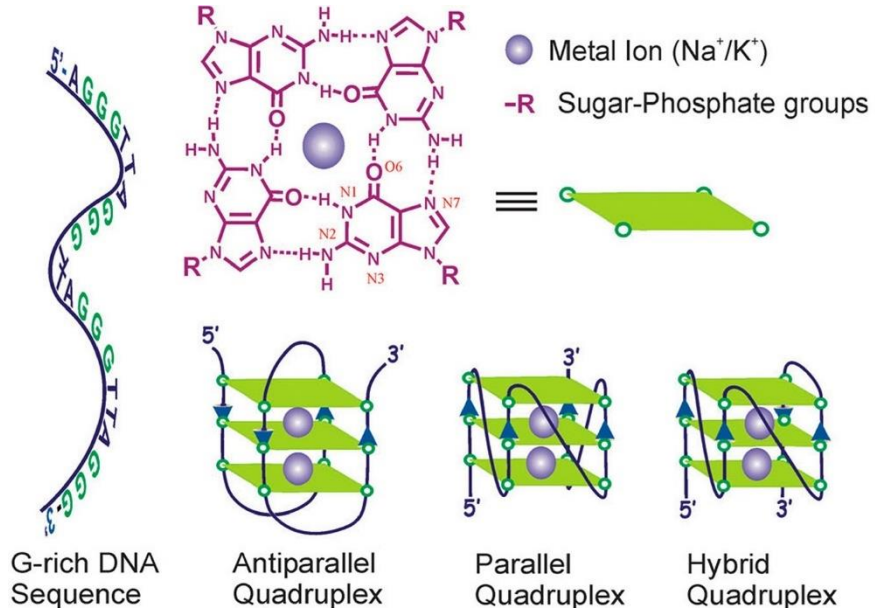

Figure 3 - Structure of a G-quartet and the different topologies of G4 (adapted from [32]).

G4s were naturally found in the human cells being present throughout the genome and in its RNA transcripts [44]. G4s have important regulatory roles in biological processes. Several studies also evidenced that G4s play an important role in growth and progression of tumours in cancer and in the development of neurological disorders, since they are present not only at telomeric regions but also at oncogene promoter regions.

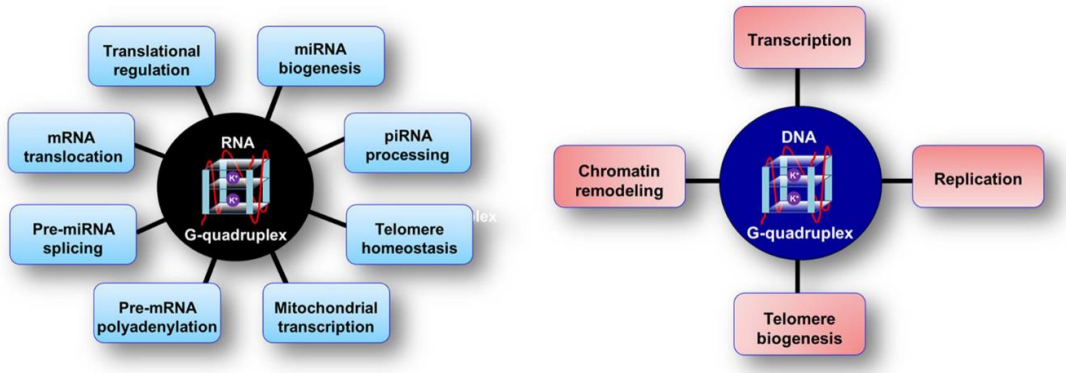

Figure 4- G4 importance in biological processes (taken from [43]).

Some molecules can stabilize the G4 structure, which are known as G4 ligands. These ligands have been applied as binders and stabilizers of G4, and can also act as therapeutic molecules (some of them have anti-cancer properties) [45]. Some examples of G4 ligands are benzothiazole, triphenylmethane, acridine, alkaloids, pyrene, naphthalene, porphyrins and acetone derivatives [45]. These ligands can be used on the stabilization of promoter regions of oncogenes and telomeric ends, and also on non-coding RNAs with importance on tumour development.

Despite all the existing G4 ligands, there are no reports of its use in retinal diseases. However, Miranda *et al.* used the ligands PhenDC3, 360A, and TMPyP4 to stabilize AS1411 aptamer and its derivate AS1411-N6. These aptamers target NCL, a protein over expressed in retinal diseases. In this study Miranda *et al.* found that the three tested ligands have promising stabilizer effects on the tested aptamers [46]. Cruz *et al.* also found that the ligand C_8 (an acridine orange derivate) is capable of stabilizing pre-miR-92b. In this case, pre-miR-92b was used as a molecular recognition probe for NCL [47]. The chemical structures of the ligands above referred are showed in Figure 5.

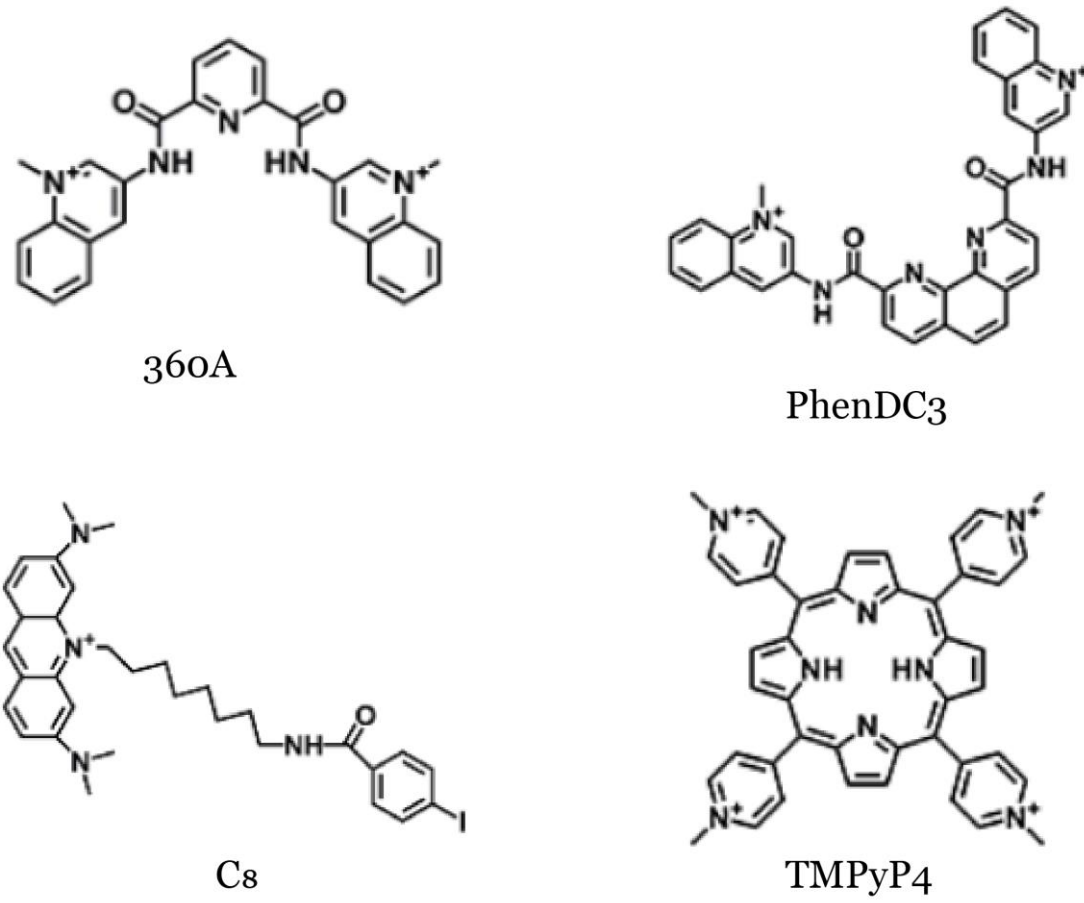

Figure 5 - Chemical structure of G4 ligands 360A, PhenDC3, C_8 and TMPyP4.

1.3.1.1 Structural characterization of aptamers using biophysical techniques

Several biophysical techniques have been developed to study aptamers conformation and their interaction with the target or ligands, namely, nuclear magnetic resonance (NMR), circular dichroism (CD), fluorescence titrations and thermal difference spectra (TDS). Other techniques can be used, such as isothermal titration calorimetry (ITC) and electrospray mass spectrometry (ESI-MS) [48,49].

NMR is a powerful tool used to study the structural, kinetic, and dynamics of G4 aptamers and ligand complexes. This technique is based on the application of magnetic fields on a solution containing the molecule of interest. Then the magnetic field variations are analysed, and the signal is converted, giving information about the chemical and physical properties of the molecule. In the case of G4 and G4/ligand complexes, one of the most important signals is the G4 imino resulting from Hoogsteen base pairing. Usually, this

signal appears in the region near 10-12 ppm and indicates that G4 is formed [48,49]. To study the interaction between the G4 and a ligand there are different types of experiments that can be performed. However, the simpler approaches depend on the hydrophobicity of the ligands (usually ligands are hydrophobic). Regarding it, usually, ligands are solubilized in a dimethyl sulfoxide (DMSO) solution and then added to an aqueous solution of the G4 aptamer. After that, chemical shifts, peak heights, and linewidth of the recovered signals are analysed. NMR can also be used for more sophisticated experiments based on polarization transfer between spins systems or on the H2O/D2O exchange rate on different parts of the G4 [48–52]. The main advantage of NMR spectroscopy is the fact that it allows determining the binding sites of a ligand in the G4 structure, characterizing the 3D structure of the complex and studying the conformation of the ligand. Despite these advantages, NMR can consume a considerable amount of time and a higher concentration of aptamer and ligands compared to other techniques [48,49].

CD is another spectroscopic technique that is commonly used to study the formation/stabilization of G4 aptamer. CD is used only with chiral molecules since this technique is based on the differential absorbance by a substance of right- and left-handed circularly polarized light. By using the CD technique, different information about the G4 aptamer topology, G4-ligand complex formation, and ligand-induced thermal stabilization can be obtained. The main advantages of CD are its simplicity and speed, the use of small sample amounts, and the type of information provided [44,53–55]. Figure 6 shows how the different G4 topologies result in different types of CD spectra.

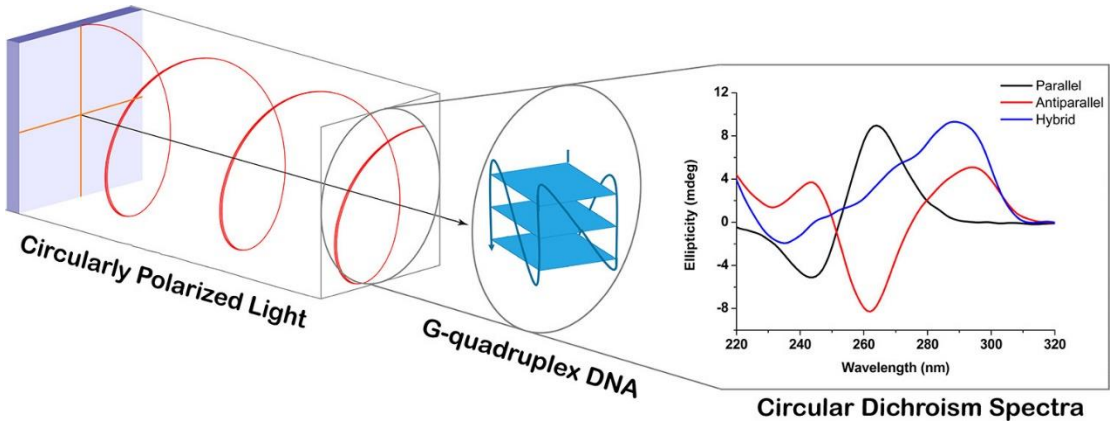

Figure 6 - Schematic representation of CD operation mode and the different spectra topologies for G4 (adapted from [44]).

As observed in Figure 6, a parallel G4 presents a positive peak located at about 260 nm and a negative peak at about 240 nm. Antiparallel G4 has two positive peaks. The first one is located at about 295 nm and the second one at about 240 nm. It also has a negative peak located at about 260 nm. Finally, hybrid G4 also presents two positive peaks and a negative

one. The positive peaks are located at about 295 and 260 nm and the negative one at about 240 nm [44,53].

Another parameter that can be determined by CD is the ligand-induced thermal stabilization of G4 aptamer that can be obtained through the analysis of spectrum before and after the addition of the ligand to G4 aptamer at different temperatures [44]. Figure 7 shows the results of a typical CD experiment for the determination of ligand-induced thermal stabilization.

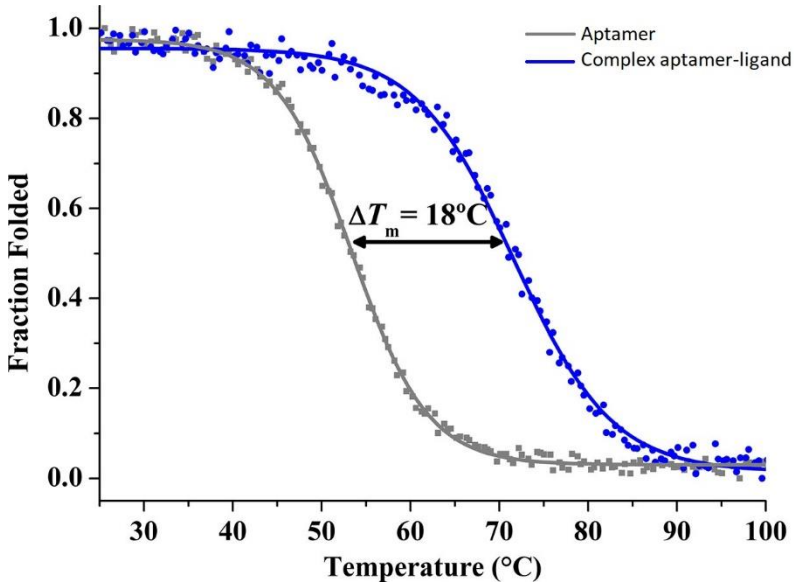

Figure 7 - Ligand-induced thermal stabilization obtained by CD (adapted from [44]).

Despite all the advantages above referred, the CD technique has a drawback that it does not allow to detect easily multiple conformations of the same molecule because it is a low-resolution technique [48,49].

Fluorescence titrations can be used to determine the binding affinity between the G4 aptamer and the ligand or the target. The aptamer or the ligand must have a fluorophore to emit fluorescence after being excited by an excitation source. This fluorescence depends on the concentration of the fluorophore, the temperature, and the intensity of the excitation source and may also depend on the interaction of the fluorophore with other molecules. Fixing the concentration of the aptamer and adding increasing concentrations of ligand, the fluorescence will decrease in each ligand addition resulting from the interaction between the G4 and the ligand. Inversely and fixing the concentration of ligand and adding increasing concentrations of the aptamer, the fluorescence will increase with each addition

of aptamer. In both cases, plotting the fluorescence intensity at its maximum with the concentration of ligand/aptamer to obtain a binding curve that can be fitted to a specific binding model allows the determination of the binding stoichiometry and the affinity constant [56–58]. The other type of experiment that can be done with fluorescence spectroscopy is fluorescence resonance energy transfer (FRET) assays. FRET-melting is used to obtain information about the stability of a G4 conformation and its interactions with ligands. This technique is based on the transference of energy between a donor (previously excited) and an acceptor molecule (quencher). Similarly, to CD-melting, which analyses the folding and unfolding state, FRET-melting assay gives information about this process. In the folding state, donor and acceptor are so close that fluorescence is quenched by the acceptor. By increasing temperature, the interactions that stabilize G4 are broken, and the molecule starts to unfold, separating the dye and quencher and it is emitted donor's fluorescence. The fluorescence maximum is achieved when the biomolecule is completely unfolded [59,60]. This process is represented in Figure 8.

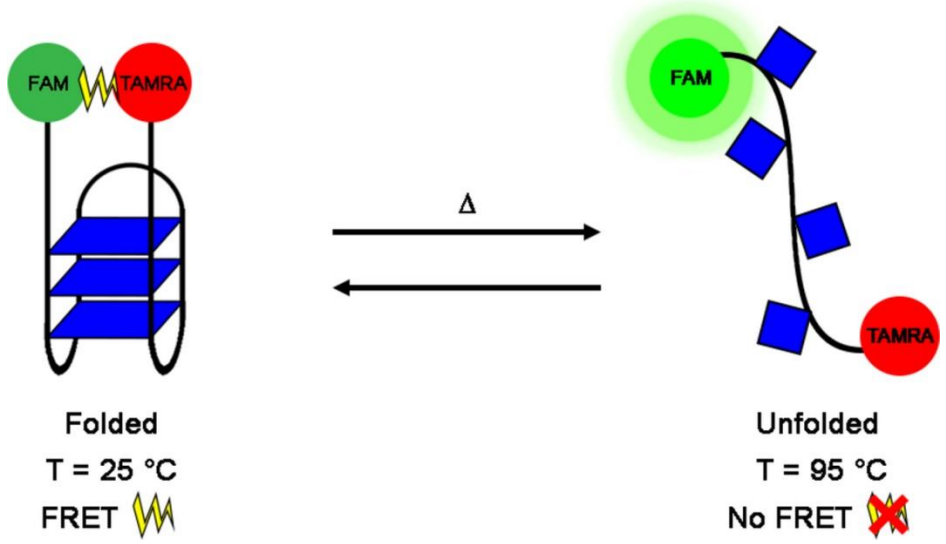

Figure 8 - Schematic representation of FRET assay in a G4 structure (taken from [60]).

FRET assay consumes a low amount of sample that may give important information about G4 structure and its interaction with ligands. However, it requires a labelled aptamer, and it only gives a limited type of information [36,37].

Finally, TDS is another technique used for the structural characterization of G4 topology. This technique provides a distinctive spectroscopic signature for different nucleic structures by the acquisition of a UV spectrum, usually between 220-320 nm, above the melting temperature and another below this temperature. These spectra are then subtracted obtaining the TDS spectrum [45]. One of the most important bands in these spectra is a

295 nm band that is known to be important in quadruplex folding. Then ΔA240nm/ΔA295nm, ΔA255nm/ΔA295nm, and ΔA275nm/ΔA295nm ratios are calculated to find out information about the G4 structure [53].

1.3.1.2 Aptamers in retinal diseases

Aptamers can be very useful to inhibit molecules associated to pathological pathways that lead to retina angiogenesis. Different aptamer-based therapies have been developed namely Macugen® that is an anti-VEGF RNA aptamer (pegaptanib sodium) approved in 2004 for the treatment of all types of neovascular AMD [39–41,61].

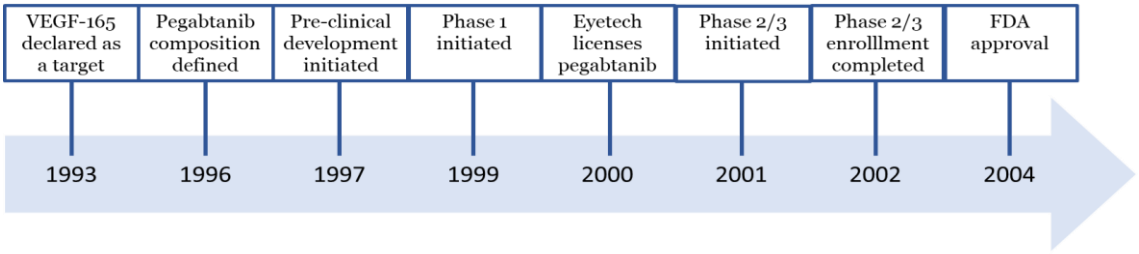

Figure 9 - Timeline for the development of Macugen® (adapted from [40]).

Macugen® is made of a short sequence of 28 nucleobases. This sequence was selected from a library of RNA and DNA tested by systematic evolution of ligands by exponential enrichment (SELEX) experiments. To improve both resistance of RNA and its affinity there have been integrated some modifications in the primary sequence. These modifications include the incorporation of 3' and 5' caps and a 2'-OMe purine substitution. This aptamer was also PEGylated to achieve a higher molecular mass that difficult the aptamer clearance by the kidneys [39–41,61]. However, Macugen® has a drawback because it only targets VEGF-165. Consequently, other VEGF isoforms keep acting and angiogenesis is not completely inhibited.

Another aptamer is Fovista® that selectively binds platelet-derived growth factor (PDGF). This aptamer of 29 nucleotides was also obtained from SELEX from a single-stranded DNA library and it targets the B chain of PDGF [40,41]. The clinical trials (NCT00569140 and NCT02214628) of this aptamer were performed using an anti-VEGF antibody named Lucentis® (ranibizumab) as a co-adjuvant, with good results in phases 1 and 2 [62,63]. However, results in phase 3 (NCT01940900) had not been as good as expected and the clinical trials had been terminated [64].

Finally, other aptamer that reached clinical trials phase 3 (NCT04435366) is Zimura® (avacincaptad pegol), an aptamer that inhibits C5 (an important molecule of the complement system). The complement system consists of a network of proteins that play an important role in the innate immune system. It means that the complement system is a non-specific mechanism of defence. Under normal physiological conditions, the complement system is maintained at low-grade activation in the eye for maintaining retinal homeostasis [65]. When activated, this defence system will originate an inflammation process and favours opsonization and cell lysis. Although these features are important to destroy unfunctional RPE cells [65], activation of complement cascades contributes to chronic inflammation and the development of retinal disease [65]. The activation of the complement system may occur from 3 different pathways. However, all the pathways will lead to the activation of C5. C5 is one of the principal molecules responsible for the inflammation process. This inflammation process will lead to the accumulation of other inflammatory cytokines that when dysregulated contribute to retinal diseases. So, as the complement system plays an important role in inflammation C5 was chosen as a target in Fovista® development [66,67].

Once again, this aptamer was obtained by SELEX using a library of nuclease resistant RNAs. This aptamer is a 38-mer sequence that was later modified with 2'-OMe substitutions, 3'-3'-linked deoxythymidine to the 3' end, and 40 kDa PEG to the 5' [40]. As in the case of Fovista®, Zimura® has also been tested in combination with Lucentis® (ranibizumab). In the clinical trials of phases II and III (NCT03362190 and NCT04435366), the results have been positive so they will be continued [14].

Despite the satisfactory results of these three aptamers, other must be studied to target other molecules associated with retinal diseases. One of the most investigated aptamers is AS1411 an aptamer with a G4 structure that can interact with NCL. NCL is a ubiquitous nonhistone phosphoprotein with several roles in biological processes. Usually, it is more expressed in the cell's nucleus where it is involved in the regulation of ribosome genesis and ribosomal RNA synthesis. This protein is also found in the cytoplasm since it acts as a shuttling protein between ribosomes and the nucleus. However, in proliferating cells, NCL is highly expressed on the cell surface playing an important role in the regulation of cell proliferation, growth and adhesion, and angiogenesis. When expressed on the cell surface it acts as a co-receptor for growth factors such as pleiotrophin, midkine and endostatin [68]. It is known that NCL translocation to the cell surface is stimulated by VEGF [69]. NCL functions are represented in Figure 10.

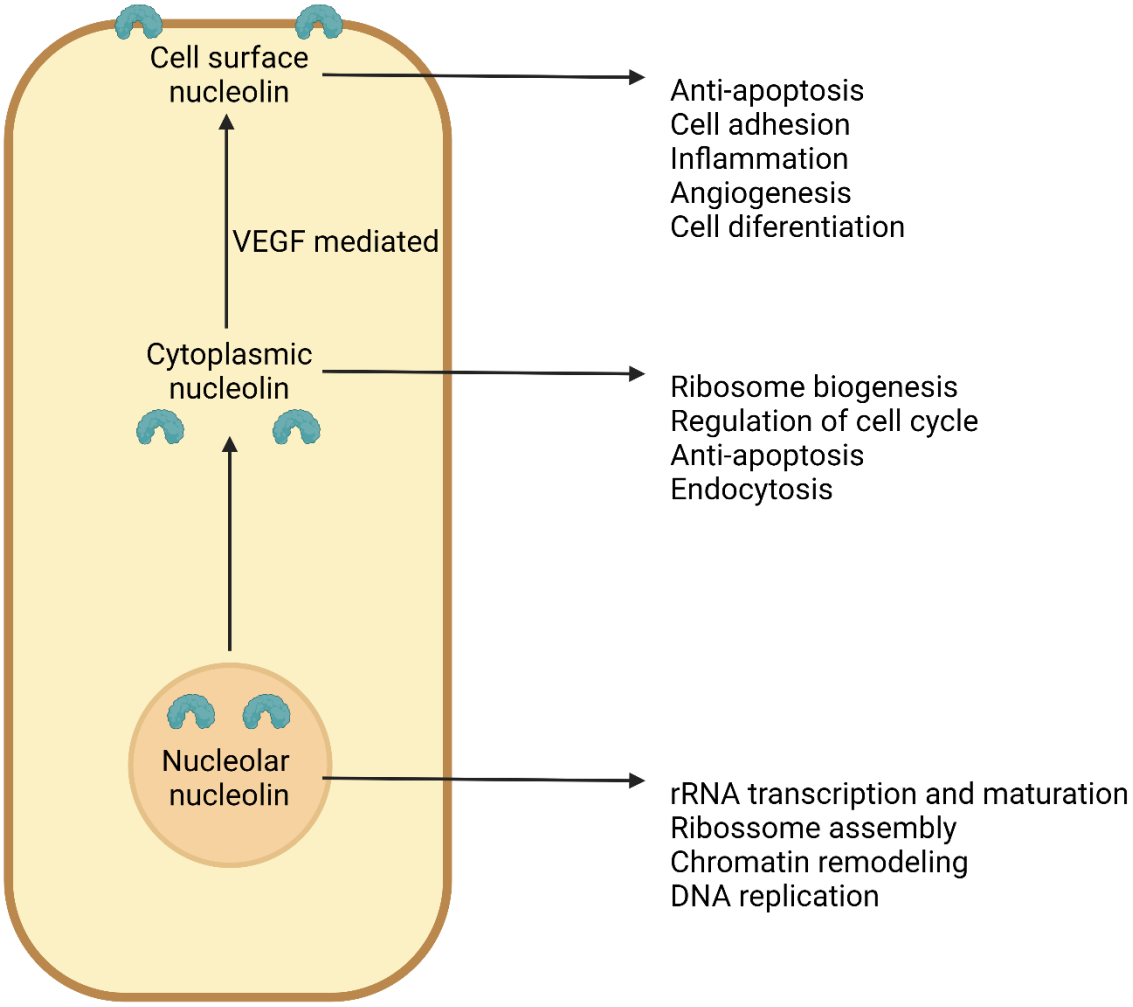

Figure 10 - NCL related functions in different cellular compartments (adapted from [70]).

An interesting investigation on retinal diseases with AS1411 have been made in 2015 by Leaderer *et al.*. They found that AS1411 attenuated the formation of angiogenesis tubes on Human Umbilical Vein Endothelial Cells (HUVEC). Using an *in vivo* AMD model, they found that this aptamer accumulates preferentially in damaged areas, where NCL is upregulated, attenuating inflammation and angiogenesis [18]. Similar results have been found in 2021 by Iturriaga-Goyon *et al.*, but on a DR model [71]. N6L is another aptamer against NCL that was found to inhibit neovascularization in retinopathies mouse models [26]. However, it is a peptide aptamer, and it will not be discussed below. In 2019, Chandola *et al.* found that the CD44 receptor is overexpressed in episodes of oxidative stress on an RPE cell line. So, they developed an aptamer (CD44 aptamer) that was able to internalize RPE cells through the CD44 receptor. Although this aptamer had not a therapeutic effect by itself, it may be an effective carrier molecule for delivering therapeutic agents into RPE cells [17].

So, it is important to identify aptamers and new targets for retinal diseases treatment since nowadays despite all the present investigations there is only one aptamer approved for the treatment of AMD.

1.3.2 Nanoparticles

NPs are delivery systems that improve the efficacy of a therapeutic molecule by helping it to reach the target at higher concentrations. In the case of ocular diseases, NPs can overcome ocular barriers, improve drug residence time on the cornea surface, and increase the permeability and bioavailability of the drug by reducing its degradation [72]. These NPs also have some advantages in terms of the production method. These advantages include an easy synthesis method with a low production cost [73].

Usually, NPs are divided into two main groups: organic and inorganic NPs. Organic NPs include all the nanocarriers that are produced using proteins, lipids, carbohydrates, or other organic compounds. Inorganic NPs include mainly metallic NPs and quantum dots. Figure 11 shows a schematic representation of the different types of NPs.

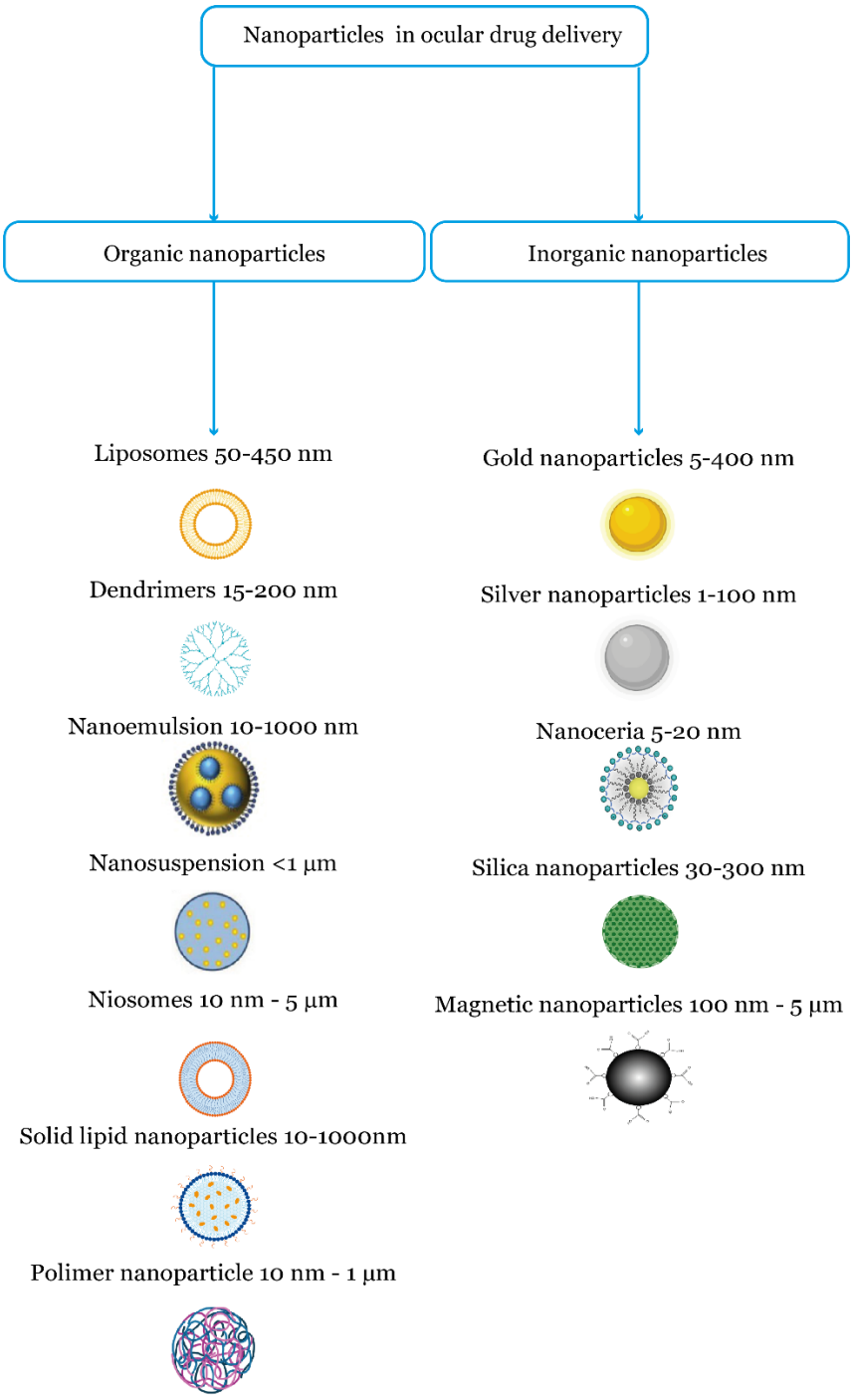

Figure 11- Schematic representation of different types of NPs (adapted from [72]).

1.3.2.1 Liposomes

The most used organic NPs are liposomes which are spherical-shaped NPs with an aqueous core composed of one or more phospholipid bilayers [72]. These NPs show several advantages since they can encapsulate both hydrophobic, hydrophilic, and amphiphilic molecules as can be seen in Figure 12. Another important advantage is that they mimic cellular membranes, so liposomes have low toxicity and are biodegradable. Finally, they can

be easily modified with molecules that help them to target a specific cell type. However, these NPs have also some drawbacks related to the fact that they are not easy to synthesize in a reproducible and cost-effective way. Another disadvantage of liposomes is the difficulty of dosing them precisely because it is not possible to control their formation process and they can even fuse between them [74-76].

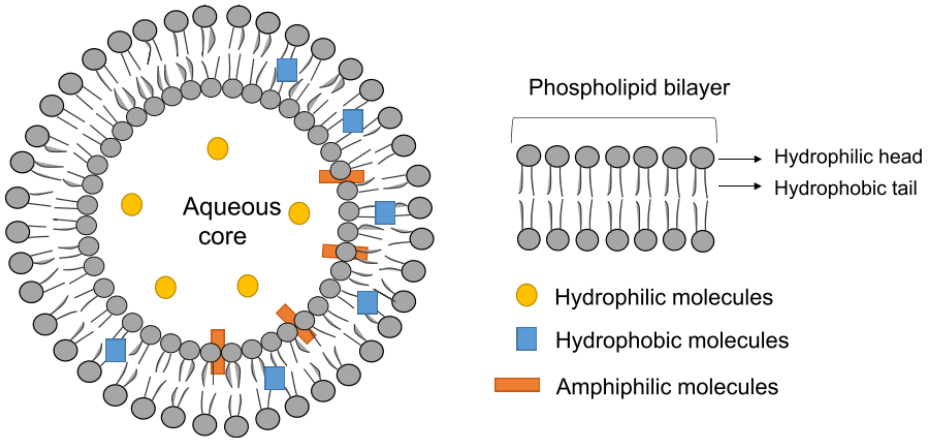

Figure 12- General structure of a unilamellar liposome with different types of molecules encapsulated (adapted from [74]).

The liposomes are characterized in terms of size, surface charge, encapsulation efficiency, and lamellarity.

Several techniques can be used to determine the size and their advantages or disadvantages are described in Table 1. The common size of the liposomes is lower than 250 nm [75].

Table 1 – Techniques used to determine liposomes' size [76].

Technique	Description	Advantages	Disadvantages
Electron microscopy methods	It uses electron microscopy to measure individually liposomes with micron size.	It allows visualizing liposomes. It may also be used to determine lamellarity and morphology.	It is not appropriate to measure large liposomes. Time-consuming method.

Fluorescence microscopy	It measures the fluorescence of labelled liposomes analysing it at the single-particle level.	It allows measuring the size distribution of polydisperse solutions. High sensitivity.	It requires a fluorescent probe. It requires the immobilization of the sample to a glass surface which may lead to sample damage. Time-consuming.
Atomic force microscopy	Based on the interaction of the sample and the tip of the cantilever.	It allows measures of size distribution, stability, and aggregation. High resolution and quick method.	The force applied may be destructive. It causes evaporation.
Field flow fractionation	It includes sedimentation, flow, electrical, and thermal field-flow fractionation. It uses the application of forces perpendicularly to the flow of the sample.	It measures size distribution and relative molecular mass. Quick, highly sensitive, selective, and automated method.	Complex and expensive method. The size range is limited.
Dynamic light scattering (DLS)	DLS measures the fluctuations of scattered light by the sample on time.	Easy, precise, accurate, and fast method. Wide range measurements.	It is not recommended for heterogeneous suspensions. Low resolution.

		Requires only a small volume.	
Flow cytometry	Each particle is measured in a continuous flow system based on the light-scattering.	Reveal the size and the inhomogeneity of the size. Quick, reliable, and reproducible method.	It requires a fluorescent label. Noise signal may be a drawback.
Centrifugal sedimentation	It is a method based on the principles of the hydrodynamic theory, so it relates the velocity of the sedimentation with the particle diameter.	High resolution and sensitivity. Powerful and versatile method.	Limited range. Results may be affected by the speed and geometry of the centrifuge and by the density of the particles.
Differential scanning calorimetry	It is based on the measurement of the temperature dependence of the liposomes' excess heat capacity due to their thermal phase transition.	Sensitive to chemical and physical properties.	Limited to lipids with a transition temperature within the limit of operation of the calorimeter. Time-consuming method.

The zeta potential (surface charge of liposomes) is another parameter used to characterize the liposomes that can be neutral, negative, or positive. Usually, it is recommended that liposomes carry a charged group. Since similar charges will repel each other, this charged group will lead to repulsion between liposomes avoiding aggregation and promoting a stable formulation. The determination of the zeta potential of liposomes is mainly based on light-scattering methods by applying an electric field that leads to particle movement. This movement is proportional to the charge of the particles and causes a shift in the light

frequency that is detected allowing calculation of the charge. Some of these techniques are laser doppler electrophoresis and capillary electrophoresis [74,76].

Encapsulation efficiency (EE) allows to determine the quantity of drug carried by a liposome. Considering that the dose administered of a drug is a key factor for therapeutic efficiency, this parameter is vital to determine that dose [74]. To calculate the EE the drug is released by destabilizing lipid membranes using organic solvents, such as Triton X-100, acetonitrile, ethanol, or even methanol. After release, the free drug can be quantified by HPLC (high-performance liquid chromatography), dialysis, ultracentrifugation, enzymatic assays or gel electrophoresis [77,78]. EE is calculated as the ratio of the free drug found in the liposome and the total drug content used in the liposome preparation [74,76]. This parameter may be influenced by several factors, such as the methods of liposome production and drug encapsulation, and also the rigidity of the membrane that depends on the lipids used and their proportions [74].

Sometimes it can be useful to quantify an individual component of the liposome. Phospholipids are the lipids that are most frequently quantified, although cholesterol can also be measured [76]. To quantify phospholipids, a suitable method is to use a reagent that forms a spectrophotometer-measurable product when reacting with. One of these methods is the Bartlett assay, which is based on the oxidation of the inorganic phosphate present in the phospholipids [79]. Another method is the ascorbic acid assay, which consists on liposomes digestion with perchloric acid that leads to the production of orthophosphates. After several reactions, these orthophosphates will form a specie that can be measured using a spectrophotometer at 820 nm [80]. However, the most used method is the Stewart assay based on the reaction of phospholipids with ammonium ferrothiocyanate, forming a complex that can be quantified in a spectrophotometer at 488 nm [81]. This is a fast, inexpensive, and reproducible method. Finally, phospholipids may also be quantified by marking them fluorescently or using HPLC or gas chromatography. HPLC can also be used to quantify cholesterol [76].

The methods used to produce liposomes are grouped in conventional and novel. The main principle of conventional methods is to dissolve lipids in an organic solvent, then this solvent is removed and finally, liposomes are isolated and purified [74]. The first conventional method used is the thin film hydration method. Basically, the lipids are dissolved in chloroform or another organic solvent and dried to form a thin lipid film by organic solvent evaporation. Then this film is hydrated using an aqueous solvent that leads to liposome formation [74]. The second conventional method is reverse-phase evaporation [82] which uses the same procedure as the previous method, but the lipid film formed is re-

dissolved in an organic solvent followed by the addition of the aqueous solution. Finally, the organic phase is removed by evaporation under reduced pressure [74]. The last conventional technique is the solvent injection method which consists of quickly injecting lipids dissolved in an organic solvent into an aqueous solution [83]. These methods are easy, low-cost, and fast. However, they showed low efficiency, and can form liposomes of several sizes, which requires the use of sonication or extrusion to homogenise the liposomes. Finally, several novel methods are modifications or improvements of the conventional methods. These methods are still under investigation with the objective of industrial production of liposomes [74].

Also the methods available to encapsulate the drug are: passive and active loading [84]. When using passive methods, the drug is dissolved in the aqueous phase used to hydrate lipids. After liposome formation, it captures a volume of the aqueous phase with theoretically the same drug concentration that was calculated for the aqueous solution. This approach is easy to make but has several drawbacks. First, this method is not so effective with hydrophobic drugs since they are not soluble in the aqueous solution. These hydrophobic drugs may be trapped inside of the lipid bilayer when using this method; however, they used low concentrations. Hydrophilic drugs are more suitable since they are charged. When it doesn't happen non-charged drugs can diffuse through the lipid bilayer leading to a low EE [74,84]. The active methods are based on the creation of a gradient of pH or ions that will drive the drug into the liposomes. First, the liposomes are formed, and the drug is carried to their interior by the electrochemical gradient. This gradient can be achieved using ethylenediaminetetraacetic acid (EDTA), phosphate, calcium acetate, or ammonium sulphate. When using these methods, high EE may be obtained without wasting a big amount of drug. However, this is a more difficult and time-consuming procedure that is only used with drugs containing a weakly basic or acid group [74,84].

Finally, it is important to characterize liposomes in terms of lamellarity. This property is related to the morphology of the liposomes, and it is based on their layers. Usually, liposomes can be divided into 4 groups: small unilamellar vesicles (SUVs), large unilamellar vesicles (LUVs), multilamellar large vesicles (MLVs) and giant unilamellar vesicles (GUVs). A representation of the different liposomes categories and their typical sizes is shown in Figure 13. Some authors also consider multivesicular vesicles (MVVs) that are vesicles that encapsulate other vesicles [76,85]. These characteristics can influence the size and the EE of the liposomes.

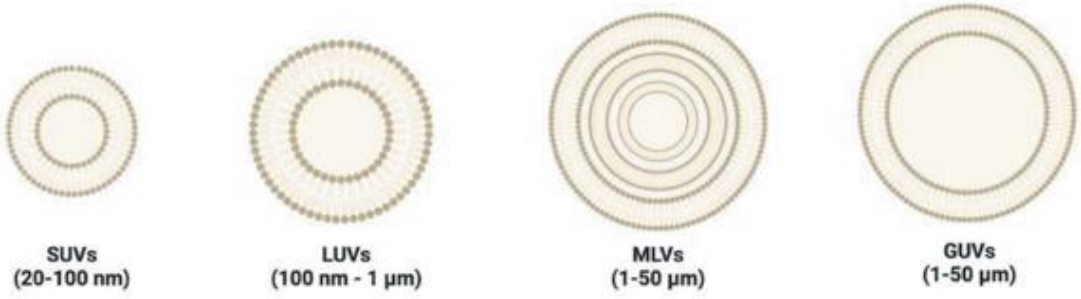

Figure 13 – Representation of liposome's lamellarity classification – small unilamellar vesicles (SUVs), large unilamellar vesicles (LUVs), multilamellar large vesicles (MLVs) and giant unilamellar vesicles (GUVs) – and their typical sizes (taken from [85]).

1.3.2.2 Liposomes in retinal diseases

Liposomes may be an important delivery system in retinal diseases. However, most of the formulations involving these NPs are still under investigation. In 2018, Karumanchi *et al.* tested different liposome formulations, using cholesterol, 1,2-dipalmitoyl-sn-gly-cero-3-phospho-(1′-rac-glycerol) (DPPG), 1,2-dipalmitoyl-sn-glycero-3-phosphocholine (DPPC) and 1,2-dioleoyl-sn-glycero-3-phosphoethanolamine (DOPE), for the delivery of an antibody anti-VEGF (bevacizumab). They showed that the release time of the drug at the vitreous humour was much higher when liposomes are used. They also conclude that the proportions of cholesterol and phospholipids can influence both sizes of liposomes and EE [86]. Also in 2018, Altamirano-Vallejo *et al.* developed liposomes, using PEG-12 glyceryl dimyristate, loaded with triamcinolone acetonide, a corticosteroid used in some vitreoretinal diseases, for vitreoretinal delivery. In this investigation, different types of liposomes were tested and some of these formulations could reach the retina efficiently. The major innovation of this work is that it was one of the first topical formulations for drug delivery in the posterior segment of the eye instead of intravitreal injections [87]. In 2020, Khalil *et al.* developed chitosan-coated liposomes, using soya lecithin and cholesterol, also containing triamcinolone acetonide for delivery in the posterior segment. This investigation showed that the liposomes increased the bioavailability of the drug by increasing the permeability, stability, and retention time of the drug on the vitreous humour. These liposomes can be used in diseases such as AMD or DR. However, all of these investigations lack a component that explores the influence of these liposomes on angiogenesis [88]. In 2019, Lai *et al.* tried to develop liposomes, using lecithin and cholesterol, for drug delivery in the posterior chamber of the eye trying to find a way to treat AMD. This study evaluated two drugs that are not usually used in ocular diseases – chrysophanol with an anti-angiogenic effect and the anti-inflammatory berberine hydrochloride. In addition, the

investigators also evaluated the influence of coating liposomes with a third-generation formulation of polyamidoamine dendrimer to improve EE and the bioavailability of the drug [89]. All these studies showed that liposomes and their functionalization with polyethylene glycol (PEG) or chitosan increase drug bioavailability. However, more studies must be performed to explore the effect of these loaded NPs on neovascular eye diseases and their potential to inhibit angiogenesis.

Despite all these recent studies, only one liposome formulation has been approved for ocular treatment. This formulation is Visudyne® (NDA 21-119) and consists of a liposomal formulation composed of unsaturated egg phosphatidylglycerol and dimyristoyl phosphatidyl choline in a 3:5 molar ratio [90]. This liposome contains verteporfin and was approved by the FDA in 2000 for intravenous administration in the treatment of choroidal neovascularization due to AMD [72].

1.3.2.3 Gold nanoparticles

The most used inorganic NPs are gold nanoparticles (AuNPs) since they present chemical stability, biocompatibility, and easy surface functionalization [72,91]. The principal applications of AuNPs include hyperthermia and photothermal therapy, imaging, tumour targeting, and delivery nanosystems [92,93]. Some of these applications are used in a synergic way to achieve better results. Hyperthermia and photothermal therapy are applications that take advantage of the optical properties of AuNPs. Indeed, AuNPs have electrons that become excited when irradiated with a near-infrared light beam. When electrons turn back into their fundamental status, they release energy and increase the surrounding temperature [94]. This property may be used for several ways such as heating a cluster of tumour cells or releasing a drug resulting from this heating process. This ability is enhanced in cancer cells since the increased permeability and retention effect resultant from the tumour environment, favours the accumulation of AuNPs in solid tumour tissues [95,96]. This potential treatment is even increased when AuNPs are used as a delivery nanosystem. It is relatively easy to functionalize their surface with some drugs, nucleic acids, or proteins. These surface modifications can be used to carry a molecule with a therapeutic effect, to target a specific site, or even to help AuNPs to evade the immune system (usually using polymers such as PEG) [92,97]. Finally, all these applications may be followed by an imaging technique, such as magnetic resonance imaging or photothermal imaging that are allowed by AuNPs [98–100].

The characterization of AuNPs is important to control variations in size, morphology, shape, colloidal stability, and surface coating determination [92,93]. Also, DLS based on the

fluctuations of the scattered light, is a non-destructive technique and appropriate to determine the size distribution of AuNPs and their aggregation state [101]. Regarding the morphology of AuNPs, they can be divided into several categories that include gold nanospheres, gold nanorods, gold nanocages, and gold nanoshells [93]. These shapes depend on the synthesis method. Transmission Electron Microscopy (TEM) is the most widely used technique for studying the morphology of NPs since it furnishes high-resolution images that allow to analyse the shape and size of the NPs [102]. Finally, UV-vis spectroscopy is useful to assess the aggregation of the AuNPs and their concentration [103,104]. This technique also allows the study of some optical properties of the AuNPs [102]. Finally, it is important to determine the surface coating using direct or indirect methods [92]. In indirect techniques, the free drug is quantified and the surface coating is calculated as the difference between the total quantity of drug and the quantity of the measured free drug. The concentration of the free drug can be quantified by UV-vis and fluorescence spectroscopies, using fluorescamine-based and ninhydrin-based assays [105]. The indirect methods consist of separating the free drug from the AuNPs using, for example, centrifugation.

1.3.2.4 Gold nanoparticles in retinal diseases

Since AuNPs can be used as a drug delivery system to treat retinal diseases, it was necessary to ensure that these NPs do not damage the eye structure. Another important factor that should be investigated is the capacity of AuNPs to cross the BRB. In 2008, Bakri *et al.* concluded that AuNPs did not cause considerable histological modifications in a rabbit model [106]. In 2009 Kim *et al.* showed that AuNPs administered intravenously could pass the BRB (depending on the AuNPs sizes) and reach the retina of CL5BL/6 mice. They also concluded that these AuNPs are distributed on different retina cell types without causing a decrease in their cellular viability. Finally, they found that AuNPs did not cause considerable changes in the expression of biological molecules [107]. Dong *et al.* produced AuNPs coated with resveratrol (a natural antioxidant) that were tested in diabetic rats for DR treatment. The results showed that these systems reduce angiogenesis and inflammation processes. These AuNPs also decreased the permeability of BRB [108]. Finally, Laradji *et al.* used an AuNPs formulation based on hyaluronic acid for topical administration in a mice model. These AuNPs were able to reach the retina and remain in it without causing adverse effects. These AuNPs may be an alternative to the actual drug delivery systems to the posterior segment of the eye since they display properties such as non-toxicity, biodistribution, and active targeting through hyaluronic acid-CD44 affinity [109].

However, it is necessary to find new targets using these nanosystems for retinal treatment. Since NCL has found to be overexpressed in some retinal diseases it may be used as a molecular target. As previously referred, some studies showed that AS1411 target this protein. Hence, this work will explore the ability of AT11-Lo to target NCL. AT11-Lo is a derivative of AT11, an aptamer of AS1411. It will also be explored the conjugation of AT11-Lo with a drug in AuNPs and liposomes.

The next chapter will describe materials and methods. After that, the obtained results will be shown and discussed. Finally, major conclusions will be indicated along with future perspectives. For a better understanding of the research work, a graphical abstract is presented in Figure 14.

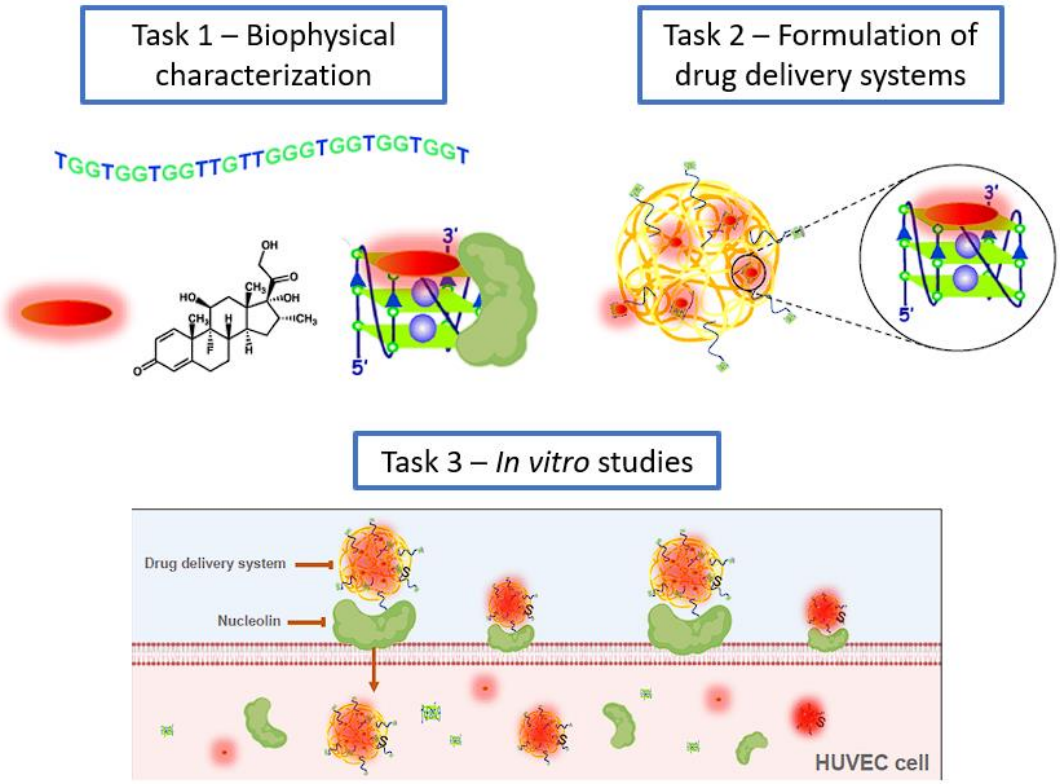

Figure 14 - Graphical abstract of the experimental work of this dissertation.

2. Aims of work

The main goal of this work is to develop NPs based on G4 aptamer, conjugated with dexamethasone and an acridine orange ligand, termed $C_{8,}$ as new intravitreal nanosystems for the targeting of NCL in retinal diseases, promoting the neoangiogenesis inhibition.

To achieve this main goal, the following objectives were defined:

1. To characterize AT11-L0 as G4 aptamer for the targeting of NCL;
2. To evaluate AT11-L0 interaction with NCL, dexamethasone, and C_8;
3. To develop NPs (AuNPs and liposomes) by conjugation with AT11-L0 and dexamethasone and C_8;
4. To structurally characterize the NPs;
5. To evaluate *in vitro* cell viability and angiogenesis inhibition of the formulated NPs in a HUVEC model.

3. Materials and Methods

In the following section there will be described all the reagents, equipment and techniques performed during this experimental work. This chapter will allow the reader to understand all the protocols used to achieve the results described later.

3.1 Materials and Reagents

The solutions used in this work have been prepared with ultrapure-grade water obtained from a Mili-Q system from Millipore (Burlington, MA, USA).

AT11-L0 (5′-TGGTGGTGGTTGTTGGGTGGTGGTGGT-3′) and ds26 (5'-CAATCGGATCGAATTCGATCCGATTG-3') were purchased from Eurogentec (Belgium) with HPLC-grade purification and a purity of 98%. Also, 5'-Cy5-TGGTGGTGGTTGTTGGGTGGTGGTGGT-3′, 5'-Thiol-TGGTGGTGGTTGTTGGGTGGTGGTGGT-3′, 5'-NH2-TGGTGGTGGTTGTTGGGTGGTGGTGGT-3′ and 5'-FAM-TGGTGGTGGTTGTTGGGTGGTGGTGGT-TAMRA-3' were obtained from the same company with the same purity. Stock solutions were prepared using Milli-Q water and stored at -20 ºC until use.

The concentration of the oligonucleotide samples has been determined by measuring the absorbance at 260 nm with a UV–Vis spectrophotometer (Thermo Scientific™ Evolution 220) using the molar extinction coefficient (ε) provided by the manufacturer.

Ligands PhenDC3 (3,3′-[1,10-phenanthroline-2,9-diylbis(carbonylimino)]bis[1-methylquinolinium] 1,1,1-trifluoromethanesulfonate; CAS: 929895-45-4; purity≥97), TMPyP4 (tetra-(N-methyl-4-pyridyl)porphyrin; CAS: 36951-72-1; purity≥90%), BRACO-19 (N,N′-(9-(4-(dimethylamino)phenylamino)acridine-3,6-diyl)bis(3-(pyrrolidin-1-yl)propanamide); CAS: 1177798-88-7; purity≥96%) and PDS 4-(2-Aminoethoxy)-N2,N6-bis[4-(2-aminoethoxy)-2-quinolinyl]-2,6-pyridinedicarboxamide; CAS: 1085412–37–8; purity≥98%) were acquired from Sigma Aldrich (St. Louis, MO, USA) and stocked on a 10 mM DMSO (Thermo Fisher Scientific, Waltham, MA, USA, CAS: 67-68-5, purity≥99,5%) solution. Synthesis and purification of the ligand C_8 (10-(8-(4-iodobenzamide)octyl))–3,6-bis(dimethylamine) acridinium iodide was performed as previously described [110].

D_2O (CAS: 7789-20-0, purity≥99.9%) was acquired from Eurisotop (France). Sucrose (CAS: 57-50-1, purity≥95%) was acquired from Fisher Scientific (Waltham, MA, USA).

Dexamethasone was acquired from Tokyo chemical industry (Japan, CAS: 50-02-2; purity≥99%) and a 10 mM DMSO stock solution was prepared (Thermo Fisher Scientific, Waltham, MA, USA, CAS: 67-68-5, purity≥99,5%).

Recombinant NCL RBD1,2 used in all experiments was synthesized and purified as reported previously [97,98].

Before each experiment, the oligonucleotide was annealed in 20 mM potassium phosphate buffer KPi containing 65 mM KCl (Labkem, Spain, CAS: 7447-40-7, purity≥99%) (annealing buffer) by heating 10 min at 95 ºC followed by an ice cooldown of 10 min. KPi (pH 6.9) was prepared using 1.945 g of KH_2PO_4 (Chemlab, Belgium, CAS: 7778-77-0, purity≥98%) and 0.990 g of K_2HPO_4 (Honeywell, USA, CAS: 7758-11-4, purity≥99%) until perform 1 L.

The lipids cholesterol (CAS: 57-88-5), 1,2-distearoyl-sn-glycero-3-phospho-(1'-rac-glycerol) (sodium salt) (PG) (CAS: 200880-42-8) and 1,2-distearoyl-sn-glycero-3-phosphoethanolamine-N-[carboxy(polyethylene glycol)-2000, NHS ester] (sodium salt) (DSPE-PEG) (CAS: 2410279-87-5) were acquired from Avanti Polar Lipids (Birmingham, AL, USA).

Chloroform (CAS: 67-66-3) was acquired from Fisher Scientific (Waltham, MA, USA). Ferric chloride hexahydrate (CAS: 10025-77-1) and ammonium thiocyanate (1762-95-4) were acquired from Acros Organics (Geel, Belgium). Centricons (MWCO=2000 Da) were acquired from Millipore (Burlington, MA, USA).

AuNPs with 5 nm diameter stabilized in a citrate buffer solution and tris-(2-carboxyethyl)-phosphine hydrochloride (TCEP) were acquired from Sigma Aldrich (St. Louis, MO, USA). D-tube Dialyzer Maxi (MWCO 3.5 kDa) was acquired from Millipore (Burlington, MA, USA).

Normal Primary Human Umbilical Vein Endothelial Cells (HUVEC) (PCS-100-010), Vascular Basal Cell Medium (PCS-100-030), and Endothelial Cell Growth Kit-VEGF (PCS-100-041) were acquired from ATCC (USA). 3-[4,5-dimethylthiazol-2-yl]-2,5 diphenyl tetrazolium bromide (MTT) was acquired from Thermo Fisher Scientific (Waltham, MA, USA, CAS: 298-93-1).

Angiogenesis Assay Kit (*In vitro*) (ab204726) was acquired from Abcam (Cambridge, UK).

3.2 Methods

3.2.1 Characterization of G4 structure from AT11-L0

3.2.1.1 NMR titration

The formation of the G4 in AT11-L0 was first proved by NMR spectroscopy. For that, a titration was performed with increasing concentrations of KCl starting at 0 mM to 65 mM. The intermediate concentrations used were 1, 5, 10, 20, 30 and 50 mM. These experiments were performed on an NMR 5 mm tube containing 600 µL of a 100 µM AT11-L0 solution containing 10% D2O/ 90% H2O. After the addition of each increasing amount of KCl and before the acquisition of each spectrum was done an annealing that consists of 10 min heating at 95 ºC followed by 10 min on ice. 1H NMR spectra were recorded on a Bruker Avance III 600 MHz spectrometer equipped with a QCI CryoProbe at 25 ºC using 256 scans. The NMR zgesgp pulse sequence was used to suppress the water signal.

3.2.1.2 CD titration

CD experiments were performed on a Jasco J-815 CD spectropolarimeter equipped with a Peltier-type temperature controller (model CDF-426S/15). Readings were achieved in a 1 mm path-length quartz cuvettes at 20ºC. Spectral width was set to 220–340 nm, with a scan speed of 200 nm/min, 1 nm bandwidth, and 1s integration time over 3 averaged accumulations. Before the CD spectra measurement, At11-L0 was annealed as described before. During KCl titrations, the required volume of solution from a 1 M stock was added directly to the quartz cell until reach the desired concentration. The concentrations of KCl used were the same that have been used on NMR titrations.

CD-melting

The most promising ligands were tested on CD-melting in order to determine the melting temperature of the G4 structure with and without ligand/drug. The parameters defined for the Jasco J-815 CD spectropolarimeter were the same as described above. AT11-L0 was annealed as previously described and the tested ligands have been added directly to the quartz cell to perform 0, 0.5, 1, and 2 molar equivalents from the 10 mM stock. The denaturation process was examined by monitoring the wavelength of maximum ellipticity (260 nm) through temperatures ranging from 20 to 100°C with a heating rate of 2°C/min. Data were converted into fraction folded (f) plots according to Eq. (1) and fitted to a Boltzmann distribution using OriginPro2021:

$$f = \frac{CD - CD_{\lambda}^{min}}{CD_{\lambda}^{max} - CD_{\lambda}^{min}} \qquad \text{Eq. (1)}$$

The melting temperatures (T_m) were determined from a two-state transition model where CD is the ellipticity at each temperature and CD^{min} and CD^{max} are the lowest and highest ellipticities, respectively. Data has been normalized and fitted to Boltzmann distribution using OriginPro2021. The melting temperatures have been calculated based on the corresponding temperature value to half of the total reached ellipticity.

3.2.1.3 Thermal difference spectra

UV-thermal difference spectra (TDS) were obtained for AT11-L0 dissolved in 65 mM of KCl and 20 mM KPi on a UV–Vis spectrophotometer (Thermo Scientific™ Evolution 220). TDS was carried out recording the absorbance spectrum from 220 to 320 nm at 95 ºC and 20 ºC. These temperatures correspond to the unfolded and folded states, respectively. TDS is the arithmetic difference between the absorbance at these two conditions. Data were normalized using OriginPro2021 and the parameters ΔA240nm/ΔA295nm, ΔA255nm/ΔA295nm, and ΔA275nm/ΔA295nm ratios were calculated to find out more information about the G4 structure [53].

3.2.1.4 FRET-melting

The ligands used in this assay were: Braco-19, PDS, PhenDC3, TMPYP4, C_8, and dexamethasone, an anti-inflammatory drug used in the treatment of retinal diseases. All these compounds were dissolved in DMSO at 10 mM concentration. FRET-melting experiments were performed in a 96-well plate, in duplicate, using a CFX Connect™ Real-Time PCR detection system (Bio-Rad, USA), equipped with a FAM filter (λex = 492 nm; λem = 516 nm). To each well it was added 20 µL of a solution containing 0.2 µM of AT11-L0 modified with FAM/TAMRA previously annealed on the annealing buffer. Then 5 µL of ligand was added at concentrations corresponding to 1, 2, 3 and 5 molar equivalents relatively to the aptamer concentration. The samples were warmed from 25ºC until 100ºC and the fluorescence was recorded during acquisition. Fluorescence output data were normalized and fitted to Boltzmann distribution using OriginPro2021. The melting temperatures were calculated based on the corresponding temperature value to half of the total reached fluorescence.

To check ligand specificity to AT11-L0 G4, 15 µL of a solution containing 0.2 µM of AT11-L0 modified with FAM/TAMRA previously annealed on the annealing buffer was added to each

well. Then 5 μL of a duplex competitor (ds26) was added at concentrations corresponding to 15 and 50 molar equivalents. Finally, 5 μL of ligand was added at a concentration corresponding to 3 molar equivalents. The samples were analysed and the data was treated as previously described. This assay was used to find information about the specificity of the ligand to the G4.

3.2.1.5 Fluorescence titrations

The most promising ligands (C_8, dexamethasone, and PhenDC3) were also tested using fluorescence titrations that have been conducted on a Horiba FluoroMax 4 fluorometer (Japan) equipped with a Peltier-type temperature control system, at 20 ºC. Samples were scanned using a high-precision quartz suprasil cuvette (light path 10 mm × 4 mm) with an optimal volume of 700 μL. Before performing the titrations 5'-Cy5-AT11-L0 has been annealed as described before on the work buffer. Solution of AT11-L0 has been prepared at a concentration of 1 μM. The excitation wavelength has been 647 nm, matching the maximum absorbance of Cy5 fluorophore. The fluorescence spectra have been acquired between 660–800 nm with an integration time of 0.5 s, an emission slit fixed at 1 nm, an excitation slit fixed at 2 nm and a step size of 1 nm, averaged over 3 scans. To assess the AT11-L0/ligand affinity, fluorescence titrations have been conducted, measuring the change in fluorescence after adding increasing concentrations of ligands (from 0 to 5 μM). After each addition, the solution has been left for 10 min for equilibration and then the spectrum has been acquired. The obtained data were converted into a fraction of bound ligand (α) plots using the following equation (Eq. 2):

$$\alpha = \frac{I - I_\lambda^{free}}{I_\lambda^{bound} - I_\lambda^{free}} \qquad \text{Eq. (2)}$$

where I is the fluorescence intensity at 667 nm at each AT11-L0/ligand ratio, and I_{free} and I_{bound} are the fluorescence intensity of the free and fully bound AT11-L0, respectively. Data points were then fitted according to the most suitable model (Two site bind, Michaelis Menten or Hill model) using Origin Pro 2021.

After that, we proceed using the same procedure to determine the affinity of AT11-L0 and AT11-L0/ligand complexes to NCL and VEGF. In the case of the AT11-L0 its concentration has been set as described before (1 μM) and increasing concentrations of the protein were added (from 0 to 800 nM). The spectra were acquired 10 min after each protein addition. In the case of the complex the concentration of the aptamer was also set to 1 μM. Then 1 equivalent of ligand were added to form AT11-L0/ligand complex. After 10 min of

equilibration, increasing concentrations of protein was added (from 0 to 800 nM). The spectra were recorded 10 min after each protein addition.

3.2.1.6 Native PAGE

Native PAGE was used to evaluate complex formation between G4 and ligands and to check AT11-L0 aptamer conformations. It was also used to verify if the complexes formed are depending on the buffer used.

Acrylamide gel was prepared with an acrylamide final concentration of 15 % and placed on an electrophoresis chamber containing a gel holder and filled with Tris/Borate/EDTA buffer (TBE). Before loading the samples, it has been performed a running of 20 min to clean gel wells. The samples containing 19 % of sucrose were then injected into the gel wells' and the electrophoresis ran for 1 h at 120 V.

The first experiment was made using two different concentrations of aptamer (2 μM and 4 μM) to see in which concentration of aptamer the bands could be better visualized. In this experiment, there have been also used two different ratios (1:1 and 1:15 AT11-L0/ligand). The ligands used were C_8 and dexamethasone to visualize if they could or not form a complex with the aptamer. Before mixing the aptamer with the ligands, the aptamer was annealed as previously described. Then, the influence of the C_8 concentration was evaluated using different ratios (1:1, 1:2; 1:5, 1:10, 1:15, 2:1) of AT11-L0/C_8 on water and on buffer.

3.2.2 Synthesis and characterization of nanoparticles

3.2.2.1 Synthesis of AuNPs functionalized with AT11-L0 and ligands

AuNPs were acquired from Sigma-Aldrich and then functionalized as described in Malik *et al.* [113] based on the original protocol of Mirkin *et al.* [114].

Thiolated aptamer AT11-L0 was first reduced by incubating with a filtrated solution of 10 mM TCEP for 6 h at room temperature on a hula mixer. The reduced aptamer was then incubated with 5 nm colloidal AuNPs in a ratio of 200 aptamer chains to each AuNP. The mixture was incubated in the hula mixer overnight. After this step, it has been made a "salting in" process with the addition of 20 mM of KPi to reach a final concentration of 10 mM. 4 h later it was added a 3 M NaCl solution to reach a final concentration of 100 mM. To finish, after four hours, a 3 M NaCl solution was added again to reach a final concentration of 300 mM. Both KPi and NaCl solutions were filtrated before being added

to the AuNP-aptamer mixture. The mixture was left on the hula mixer between each salt addition. After the last salt addition, the mixture was left rotating overnight.

AuNP solution was lyophilized on a ScanVac Coolsafe freeze dryer (Labogene, Denmark) and resuspended on 2-3 mL of milli-Q water. The sample was then inserted in a D-tube Dialyzer Maxi (MWCO 3.5 kDa). To remove the salts of the solution of aptamer functionalized NPs the D-tube was inserted into Milli-Q water to perform dialysis for 48 hours. Milli-Q water was changed two times a day. Finally, the sample was recovered, lyophilized again, and resuspended on 50 μL of working buffer to determine the concentration of the aptamer in the solution by UV–Vis spectrophotometry.

Functionalized NPs were mixed with C_8 and dexamethasone. C_8 was mixed with the AuNP's solution in a molar ratio of 1 M of C_8 for 15 M of DNA. Dexamethasone was mixed with the AuNP's solution in a molar ratio of 4 M of dexamethasone for 15 M of DNA. AuNPs were stocked at 4 ºC until further use.

3.2.2.2 Synthesis of liposomes functionalized with AT11-L0 and ligands

Liposomes were made using the thin film hydration method using three different lipids: Cholesterol, PG, and DSPE-PEG. To start the liposomes' synthesis, lipid solutions were dissolved on chloroform and mixed in a molar ratio of 2:1:0.16 – PG:Cholesterol:DSPE-PEG [115] on a 2 mL previously weighted eppendorf that was left opened overnight to evaporate the chloroform. When the chloroform was fully evaporated a lipid thin film were observed on the bottom of the eppendorf, which was weighted again to calculate the lipid mass. Then lipids were resuspended on a PBS solution containing C_8 or dexamethasone. The volume of solution added was calculated as function of the mass of lipids thin film to achieve a final lipid concentration of 1 mg/mL. C_8 was added to PBS to perform a mass ratio of 0.025 mg for each g of lipids and 0.1 mg of dexamethasone for each g of lipids. To homogenize the size and the lamellarity of the formed liposomes we performed 5 cycles of "freeze and thaw". The mix was then extruded using an Avanti mini-Extruder (Avanti Polar Lipids, Birmingham, AL, USA) containing a polycarbonate membrane. Then, samples were washed with water on a centricon centrifugal filter unit (MWCO=2000 Da) four times at 200 RCF for 40 min. Finally, samples were incubated with the aptamer with an amino modification in a DNA:liposome mass ratio of 1:10 to functionalize the liposomes with the aptamer. After that, samples were washed again as previously described and stocked at 4 ºC until use.

3.2.2.3 Structural characterization of NPs

AuNP's were characterized using two different techniques. The first one was DLS to give us information about the size and the polydispersity of the sample. For this technique after determining the concentration of the aptamer in the solution by UV–Vis spectrophotometry, it was made a dilution of the sample to obtain a 1 mL solution with a concentration of 10 μM. This solution was then measured on a disposable 1-cm beam plastic cell using Zetasizer Nano ZS equipment (Malvern Instruments, UK) and the Malvern Zetasizer software v6.34. Briefly, the average size and the polydispersity dispersion index (PDI) were obtained by analysing 1 mL of sample 3 times at 25 ºC. The second technique was TEM which gives information about the size and morphology of AuNP's. To perform this technique, 20 μL of sample at 10 μM was put on a circular coverslip at room temperature and let dry overnight in a place protected from direct sunlight. The coverslips containing the dried samples were fixed in a metallic sample holder with two-sided tape. The sample holder was inserted into the anode stage of an Emitech K550 (London, UK) sputter coater. The coater was vacuum closed, and the samples were carbon coated for 1.5 min. Samples were observed using a Hitachi S-2700 (Tokyo, Japan) scanning electron microscope, with an accelerating voltage of 20 kV using various magnifications until reach a clear image of AuNPs.

Liposomes were also characterized by DLS to give information about the size and the polydispersity of the sample. 1 mL of the liposome's solution at the concentration obtained by the synthesis process was directly inserted into a disposable 1-cm beam plastic cell using a Zetasizer Nano ZS equipment (Malvern Instruments, UK) and the Malvern Zetasizer software v6.34. Each sample was measured 3 times at 25 ºC.

SEM was also used to confirm size and morphology of liposomes. To perform this technique, 20 μL of the sample at the concentration obtained in the synthesis process was put on a circular coverslip at room temperature and let dry overnight in a place protected from direct sunlight. The coverslips containing the dried samples were fixed in a metallic sample holder with two-sided tape. The sample holder was inserted into the anode stage of an Emitech K550 (London, UK) sputter coater. The coater was vacuum closed, and the samples were gold coated for 1.5 min. Samples were observed using a Hitachi S-2700 (Tokyo, Japan) scanning electron microscope, with an accelerating voltage of 20 kV using various magnifications until reach a good image of liposomes.

To quantify the number of liposomes formed and their size it was employed the Nanoparticle Tracking Analysis (NTA) technique which uses the properties of both light scattering and Brownian motion to obtain the NPs size distribution of samples in liquid

suspension. 300 μL of sample was loaded into a sample chamber of Malvern NanoSight NS300 (Malvern Instruments, UK) after diluting it 100 times from the concentration obtained by the synthesis process. The acquisition was run at 25 frames per second until performing 749 frames using NTA 3.2 Dev Build 3.2.16 at 22.6 ºC.

For assuring that the aptamer was bound to liposomes, NMR spectra of liposomes conjugated with the aptamer and loaded with C_8 was acquired. It was also acquired a spectrum of liposomes without the aptamer. Spectrum of both samples were compared to find out if the aptamer was bound to liposomes. For acquiring spectra, liposomes were mixed with 10% D2O/90% H_2O to perform 180 μL on a 3 mm NMR tube. Standard 1H NMR spectra were recorded on a Bruker Avance III 600 MHz spectrometer equipped with a QCI CryoProbe at 25 ºC. The NMR zgesgp pulse sequence was used to suppress the water signal.

The association of C_8 and dexamethasone on liposomes was evaluated using UV–Vis spectrophotometry. For that, it was made a calibration curve using the compounds at the concentrations of 15, 20 ,25, and 30 μM for C_8 and of 25, 50, 75 and 100 μM for dexamethasone. Absorbances were recorded on a 1×1 cm suprasil quartz cell using 1 mL of the solutions at the concentrations reported. Measurements were performed using a UV–Vis spectrophotometer (Thermo Scientific™ Evolution 220). C_8 and dexamethasone have a maximum at 496 nm and 242 nm, respectively. After the determination of the calibration curves, 1 mL of liposome solutions were measured at the reported wavelengths to calculate the concentration of the compounds in the samples.

This technique was also used to evaluate the presence of aptamer (260 nm) and cholesterol (206 nm). For that the UV spectra of 1 mL of liposome sample was measured between 200 and 400 nm to see if bands at 206 and 260 nm were present. This experiment was also performed on a UV–Vis spectrophotometer (Thermo Scientific™ Evolution 220) using a 1×1 cm suprasil quartz cell.

Finally, it was made the quantification of DSPE-PEG using the Stewart method [81]. It was chosen this lipid since this technique is adequate for phospholipids. For that, we prepared a solution of ammonium ferrothiocyanate by dissolving 27.03 g of ferric chloride hexahydrate and 30.4 g of ammonium thiocyanate in milli-Q water until perform 1 L. Then a calibration line was made using different concentrations of DSPE-PEG. The first step was to prepare a 0.1 mg/mL DSPE-PEG solution on chloroform. Then we made solutions mixing 100, 200, 400, 600, and 800 μL of this stock solution with 2.0 mL of ammonium ferrothiocyanate and chloroform until perform 4 mL. This solution was then vortexed and after 15-20 min the lower phase was measured using UV–Vis spectrophotometry at 502 nm. Absorbances were plotted vs the lipid mass. 20 μL of the liposome samples were diluted

(100×) on phosphate buffer. 200 μL of this dilution was mixed with 1.8 mL of chloroform and 2 mL of ammonium ferrothiocyanate. After that, absorbance was measured at 502 nm and the mass of lipid was calculated using an calibration curve.

3.2.3 *In vitro* assays

3.2.3.1 Cell line

In vitro studies were performed with HUVEC (PCS-100-010) acquired from ATCC (USA). They are adherent cells that may proliferate in a Vascular Basal Cell Medium (ATCC, PCS-100-030, USA) where it can be added or not VEGF. The addition of VEGF allows a faster proliferation rate that simulates what occurs in retinal diseases. This cell line presents a high mitotic index. Cells have a cobblestone appearance with large dark nuclei. However, during proliferation cells are small and evenly sized. HUVEC cell line was chosen because it is the typical model used for evaluating the anti-angiogenic effects of any substance. This evaluation can be performed since HUVEC after the addition of an adequate extracellular matrix form tubes that simulate what happens in angiogenesis processes [58,103].

3.2.3.2 MTT assay

MTT assay was used to evaluate the cellular viability when exposed to the tested NPs. For these assays, HUVEC were harvested when reaching 80-90% confluency and seeded on 96-wells using 100 μL of Vascular Basal Cell Medium supplemented with an Endothelial Cell Growth Kit-VEGF from ATCC at a density of 5×10^3 cells per well. After 24 h the medium was removed, and it was added new medium containing the formulations of NPs that we wanted to evaluate at distinct concentration (0.01, 0.05, 0.1, and 0.25 μM of C_8 loaded liposomes, and 10 μM of dexamethasone loaded liposomes). After 72 h, the medium was removed and 100 μL of a 3-[4,5-dimethylthiazol-2-yl]-2,5 diphenyl tetrazolium bromide (MTT) solution was added at a concentration of 1 mg/mL. After 4 h, MTT was removed and the insoluble formazan crystals were completely dissolved on DMSO. Finally, absorbance was read on a plate reader (Bio-rad xMark spectrophotometer from Bio-rad, USA) at 570 nm.

3.2.3.3 Angiogenesis assay

The anti-angiogenic properties of the tested compounds/formulations were tested using an Angiogenesis Assay Kit (*In vitro*) acquired from Abcam, according to the manufacturer's

guidelines. Briefly, HUVEC were harvested when reaching 80-90% confluency and seeded on 96-wells using 50 µL of extracellular matrix provided with the kit at a density of 5×10^3 cells per well. Negative controls were seeded without this matrix. The compounds/formulations were added at the desired concentrations (10 µM of dexamethasone and dexamethasone loaded liposomes, and 0.05 µM of C_8 and C_8 loaded liposomes), and suramin was added to another negative control. Cells were incubated with the compounds/formulations for 18 h. Then they were incubated with the staining dye provided at the kit, for 30 min, after being carefully washed and finally observed on a microscope using light and fluorescence. Results were analyzed using ImageJ software.

3.2.3.4 Statistical analysis

Data from assays comprising more than one sample were presented as mean ± standard error (SE) of at least three independent experiments. Statistical significance of the studies was evaluated by using one-way ANOVA and p-values ≤ 0.05 were considered as significant. All data were analyzed using GraphPad Prism version 8.0, GraphPad Software, La Jolla California USA.

4. Results and discussion

In this chapter the data obtained will be presented and forwardly discussed.

The results will be presented in a logical sequence that allows the reader to understand the sequence of experiments that were made. These results will be used to take conclusions about the potential of NPs containing AT11-L0/ligand complexes to inhibit angiogenesis in neovascular diseases.

4.1 Characterization of G4 structure from AT11-L0

4.1.1 NMR titration

NMR titration of AT11-L0 was performed with increasing concentrations of KCl at a fixed temperature of 20 ºC to check cation (K^+) effect on the G4 formation. The spectra of the titration are shown in Figure 15.

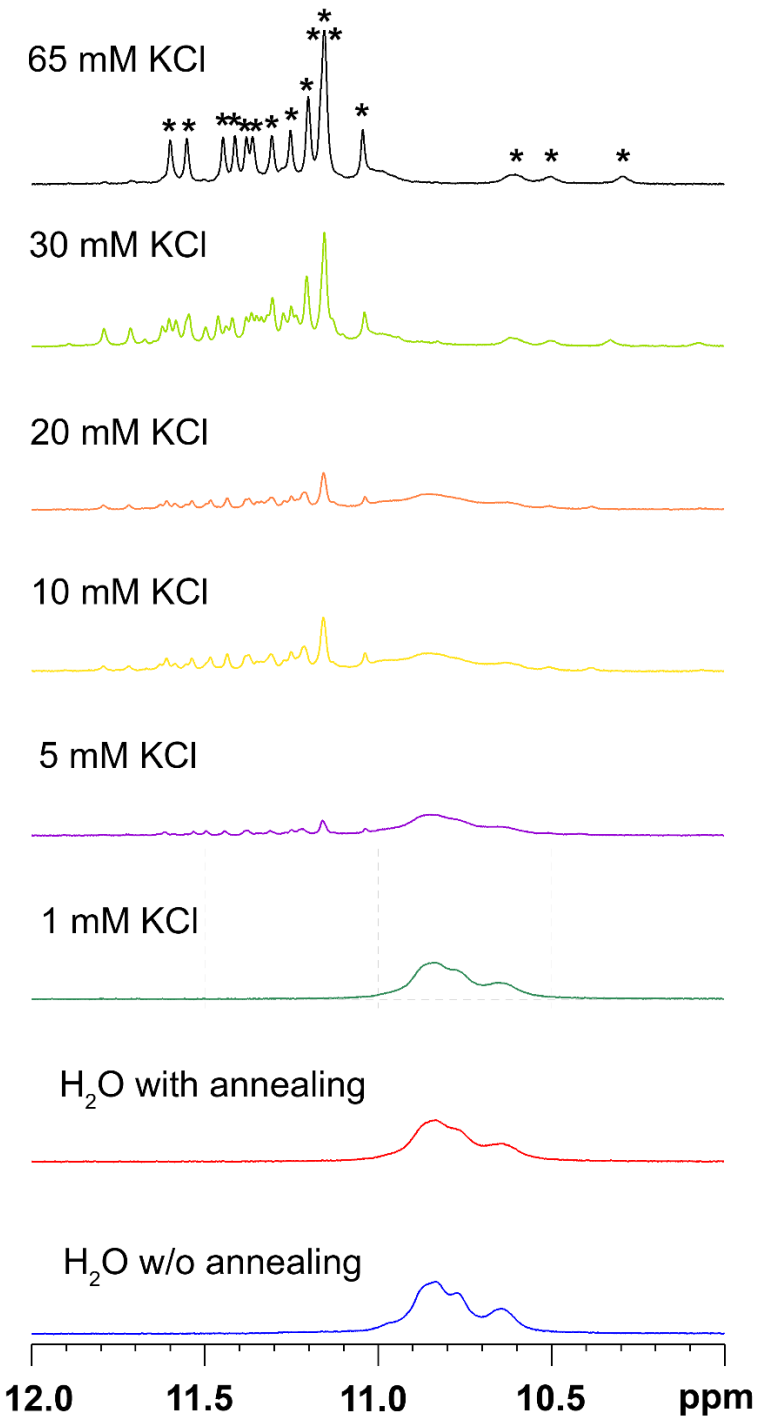

Figure 15 – NMR titration of AT11-Lo with KCl (concentrations from 0 to 65 mM). Signals from imino protons of AT11-Lo are indicated with asterisks (∗) in the 65 mM spectrum.

The NMR spectra in water showed a signal near 11 ppm. This signal is typical of the G4 structure (10 -12 ppm) being originated by the imino proton resonances characteristic of Hoogsteen hydrogen bound. However, this signal is broad with no well-defined peaks. It may indicate that in water without the addition of KCl, AT11-Lo form an unstable G4 structure.

With the increase of KCl concentration to 10 mM in the AT11-L0 solution, the signals start to be more well-defined. These signals are more evident for concentrations above 30 mM. As we can observe on the 65 mM spectra, there are 16 peaks corresponding to the imino protons forming the Hoogsteen bounds of the G-tetrads in the G4 structure. The spectra suggest a single G4 conformation, and the signals with low intensity can be indicative of minor G4 conformations. AT11-L0 is a derivative of AT11 by eliminating a thymine residue in the linker. This modification in the linker is not expected to affect the overall conformation of the G-tetrads, as indicated by the similarity of the 1 H NMR imino region to the one reported by Phan *et al.* [116].These results confirm that the formed G4 structure is composed of two subunits of two G-tetrads each, as previously reported by Carvalho *et al.* [58].

4.1.2 CD titration

CD titration of AT11-L0 was performed by adding increasing concentrations of KCl between 0 and 65 mM to confirm the results of NMR titration and to characterize topology. The spectra obtained are presented in Figure 16.

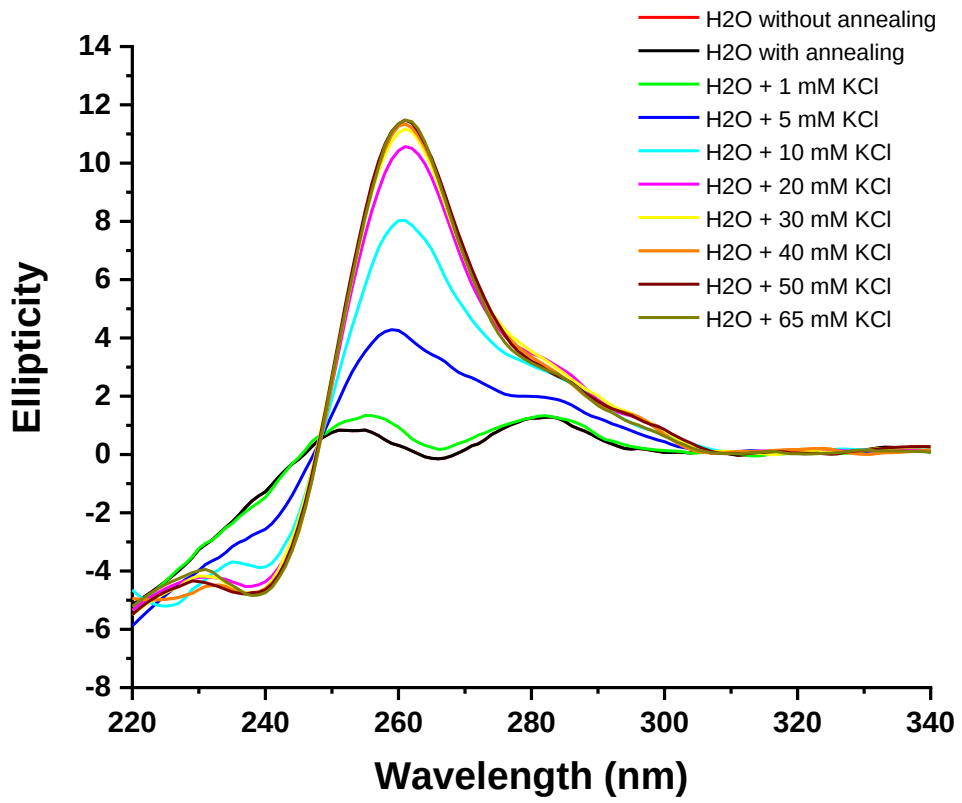

Figure 16 - CD spectra of AT11-L0 with concentrations of KCl from 0 mM to 65 mM.

The spectra presented in Figure 16 showed a typical parallel G4 structure characterized by a positive peak at 260 nm and a negative one at 240 nm, which are more evident with increasing KCl salt concentrations. However, at low concentrations of KCl (0 to 5 mM) the spectra have a peak at about 295 nm (this peak is also present at higher concentrations despite being less evident). This peak may result from the contribution of other conformations, namely anti-parallel G4 structure, or even from the contribution of other contaminating cations (Na^+ for example) resulting from the synthesis of the AT11-L0 that may induce other structures.

We may also observe in the spectra that ellipticity increases with increasing KCl concentrations. This behaviour suggests a dependence on K^+ for the G4 structure stabilization. However, increases in the ellipticity are not perceived at concentrations higher than 30 mM. These data corroborate what we found on NMR, showing that at 30 nM AT11-L0 forms a well-defined G4 structure with a parallel topology. According to the results, a concentration of 65 mM was used for further studies since it is the concentration that shows the most well-defined peaks at NMR and a typical parallel topology CD spectrum. We conclude that this concentration promotes the formation of a G4 structure with one well-defined structure. The use of this concentration was also reported by Carvalho *et al.* [58] allowing the comparison with the obtained results.

4.1.3 Thermal difference spectra

TDS spectrum was acquired to check G4 formation and topology.

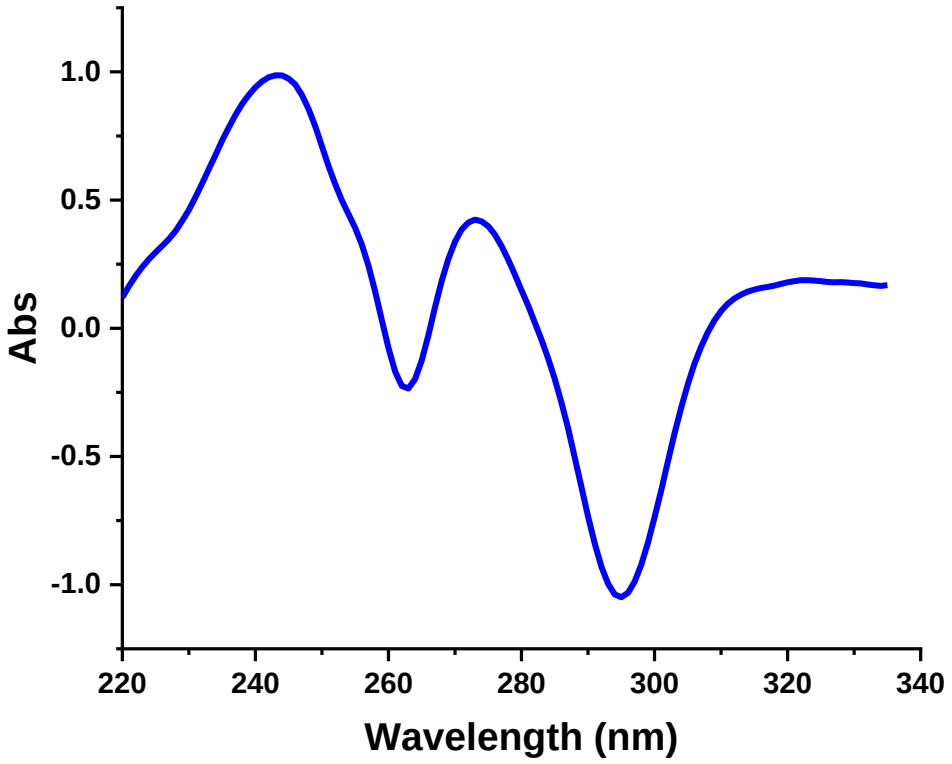

Figure 17 - Thermal difference spectra of AT11-Lo. This spectrum was obtained from the difference between the absorbance recorded at high temperature and that recorded at low temperature under the same conditions.

TDS shown in Figure 17 has the typical signature of a G4 structure with a negative band at 295 nm and two positive bands at about 295 nm and 275 nm. The parameters ΔA240nm/ΔA295nm, ΔA255nm/ΔA295nm, and ΔA275nm/ΔA295nm ratios have been calculated and are shown in Table 2.

Table 2 - TDS ratios

Parameter	**$\Delta A_{240}/\Delta A_{295}$**	**$\Delta A_{255}/\Delta A_{295}$**	**$\Delta A_{275}/\Delta A_{295}$**
Ratio	0.896	0.373	0.379

The data presented in Table 2 are supported by the formation of anti-parallel G4 since ΔA240/ ΔA295 are lower than 2, ΔA255/ ΔA295 is lower than 1.5 and ΔA275/ ΔA295 is lower than 2. These results contradict the information obtained by CD. However, as previously discussed concerning the results of CD spectra, G4 solution could present a small contribution of anti-parallel species or a contamination of other cations like Na^+ that could favour other topologies, which may explain the differences between CD and TDS spectra.

4.2 Interaction AT11-L0 G4 with ligands

4.2.1 FRET-melting assay

FRET-melting assay was performed to select the ligands that could stabilize the G4 structure in AT11-L0. The ligands chosen were PhenDC3, Braco-19, TMPyP4 and PDS since they are commercially available stabilizers of G4 structures. In addition to these, it was also studied C_8, an acridine derivative and a stabilizer of G4 structures with some anti-tumoral properties, as previously described, and dexamethasone, a costicosteroid already used in the treatment of retinal diseases.

This assay was performed with a concentration of 0.2 μM of aptamer and with different concentrations of ligands (0.2, 0.4, 0.6, and 1.0 μM) in duplicate. The T_m for each condition was calculated, and its variation is presented in Figure 18.

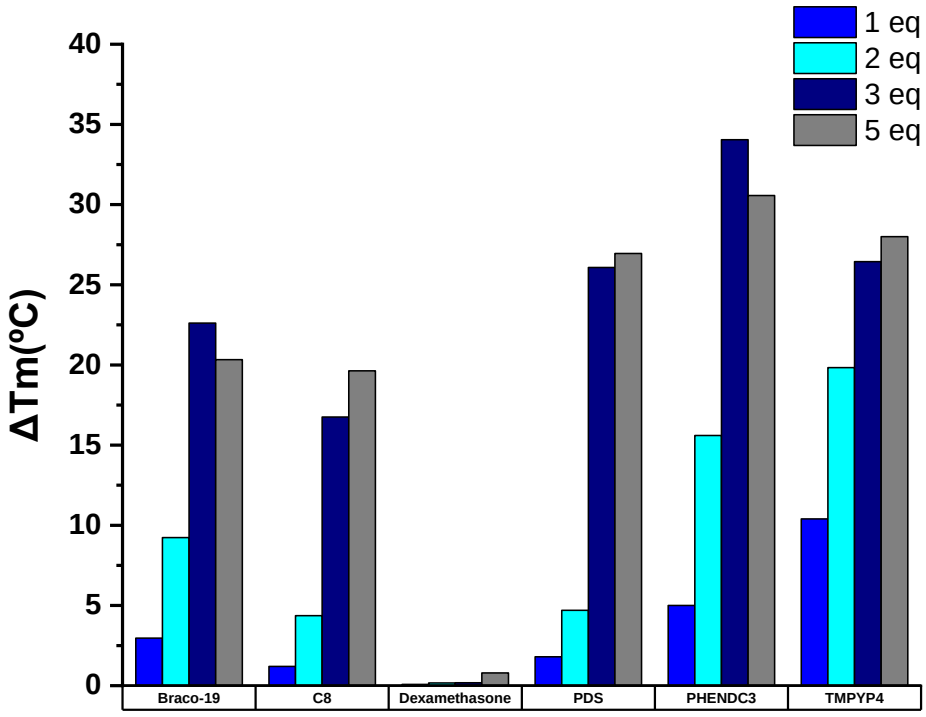

Figure 18- Variation of the melting temperature of AT11-L0 with ligands Braco-19, C_8, dexamethasone, PDS, PhenDC3 and TMPyP4 at 0.2, 0.4, 0.6 and 1.0 μM.

The T_m of AT11-L0 G4 obtained by FRET-melting assay on 65 mM KCl was 48.1 ºC. All the ligands can stabilize the G4 structure of AT11-L0, except dexamethasone which does not

stabilise the G4. Almost all ligands present a dose-dependent response since the increase in their concentration increases the T_m of the G4 structure. As expected, commercial ligands present higher T_m. At 1 molar equivalent the ligand that promotes the highest T_m is TMPyP4 with a T_m of 58.5 ºC. PhenDC3, Braco-19, PDS and C_8 also present a high T_m of 53.1, 51.1, 49.9, and 49.3 ºC respectively. Dexamethasone presents the lowest T_m (48.2 ºC). However, at 5 molar equivalents, PhenDC3 is the ligand that promotes the highest T_m (78.7 ºC). TMPyP4, PDS, BRACO-19 and C_8 present a T_m of 76.1, 75.1, 68.4 and 67.7 ºC. At these conditions, dexamethasone continues to present the lowest T_m (48.9 ºC).

In addition, a competition assay was conducted with the self-complementary DNA sequence ds26 in order to evaluate the specificity of the ligands towards G4 AT11-L0 over duplex DNA (Figure 19). Competition melting studies have been used before to assess whether 3 equivalents of ligands can bind preferentially to G4 structures compared to duplex DNA. The concentrations of DNA sequence ds26 used were 3 μM and 10 μM.

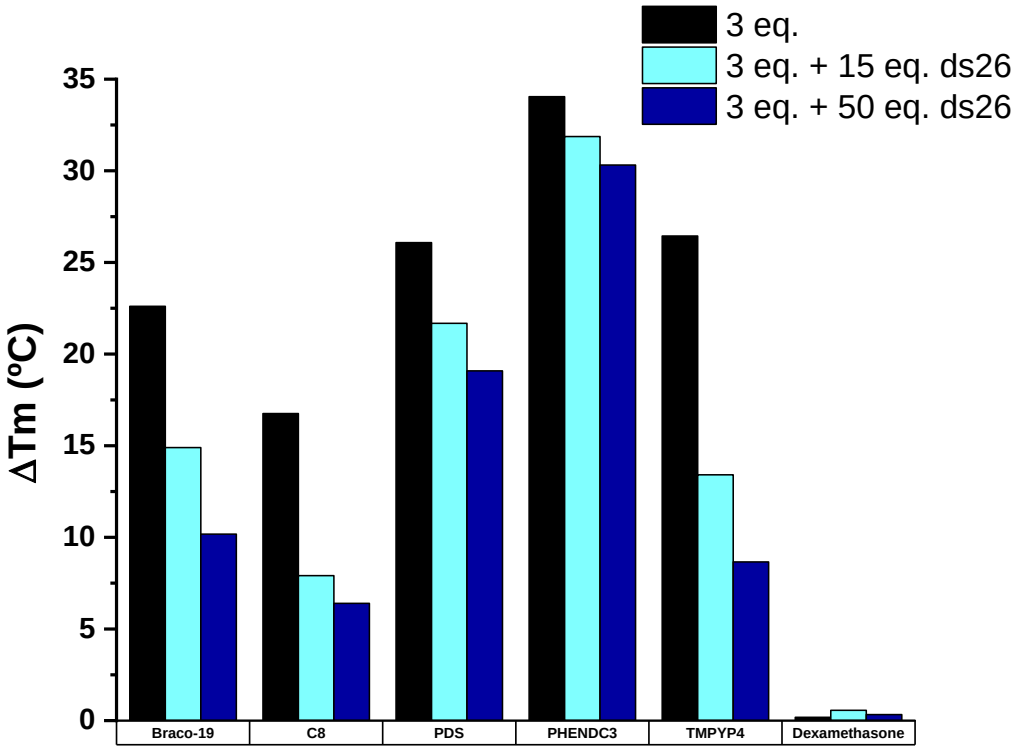

Figure 19 - Variation of melting temperatures of AT11-L0 in the presence of 3 molar equivalent of ligands and a duplex competitor (ds26) at 3 and 10 μM.

Dexamethasone results of the competition assay are not relevant since this drug did not promote a thermal stabilization of the AT11-L0 G4 structure. However, for the remaining ligands, it was calculated the S factor that corresponds to the ratio between ΔT_m obtained in the presence and absence of ds26 [117]. This S factor gives information about the selectivity that ligands have for the G4 structure.

Table 3- Selectivity factor of BRACO-19, C8, PDS, PhenDC3, and TMPyP4 for AT11-L0 G4 in the presence of 15 and 50 molar equivalents of ds26.

	S factor	
Ligand	15 molar eq. ds26	50 molar eq. ds26
BRACO-19	0,66	0,45
C_8	0,47	0,38
PDS	0,83	0,73
PhenDC3	0,94	0,89
TMPyP4	0,51	0,33

Ligands with S factors near 1 are more selective for AT11-L0 G4 whereas the ones with S factors near 0 are less selective. Thermal stabilization induced by PhenDC3 is not strongly affected by ds26 competitor since S value is 0.89 for 50 molar equivalents. The presence of the competitor has strongly affected TMPyP4, C_8 and Braco-19 thermal stabilization of AT11-L0 G4 since they present low S values (0.33, 0.38, and 0.45, respectively for 50 molar equivalents). PDS thermal stabilization was also affected by the presence of the competitor as its S factor is 0.73 for 50 molar equivalents.

With these data, we conclude that PhenDC3 is the more stabilizing and the more selective ligand for AT11-L0 G4.

4.2.2 CD-melting

To have more precise data about the real ΔT_m and the grade of stabilization of the G4 structure for each ligand, CD-melting assays were performed with ligands C_8, dexamethasone and PhenDC3. The obtained melting curves are shown in Figure 20. In FRET-melting assays, a modified sequence of the AT11-L0 aptamer containing FAM and TAMRA is used, so the interaction of the ligand with the aptamer may suffer some differences from what occurs with the non-modified sequence. These differences may occur

resulting from an abnormal stacking of the aromatic portion of the ligand in the G-tetrads caused by the increased occupied volume from FAM and TAMRA.

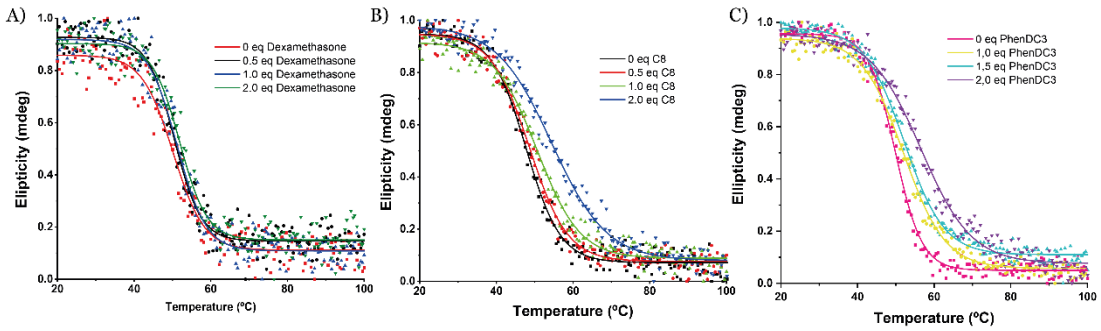

Figure 20- CD-melting curves from 0 to 2 molar equivalents of A) dexamethasone; B) C_8; C) PhenDC3.

The T_m obtained by CD-melting of AT11-L0 G4 49.3 °C. This value agrees with the value obtained by FRET-melting assay.

Upon the addition of dexamethasone, all the curves are almost overlapped showing there is no stabilization of G4. In fact, for 2 molar equivalents of dexamethasone, the ΔT_m of AT11-L0 G4 is 1.71°C, showing that dexamethasone doesn't promote a thermal stabilization of the G4 structure. However, C_8 and PhenDC3 promote a ligand-induced thermal stabilization of the structure in a concentration-dependent manner. For 2 molar equivalents, C_8 and PhenDC3 present similar thermal stabilizations (6.68 and 6.67 °C, respectively).

Table 4 – T_m of AT11-L0 with C_8, dexamethasone, and PhenDC3 at different concentrations.

Ligand	Dexamethasone			C_8			PhenDC3		
Concentration (molar equivalents)	0.5	1.0	2.0	0.5	1.0	2.0	0.5	1.0	2.0
ΔT_m (°C)	0.32	1.03	1.71	0.91	2.91	6.68	2.15	2.27	6.67

The results of dexamethasone are coherent with FRET-melting results. We prove that dexamethasone is not capable of promoting thermal stabilization on the G4 structure of AT11-L0, as expected. C_8 and PhenDC3 have similar melting stabilization on the AT11-L0 G4. These results agree with FRET-melting assay results. However, the increase in the T_m value is not as evident as FRET-melting assay suggested. As discussed before, it may be explained because of the interference of the fluorophores with the ligand's stacking on the

tetrads. Regarding these results, we can assume that C_8 is the most promising ligand since it promoted the highest thermal stabilization on the AT11-Lo G4 structure.

4.2.3 Fluorescence titrations

We further determined the apparent equilibrium constants (K_D) of C_8, dexamethasone, and PhenDc3 via fluorometric titrations. Upon adding the ligands to the pre-folded 5´Cy5-AT11-Lo a decrease in the intensity was observed.

Spectra were acquired between 660-800 nm and K_D was determined by plotting the maximum fluorescence intensity recorded at 667 nm.

Figure 21 shows the fluorescence titrations between the AT11-Lo G4 C_8, dexamethasone, and PhenDC3.

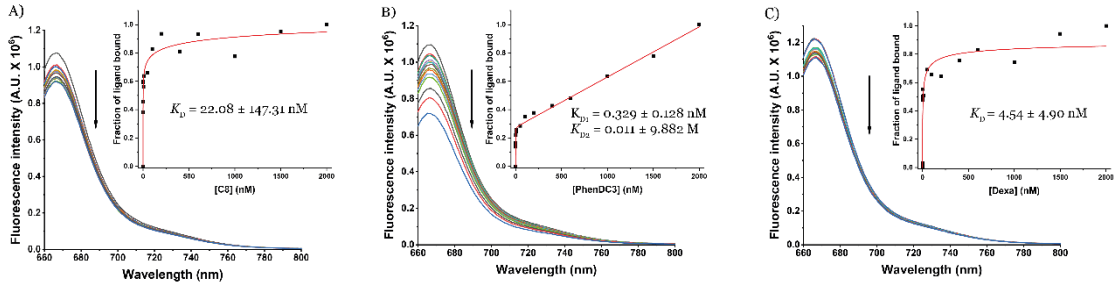

Figure 21 - Fluorescence intensity spectra and K_D determination of AT11-Lo titrated with A) C_8; B) PhenDC3; C) dexamethasone.

Titrations were performed until reaching 2 molar equivalents of each ligand, similar to the CD titrations. PhenDC3 has a behaviour different from C_8 and dexamethasone since fit had to be done differently (Two-site binding model for PhenDC3 and Hill saturation binding model for C_8 and dexamethasone). The relative enhancement of the fluorescence intensity upon titration with 5 equivalents of PhenDc3 didn't stabilize and the K_D values are K_{D1} = 0.329 ± 0.128 nM and K_{D2} = 0.011 ± 9.9882 M. The K_{D1} is low (in the nanomolar range) and indicates that PhenDC3 has a high affinity to the aptamer as expected since PhenDC3 is a commercial G4 ligand. However, K_{D2} is high (in the mM range) indicating that in higher concentrations of PhenDC3 it loses its affinity to the G4 structure. Since it is a commercial G4 ligand it was not expected that it loses its affinity. This result can be explained because only a small concentration of PhenDC3 is necessary to interacting with all the binding sites available in the G4 structure due to its higher affinity. After that, excess of PhenDC3 concentration promote a saturation of the plot indicating that the second K_D may not be considered.

C_8 and dexamethasone also showed K_D in the nanomolar range. These values were obtained using the Hill model. Both ligands have an affinity to the aptamer despite dexamethasone didn't stabilize it. It is interesting to see that Carvalho *et al.* found a K_D for C_8 that was slightly lower (10^{-7} M order) [58]. However, these experiments were performed following the C_8 fluorescence instead of the aptamer-labelled fluorescence. These differences can be explained by π–π stacking interactions of C_8 in the G4 structure that may quench some fluorescence. When using a labelled aptamer, the interaction of the ligand with the aptamer may suffer some differences from what occurs with the non-modified sequence. These differences may occur resulting from an abnormal stacking of the aromatic portion of the ligand in the G-tetrads caused by the fluorophore.

Regarding the high affinities of the G4 structure to PhenDC3 and C_8 it was necessary to evaluate if they did not affect the normal interaction of the G4 structure with proteins. Therefore, we determined the apparent equilibrium constants (K_D) AT11-L0 G4/ligand complexes via fluorometric titrations. Upon adding NCL to the pre-folded 5´Cy5-AT11-L0 a decrease in the intensity was observed. Figure 22 shows the fluorescence titration studies between the AT11-L0 G4/ligand complexes 1:1 ratio with NCL.

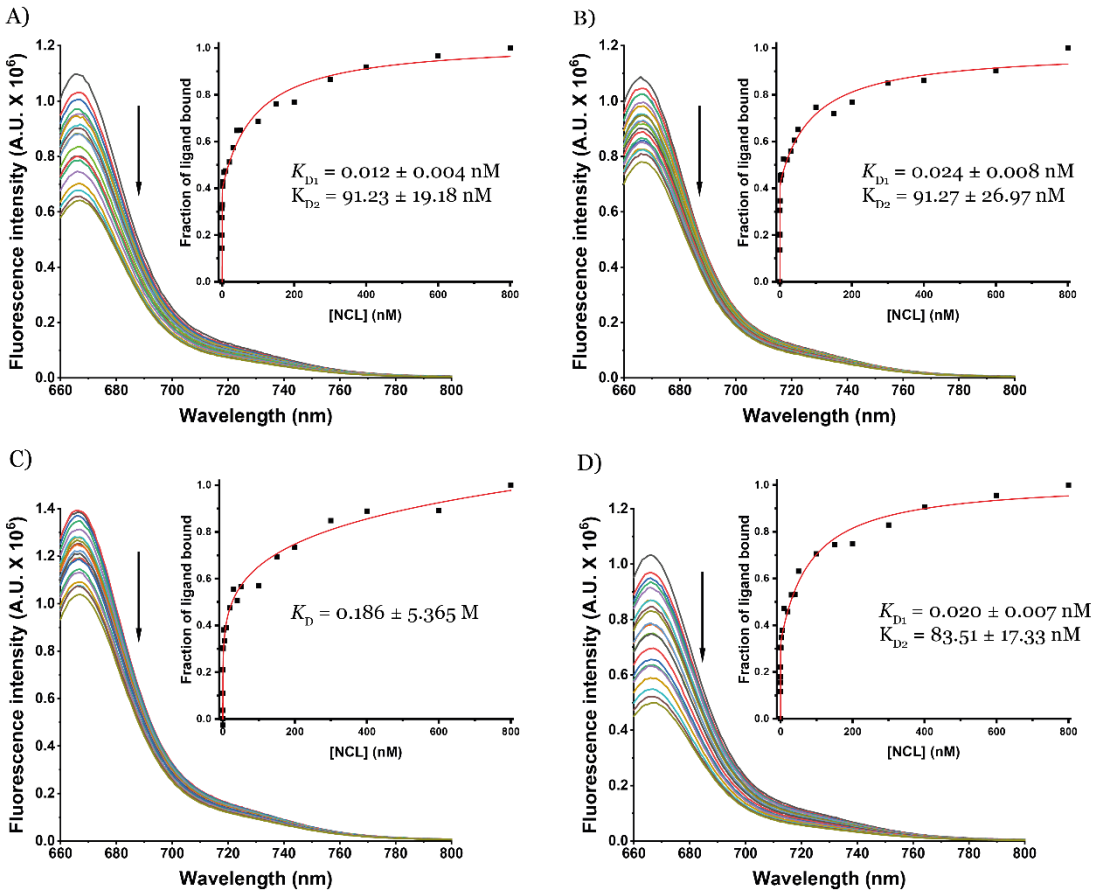

Figure 22 - Fluorescence intensity spectra and K_D of A) AT11-Lo G4 and of AT11-Lo G4 complexed with B) C_8; C) dexamethasone and D) PhenDC3 titrated with NCL.

The fluorometric data of NCL and AT11-Lo G4, NCL and AT11-Lo G4/C_8, NCL and AT11-Lo G4/PhenDC3 was fitted using the two-site binding model. The fluorometric data of NCL and AT11-Lo G4/dexamethasone was fitted using the Hill model. The K_D values of AT11-Lo G4/PhenDC3 and AT11-Lo G4/C_8 with NCL remaining in the nM range, suggesting high complex formation and PhenDC3 and C_8 did not affect the recognition of NCL by AT11-Lo G4. The nanomolar range obtained for the K_D agrees with the ones found in the literature [58]. The two K_D values obtained for NCL and AT11-Lo G4, NCL and AT11-Lo G4/C_8, NCL and AT11-Lo G4/PhenDC3 can indicate that AT11-Lo G4 interacts with two domains of NCL [118]. However, only one K_D was determined between NCL and AT11-Lo G4/dexamethasone. This K_D is in the mM range suggesting low affinity and maybe the AT11-Lo G4/dexamethasone complex is unable to recognise NCL. Therefore, dexamethasone was used for further assays as an isolated therapeutic molecule instead of a AT11-Lo/G4/dexamethasone complex.

Regarding the importance of VEGF on retinal diseases and on NCL migration to the cell surface we evaluated AT11-Lo G4 and AT11-Lo G4/ligand affinity to VEGF. Upon adding VEGF to the pre-folded 5´Cy5-AT11-Lo, a decrease in the intensity was observed. Figure 23

shows the fluorescence titration studies between the AT11-Lo/ligand complexes 1:1 ratio when titrated with VEGF. This experiment will allow us to see if AT11-Lo G4 has also an affinity to this protein which is overexpressed in retinal diseases.

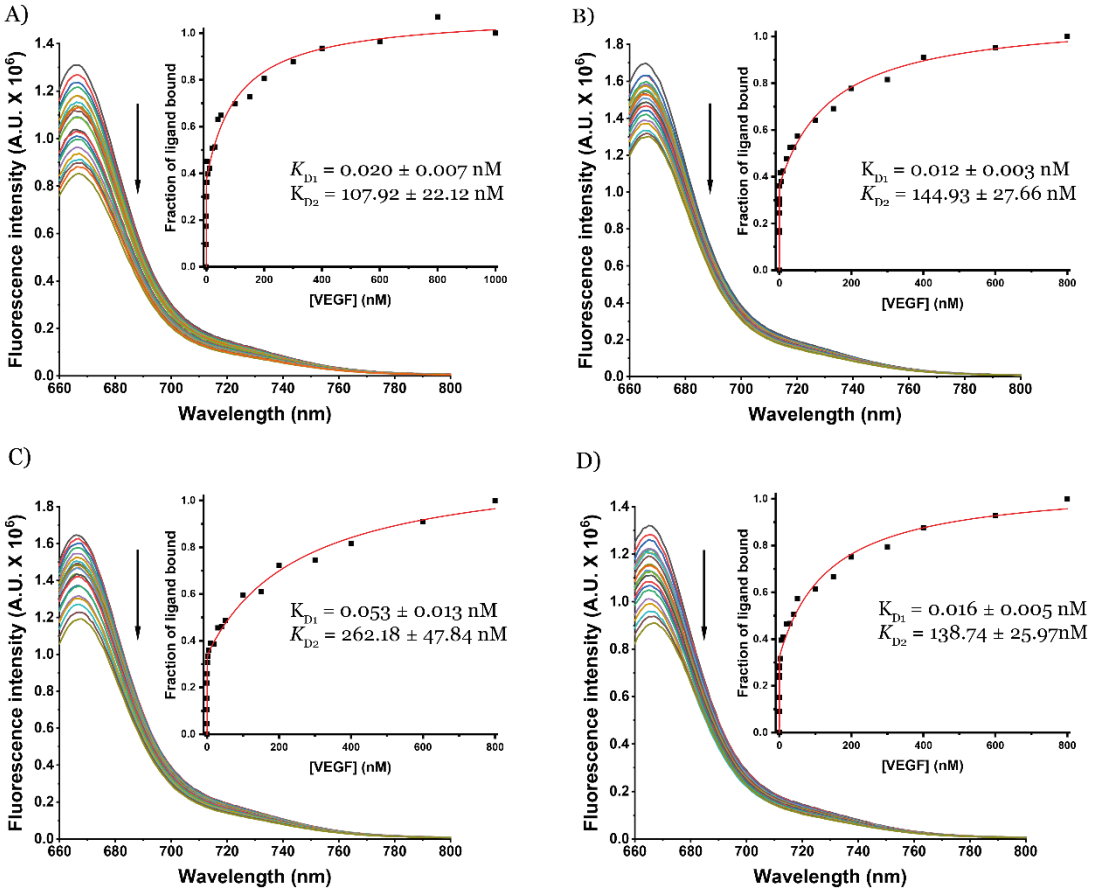

Figure 23 – Fluorescence intensity spectra and K_D of A) AT11-Lo G4 and of AT11-Lo G4 complexed with B) C_8; C) dexamethasone and D) PhenDC3 titrated with VEGF.

Titrations with VEGF were similar to those performed with NCL. The fit model used was the same (two-site binding model) and we obtained two K_D for the aptamer and the complexes. The affinity is also very similar to the ones obtained with NCL being in the nanomolar order. Since aptamers are highly specific, we expected different affinity between AT11-Lo G4 and both proteins, VEGF and NCL. However, these proteins are intimately interrelated. NCL can bind to VEGF G4 promoter and VEGF can bind to cell surface NCL [119, 120]. These described interactions established between NCL and VEGF may explain why AT11-Lo G4 is capable to bind to both proteins.

4.2.4 Native PAGE

Native PAGE analysis was performed with C_8 since it presents a high affinity and improves the thermal stabilization as G4 ligand. On the other hand, dexamethasone was also analysed because of its therapeutic properties and application in clinical practice for the treatment of neovascular retinal diseases. Native PAGE was performed to evaluate the distinct species formed by AT11-Lo G4 with C_8 and dexamethasone.

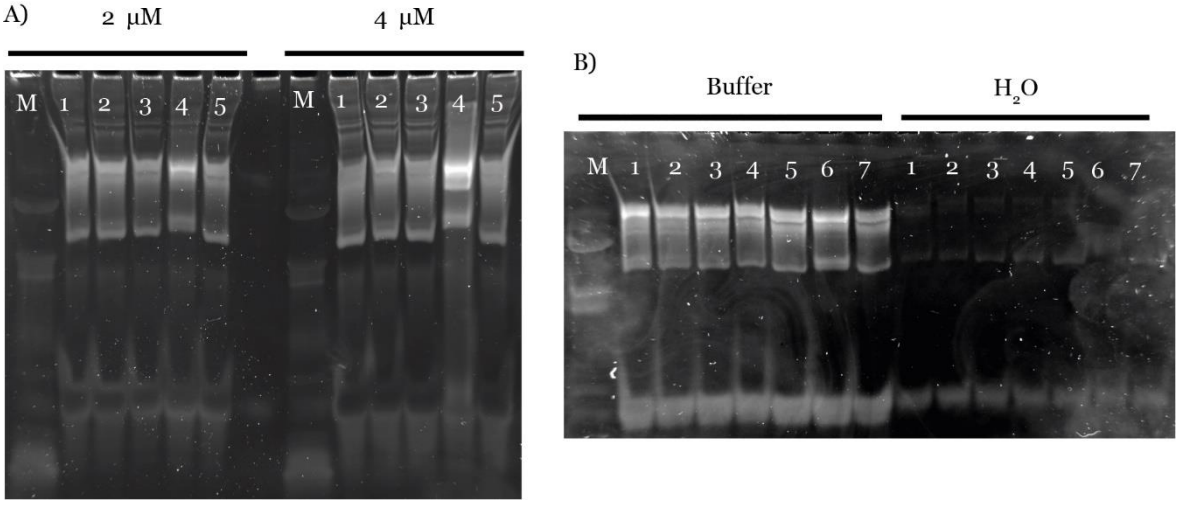

Figure 24 – Native PAGE gel results. M: Weight marker (90 nt, 60 nt, 30 nt, 21 nt, 15 nt) A) 1: AT11-Lo, 2: AT11-Lo+C_8 (1:15), 3: AT11-Lo+Dexamethasone (1:15), 4: AT11-Lo+C_8 (1:1), 5: AT11-Lo+Dexamethasone (1:1); B) 1: AT11-Lo, 2) AT11-Lo+C_8 (1:1), 3) AT11-Lo+C_8 (1:2), 4) AT11-Lo+C_8 (1:5), 5) AT11-Lo+C_8 (1:10), 6) AT11-Lo+C_8 (1:15), 2) AT11-Lo+C_8 (2:1); C) AT11-Lo+H_2O.

Based on the gel results presented in Figure 24, AT11-Lo G4 forms not just the G4 structure that was already described but also dimers and tetramers. The band that appears near 30 nt is AT11-Lo (27 nt). Then we observe another band near 60 nt that shows the formation of dimers and finally another one above 90 nt that indicates the formation of tetramers. There is no difference between the bands of dexamethasone at different concentrations (Figure 24A) indicating that dexamethasone concentrations did not influence AT11-Lo G4/dexamethasone formation. In contrast, the difference between bands is visible indicating that increasing C_8 concentration can influence the formation of the AT11-Lo G4/C_8 complex. The formation of as AT11-Lo G4/complex is absent in water since no intense bands are visible, which confirms our results in NMR titration that indicat the G4 structure is unstable in water. Also, the formation of higher-order species is not observed in water (Figure 24B).

4.2.5 NPs synthesis

AuNPs conjugation with the AT11-Lo G4 aptamer was achieved following the reaction presented in Figure 25. As described in the section 3, the first step is to reduce the disulfide

bond on the 5'-Thiol-AT11-L0, since the aptamers acquired have the sulfur atom protected by a disulfide bond to prevent unspecific reactions from occurring. Thus, TCEP was used to reduce this disulfide bond. After that, the reduced thiol groups were linked to gold. However, since AuNPs are stabilized by citrate (with a negative charge) AT11-L0 will be repulsed due to the negatively charged phosphate groups. Therefore, to promote the linkage, NaCl is added to the mixture to minimize charge repulsion effects and allow DNA to approach AuNPs for adsorption.

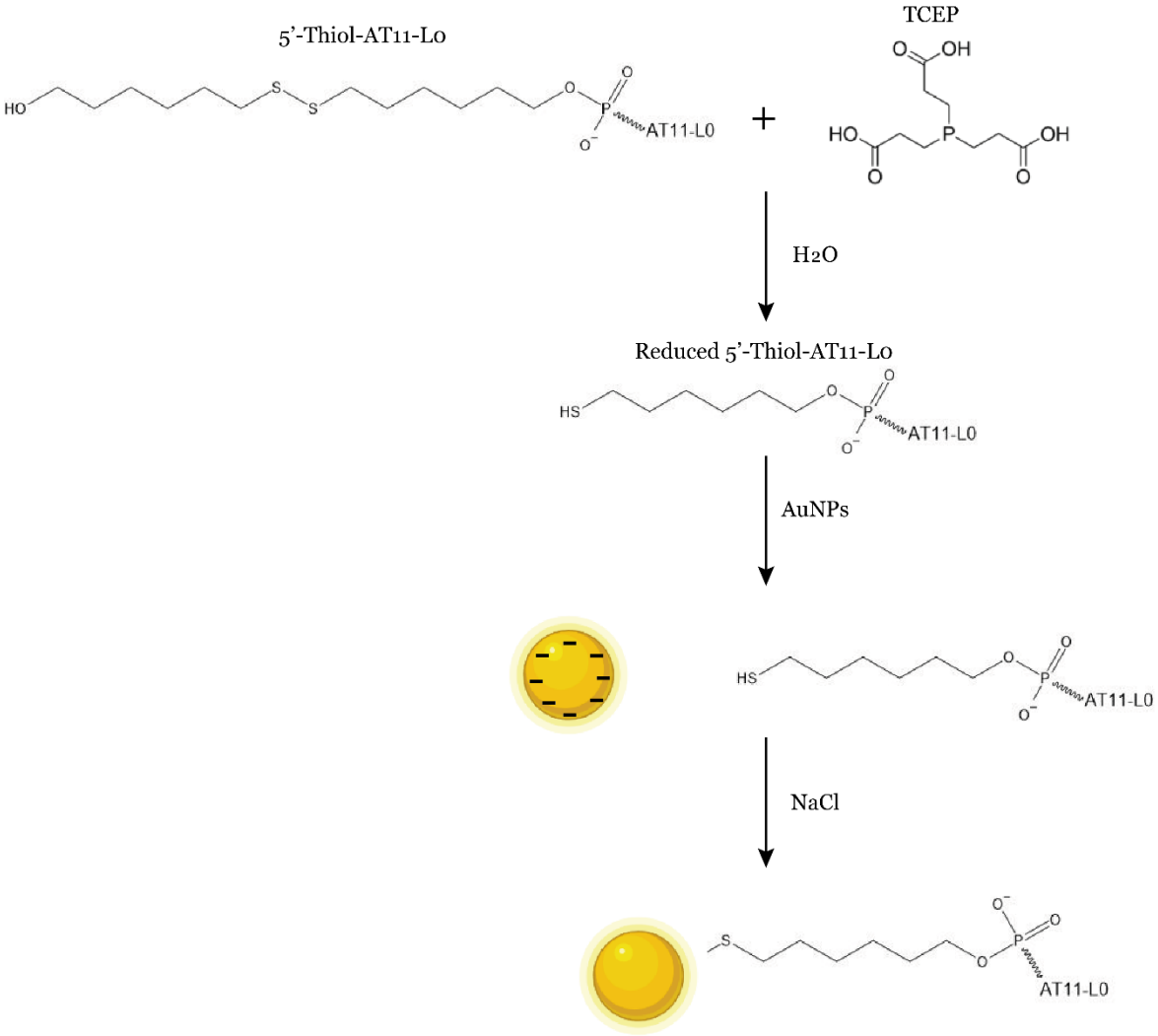

Figure 25 - Reactional scheme of AT11-L0 conjugation to AuNPs.

Liposomes synthesis was achieved as described in the materials and methods section by the thin film hydration method [121]. After the formation of liposomes, they were homogenised and purified using an extrusion process followed by centrifugations on centricon filter units. The mechanism behind the AT11-L0 aptamer conjugation to the liposomes was achieved using 5'-NH2-AT11-L0. The conjugation of the aptamer by reacting the AT11-L0 amine group with the NHS ester present in DSPE-PEG is shown in Figure 26.

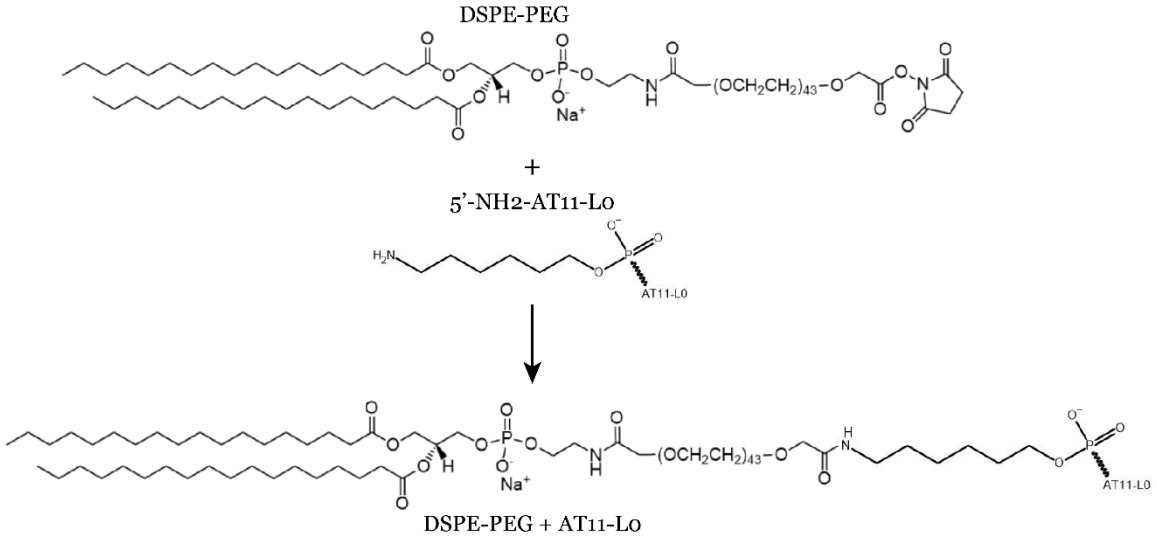

Figure 26 - Reactional scheme of AT11-L0 conjugation with DSPE-PEG (present in liposomes).

4.2.6 Characterization of NPs functionalized with AT11-L0

The characterization of AuNPs was made using DLS and TEM.

TEM image was acquired to confirm the presence of the AuNP's in our samples. After that DLS was performed to measure the size of the AuNP's. Results are shown in Figures 27 and 28.

TEM images show that AuNPs have a well-defined round shape and a high homogeneity in terms of size.

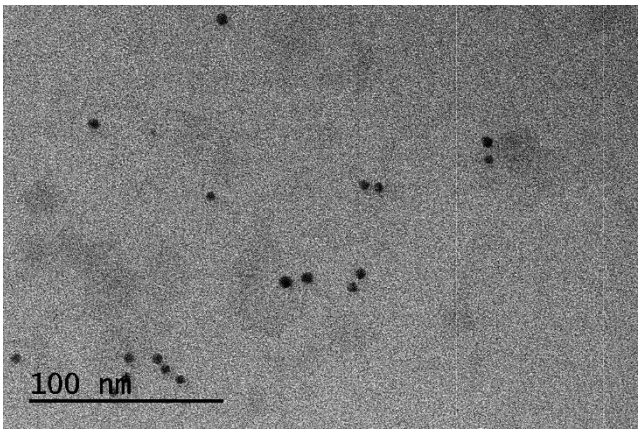

Figure 27 - TEM image of AuNP's.

DLS analysis showed that AuNP's have a size of 24 nm and a polydispersity index of 0.561. These results are coherent with those we find in the literature, since AuNPs conjugated with AS1411 aptamer synthetised by Malik *et al.* have a size of 33 nm [113]. The high polydispersity index is common in solutions of very small NPs.

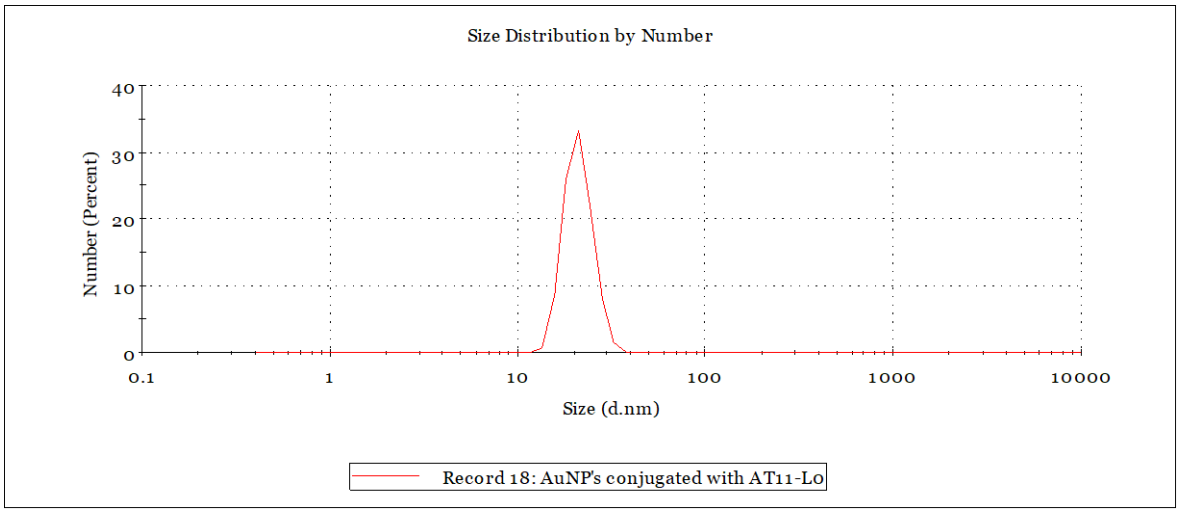

Figure 28 – DLS of AuNP's conjugated with AT11-Lo.

The characterization of liposomes was performed by SEM, DLS, and NTA. SEM was used to prove the formation of the liposomes and then their size was measured with DLS and NTA.

SEM image (Figure 29) shows that liposomes present a high homogeneity in terms of size. However, liposome's morphology is not uniform and varies from round-shaped liposomes to rod-shaped liposomes. It is also possible to observe a small fraction of liposomes agglomerate.

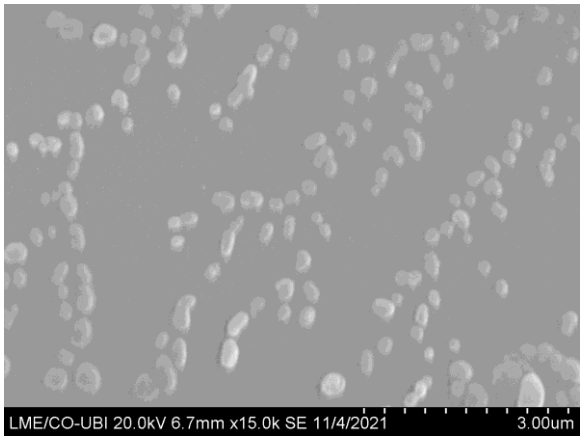

Figure 29 – SEM image of liposomes functionalized with AT11-Lo.

The size of liposomes obtained by DLS was 164.4 nm with a polydispersity index of 0.231. These results (Figure 30) show that the liposomes have the appropriate size homogeneity and this values are the according to the referred in the literature [88,89].

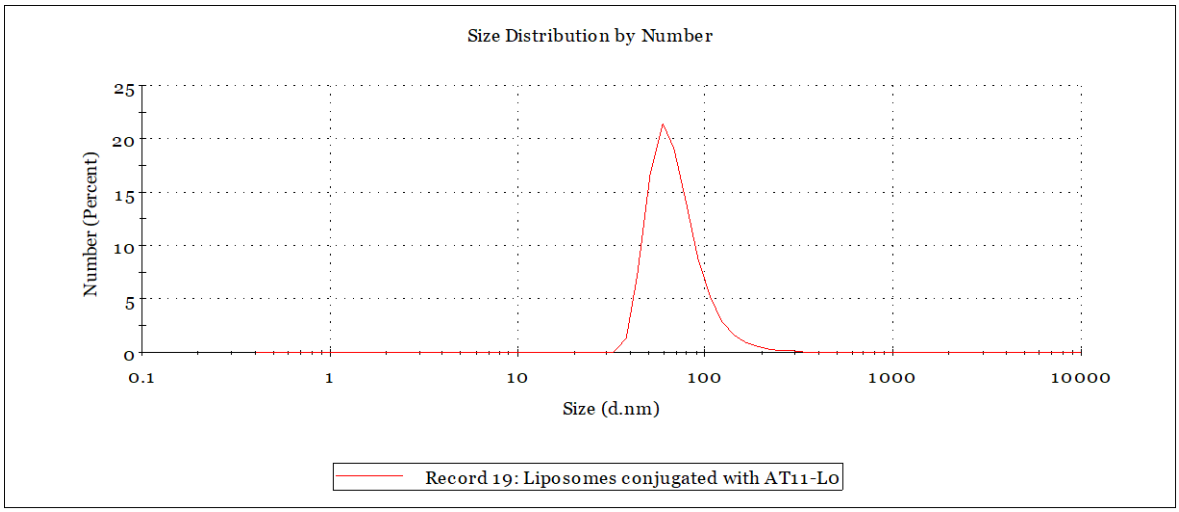

Figure 30 – DLS of liposomes functionalized with AT11-L0.

NTA was made to determine the concentration of liposomes since DLS and SEM did not give information about this parameter. NTA was also performed to confirm liposome's sizes. NTA results were similar since liposome sizes and were 147.4 nm with 90% of the liposomes having sizes below 188.5 nm. The concentration of liposomes in the samples was $4.82\times10^{10} \pm 3.85\times10^{7}$ particles/mL.

Finally, to prove that AT11-L0 G4 is linked to the liposomes, ^{1}H NMR spectrum of liposome's solution was acquired to check the presence of G4 signals. The presence of C_8 in liposomes was also checked in the NMR spectrum. The ^{1}H NMR spectrum was acquired after washing samples on centricons to remove free AT11-L0 G4 and free C_8 and it is presented in Figure 31. The ^{1}H NMR spectrum of liposomes without AT11-L0 and C_8 was also acquired as a control sample.

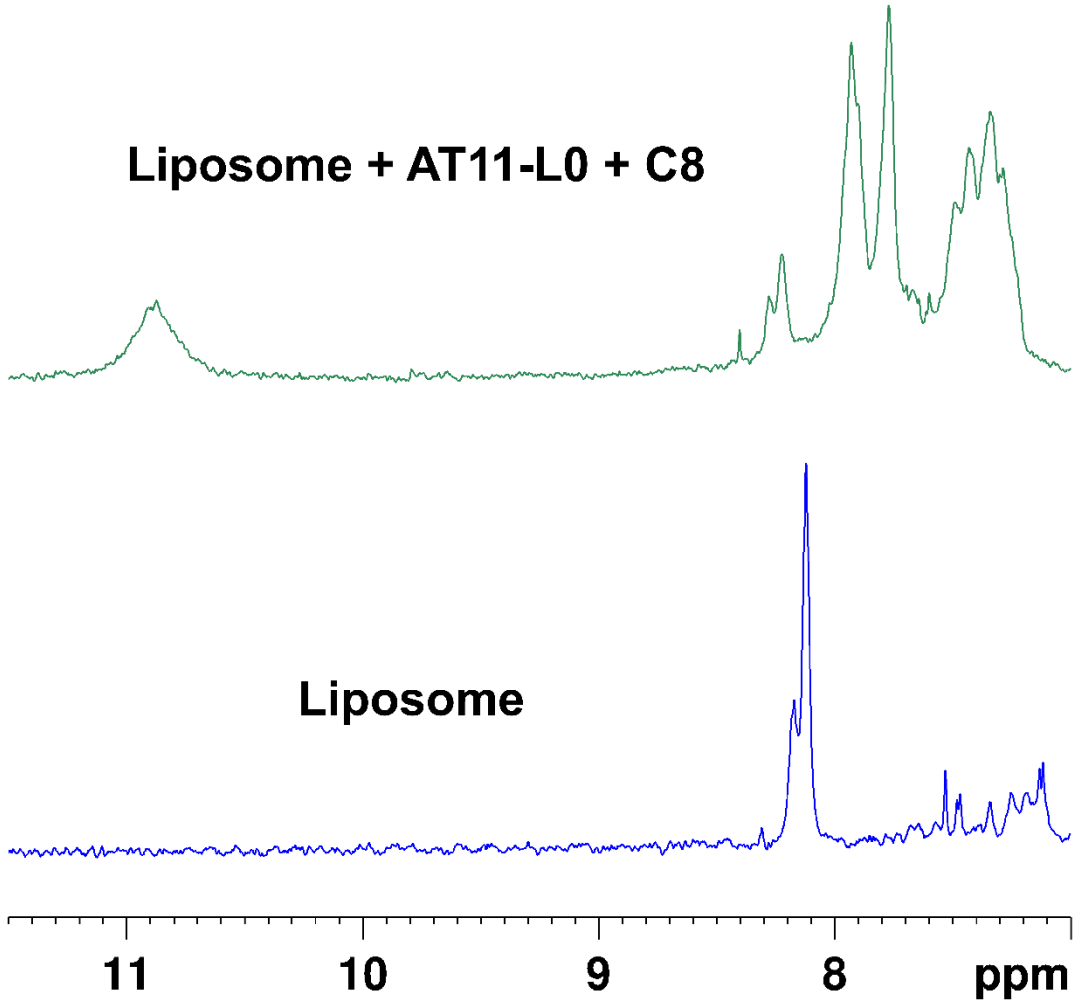

Figure 31 – NMR spectra of liposomes and liposomes conjugated with AT11-L0 G4 and loaded with C_8.

Figure 31 shows on the bottom a spectrum of liposomes with no C_8 and no AT11-L0. There are no signals between 10-12 ppm. However, when conjugated with AT11-L0 signals between 10-12 ppm are visible. These signals resulted from the imino protons resonances characteristic of Hoogsteen hydrogen bonds attributed to the G-tetrads formation. This result indicates that G4 formation in AT11-L0 was not affected by the linkage to the liposome. The spectrum of liposome loaded with C_8 and functionalized with AT11-L0 also showed differences at 7-9 ppm. These signals are attributed to the aromatic protons of C_8 in the liposomes. By this way we conclude that liposomes were efficiently loaded with C_8 and conjugated with AT11-L0.

UV-Vis also confirmed the association of the ligands with AT11-L0 and encapsulation in liposomes.

4.2.7 MTT assay

In a first approach, the viability of HUVEC was evaluated when exposed to different concentrations of C_8, dexamethasone, and the AT11-Lo aptamer. The results obtained are shown in Figure 32.

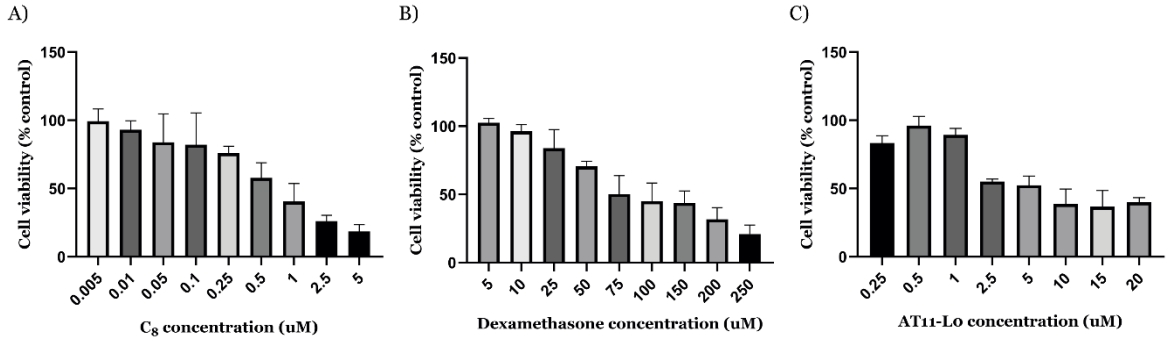

Figure 32 – Percentage of viable HUVEC after 72 h incubation with A) C_8 in concentrations from 0.005 to 5 μM, B) dexamethasone in concentrations from 5 to 250 μM and C) AT11-Lo in concentrations from 0.25 to 20 μM.

C_8 greatly reduces the viability of HUVEC at concentrations from 0.5 to 5 μM. This may indicate that C_8 at these concentrations are capable of reducing cell proliferations or even having cytotoxic effects. These results are in line with those reported by Carvalho *et al.*, in which they found that the viability of normal human dermal fibroblast cells exposed to 1 μM was near 40% [58]. On the other hand, dexamethasone showed a considerably lower effect on the HUVEC viability, since only at concentrations from 75 to 250 μM the viability drops to under 50%.

As the main objective of this work was to inhibit the formation of new blood vessels without reducing cell viability, we evaluated the viability of HUVEC exposed to C_8 and dexamethasone loaded liposomes at concentrations below 0.5 μM and 75 μM, respectively. AT11-Lo also promoted a considerable reduction in the HUVEC viability when concentrations from 2.5 to 20 μM were used. This result is the most unexpected since Iturriaga-Goyon *et al.* reported that AS1411 did not cause a reduction of HUVEC viability in concentrations from 0.75 to 10 μM. However, AS1411 has at least eight polymorphisms and it is not known which one is the more relevant. So, this result may indicate that AT11-Lo has more biological activity resulting from having just one predominant G4 topology. Carvalho *et al.* also reported that AT11-Lo at 15 μM did not appreciably affect the viability of normal human dermal fibroblast cells. In this case, results were not coincident. However, since the cell line evaluated on this work was different from HUVEC, this result may be a consequence of different cell line susceptibilities to the same compound.

Since it was observed a considerable reduction in the viability of HUVEC, at concentrations of AT11-Lo greater than 2.5 μM, the evaluation tests with liposomes were performed at

concentrations below this value. However, the quantity of NPs used was defined in function of the drug encapsulated instead of the AT11-L0 concentration. We followed this approach because the total concentration of AT11-L0 in the liposomes was about 500 nM.

After defining the concentrations of C_8, dexamethasone and AT11-L0 that does not considerably affect the viability of HUVEC, the MTT assay was performed with the formulations containing liposomes and the compounds at the defined concentrations. MTT results are shown in Figure 33. AuNPs were not used in this assay since in this formulation the drug was conjugated on the G4 structure resulting in a lower concentration of drug in the final formulation. Regarding this lower concentration we focused our efforts on liposomes formulations.

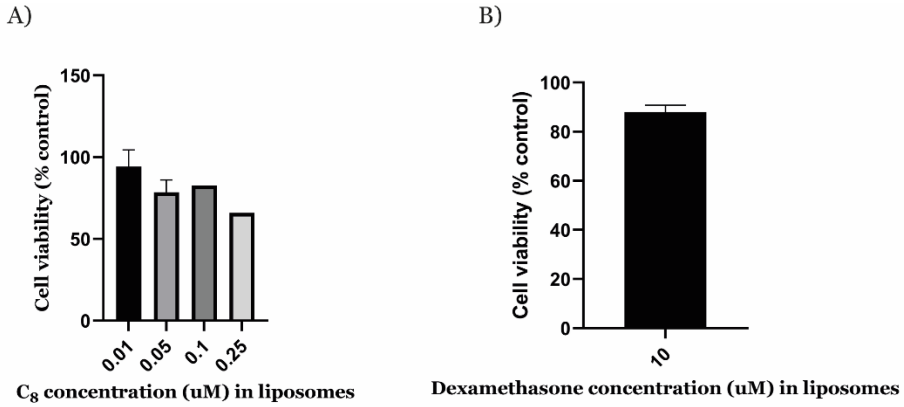

Figure 33 – Percentage of viable HUVEC after 72 h incubation with A) C_8 loaded liposomes in concentrations from 0.01 to 0.25 μM and B) dexamethasone loaded liposomes at a concentration of 10 μM.

MTT assay revealed that both C_8 and dexamethasone-loaded liposomes did not considerably affect the viability of HUVEC. We may conclude that liposomes formulations in the tested concentrations are suitable for being evaluated in the angiogenesis assay without disturbing normal cell proliferation.

4.2.8 Angiogenesis assay

The formation of new blood vessels is characteristic of vascular diseases of the retina. The study of how compounds can promote or inhibit it is therefore essential in the research related to these processes. The tube formation assay studies the development of blood vessels by measuring the angiogenesis stage of endothelial cell reorganization to form tubes or capillary-like structures, usually using an extracellular matrix as a scaffold. The main advantage of this assay is the analysis of angiogenesis over time allowing to determine the effects of inhibitors or activators of neovascularization over time.

To determine the angiogenic activity of the NPs, the concentration of drug used was defined regarding the MTT results. Dexamethasone NPs were tested using a dexamethasone

concentration of 10 μM and C_8 NPs using a C_8 concentration of 0.05 μM. These concentrations were chosen since they are the highest concentrations that do not cause a considerably decrease on the cell viability. As shown in Figure 34, when seeded on a Matrigel, HUVEC can organize themselves on capillary-like structures. After 18 h, these structures are well visible in the untreated control group. In contrast, tube formation was significantly inhibited by dexamethasone and by C_8 and also by NPs containing AT11-L0 loading these compounds. However, these NPs did not show a significant difference when compared with the isolated compounds, dexamethasone and C_8.

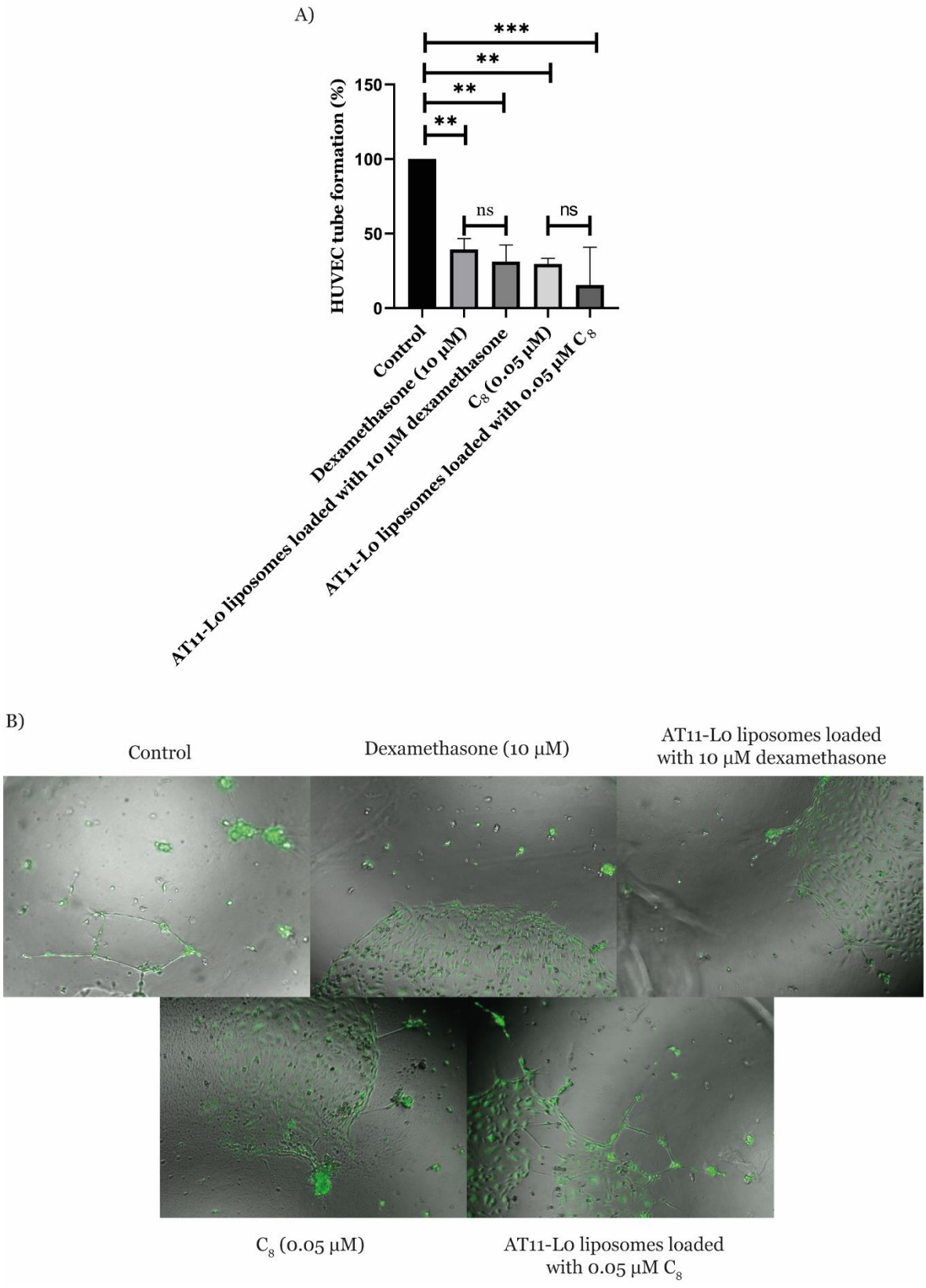

Figure 34 - A) HUVEC tube formation. Data are expressed as mean ± SD, **p<0.01, ***p<0.001. B) Representative image of tube formation on HUVEC.

Regarding the obtained data, C_8 showed antiangiogenic properties similar to those presented by dexamethasone. It was already known that C_8 had anticarcinogenic and antiproliferative properties [122]. However, antiangiogenic assays were never performed with this molecule. Since dexamethasone is already used in the treatment of retinal vascular diseases because of its antiangiogenic properties [123], C_8 may be a potential candidate for use in these diseases as it presents a similar effect in a much lower concentration. Other important advantage of C_8 is that it may be used in combination with G4 aptamer since it induces a thermal stabilization of the G4 structure.

Nevertheless, AT11-L0 liposomes did not induce a reduction of the angiogenesis, when compared with the compounds alone. This result can be explained because the concentration of AT11-L0 on the liposomes was about 500 nM. Since AS1411 presented a significant reduction of the angiogenesis at 10 μM [71], the concentration used in this work may be too low. However, liposomes conjugated with AT11-L0 can have an important role since they improve dexamethasone and C_8 targeting to cells with overexpression of NCL. In the angiogenic assay, the HUVEC were VEGF dependent which means they have an overexpression of VEGF (and consequently of cell surface NCL). In a retinal eye disease, only some cells have this overexpression and liposomes conjugated with AT11-L0 may be useful to help the compounds to reach only the cells with an overexpression of VEGF and NCL that will trigger the angiogenesis process.

5. Conclusion and Future Perspectives

This work used AT11-L0 aptamer conjugated with a NP to deliver drug/compound to inhibit angiogenesis in retinal diseases. AT11-L0 is an aptamer derivative from AS1411 that targets NCL.

Through CD spectroscopy it was observed that AT11-L0 formed a majority parallel-stranded G4 structure with a well-defined profile specially when using a 65 mM KCl buffer. This result shows that AT11-L0 surpassed one of the principal drawbacks of AS1411 that is the fact that it can adopt several G4 structures.

It was also demonstrated that AT11-L0 is stabilized by commercial ligands such as PhenDC3 but also by the orange acridine derivative C_8. However, dexamethasone did not present a stabilization of the G4 in AT11-L0 structure. Regarding the affinity of the ligand/G4 complex to NCL C_8 promotes higher affinity.

In the second part of the work, it was demonstrated that it is possible to conjugate AT11-L0 with AuNPs and with liposomes. AuNPs may be a useful tool to carry AT11-L0 aptamer in retinal diseases. However, it is difficult to conjugate a considerable amount of an antiangiogenic drug in the G4 structure. On the other hand, liposomes showed to be able to encapsulate a larger amount of an antiangiogenic drug and, at the same time, conjugate on the surface AT11-L0 in order to target NCL. These liposomes have a size of about 160 nm and are the most promising NP in this work to use in retinal vascular diseases.

When tested *in vitro,* liposomes did not promote a significant reduction in the angiogenic process when compared to the tested drugs (dexamethasone and C_8). However, this work demonstrated that C_8 may be a useful molecule in the treatment of vascular retinal diseases, since it has a similar antiangiogenic effect to the one showed by dexamethasone. In addition to this characteristic, C_8 is capable to promote a thermal stabilization of G4 structures and present these effects in low concentrations, when compared to dexamethasone.

Regarding future perspectives related to this work we can say that there is still a long way to go on the study of the therapeutic potential of these molecules in vascular retinal diseases. First it will be important to validate the antiangiogenic effect of C_8. For that, more angiogenic assays must be done. It should be repeated the assay performed on this work, but also tested different approaches like the Rat Aortic Ring Assay.

It will be important to try to improve the liposome formulation in order to achieve better encapsulations and higher conjugation of the aptamer. It will also be interesting to test

antiangiogenic effect of AT11-L0 aptamer in a concentration of 1 μM (the highest concentration that did not considerably affect cell viability) conjugated with 0.05 μM C_8 (the same concentration tested in this work) to see if it improves C_8 antiangiogenic effect. AuNPs antiangiogenic effect may also be tested following the same approach used with liposomes.

Finally, it may be important to test the formulations in a more complex biologic sample. These formulations can be tested using HUVEC cells treated with the humour vitreous of patients with proliferative DR or using the Oxygen Induced Retinopathy Mouse Model. These assays would allow to achieve results on *in vitro* and *in vivo* models more similar to the real concentration of VEGF or NCL, but also of other angiogenic and inflammatory proteins that are implicated in the development of vascular retinal diseases.

References

[1] A. C. Galloway, N. R., Amoaku, W. M. K., Galloway, P. H., & Browning, "Basic Anatomy and Physiology of the Eye," *Common Eye Dis. their Manag.*, 2016, doi: 10.1007/978-3-319-32869-0_2.

[2] A. Lens, S. C. Nemeth, and J. K. Ledford, *Ocular anatomy and physiology*, 2º Edition. SLACK, 2008.

[3] R. R. A. Bourne *et al.*, "Magnitude, temporal trends, and projections of the global prevalence of blindness and distance and near vision impairment: a systematic review and meta-analysis," 2017, doi: 10.1016/S2214-109X(17)30293-0.

[4] C. Sabanayagam and C.-Y. Cheng, "Global causes of vision loss in 2015: are we on track to achieve the Vision 2020 target?," *Lancet Glob. Heal.*, vol. 5, pp. e1164–e1165, 2017, doi: 10.1016/S2214-109X(17)30412-6.

[5] "Keeffe J, Resnikoff S (2019) Prevalence and Causes of Vision Impairment and Blindness: The Global Burden of Disease. In: Khanna RC, Rao GN, Marmamula S (eds) Innovative Approaches in the Delivery of Primary and Secondary Eye Care. Springer International P."

[6] R. Seeley, T. Stephens, and T. Philip, "Anatomy & Physiology," in *Anatomy & Physiology*, 6th ed., McGraw-Hill Science, 2003, p. 511.

[7] C. E. Willoughby, D. Ponzin, S. Ferrari, A. Lobo, K. Landau, and Y. Omidi, "Anatomy and physiology of the human eye: effects of mucopolysaccharidoses disease on structure and function – a review," *Clin. Experiment. Ophthalmol.*, vol. 38, no. SUPPL. 1, pp. 2–11, Aug. 2010, doi: 10.1111/J.1442-9071.2010.02363.X.

[8] H. Ragelle, A. Goncalves, S. Kustermann, D. A. Antonetti, and A. Jayagopal, "Organ-On-A-Chip Technologies for Advanced Blood–Retinal Barrier Models," *J. Ocul. Pharmacol. Ther.*, vol. 36, no. 1, p. 30, Jan. 2020, doi: 10.1089/JOP.2019.0017.

[9] C. Gilbert and A. Foster, "Childhood blindness in the context of VISION 2020-The Right to Sight."

[10] D. Yorston, "Retinal Diseases and VISION 2020," *Community Eye Heal.*, vol. 16, no. 46, p. 19, 2003, Accessed: Oct. 27, 2021. [Online]. Available: /pmc/articles/PMC1705858/.

[11] J. Birtel, I. H. Yusuf, C. Priglinger, G. Rudolph, and P. C. Issa, “Diagnosis of Inherited Retinal Diseases,” *Klin. Monbl. Augenheilkd.*, vol. 238, no. 03, pp. 249–259, Mar. 2021, doi: 10.1055/A-1388-7236.

[12] E. Margalit and S. R. Sadda, “Retinal and Optic Nerve Diseases,” *Artif. Organs*, vol. 27, no. 11, pp. 963–974, Nov. 2003, doi: 10.1046/J.1525-1594.2003.07304.X.

[13] A. Yoshida, S. Yoshida, T. Ishibash, and H. Inomata, “lntraocular neovascularization,” *Histol. Histopathol.*, vol. 14, pp. 1287–1294, Jan. 1999, doi: 10.1007/S00109-013-0993-5.

[14] G. J. Jaffe *et al.*, “C5 Inhibitor Avacincaptad Pegol for Geographic Atrophy Due to Age-Related Macular Degeneration: A Randomized Pivotal Phase 2/3 Trial,” *Ophthalmology*, vol. 128, no. 4, pp. 576–586, Apr. 2021, doi: 10.1016/J.OPHTHA.2020.08.027.

[15] R. S. Apte, “Age-Related Macular Degeneration,” *https://doi.org/10.1056/NEJMcp2102061*, vol. 385, no. 6, pp. 539–547, Aug. 2021, doi: 10.1056/NEJMCP2102061.

[16] Y. Usui *et al.*, “Angiogenesis and Eye Disease,” *Annu. Rev. Vis. Sci.*, vol. 1, no. 1, pp. 155–184, Nov. 2015, doi: 10.1146/ANNUREV-VISION-082114-035439.

[17] C. Chandola, M. G. Casteleijn, U. M. Chandola, L. N. Gopalan, A. Urtti, and M. Neerathilingam, “CD44 aptamer mediated cargo delivery to lysosomes of retinal pigment epithelial cells to prevent age-related macular degeneration,” *Biochem. Biophys. Reports*, vol. 18, p. 100642, Jul. 2019, doi: 10.1016/J.BBREP.2019.100642.

[18] D. Leaderer, S. M. Cashman, and R. Kumar-Singh, “Topical application of a G-Quartet aptamer targeting nucleolin attenuates choroidal neovascularization in a model of age-related macular degeneration,” *Exp. Eye Res.*, vol. 140, pp. 171–178, 2015, doi: 10.1016/j.exer.2015.09.005.

[19] A. Sharma *et al.*, “Terms non-exudative and non-neovascular: awaiting entry at the doors of AMD reclassification,” *Graefe’s Arch. Clin. Exp. Ophthalmol. 2021 2596*, vol. 259, no. 6, pp. 1381–1383, Mar. 2021, doi: 10.1007/S00417-021-05164-6.

[20] R. F. Spaide *et al.*, “Consensus Nomenclature for Reporting Neovascular Age-Related Macular Degeneration Data: Consensus on Neovascular Age-Related Macular Degeneration Nomenclature Study Group,” *Ophthalmology*, vol. 127, no. 5, pp. 616–

636, May 2020, doi: 10.1016/J.OPHTHA.2019.11.004.

[21] E. Makarev, C. Cantor, A. Zhavoronkov, A. Buzdin, A. Aliper, and A. B. Csoka, "Pathway activation profiling reveals new insights into Age-related Macular Degeneration and provides avenues for therapeutic interventions," *Aging (Albany. NY).*, vol. 6, no. 12, pp. 1064–1075, Dec. 2014, doi: 10.18632/aging.100711.

[22] I. M. Nawaz *et al.*, "Human vitreous in proliferative diabetic retinopathy: Characterization and translational implications," *Prog. Retin. Eye Res.*, vol. 72, p. 100756, Sep. 2019, doi: 10.1016/J.PRETEYERES.2019.03.002.

[23] J. Lechner, O. E. O'Leary, and A. W. Stitt, "The pathology associated with diabetic retinopathy," *Vision Res.*, vol. 139, pp. 7–14, Oct. 2017, doi: 10.1016/J.VISRES.2017.04.003.

[24] S. Pillar, E. Moisseiev, J. Sokolovska, and A. Grzybowski, "Recent Developments in Diabetic Retinal Neurodegeneration: A Literature Review," *J. Diabetes Res.*, vol. 2020, 2020, doi: 10.1155/2020/5728674.

[25] M. G. Rossino, M. Dal Monte, and G. Casini, "Relationships Between Neurodegeneration and Vascular Damage in Diabetic Retinopathy," *Front. Neurosci.*, vol. 13, p. 1172, Nov. 2019, doi: 10.3389/FNINS.2019.01172/BIBTEX.

[26] M. Darche *et al.*, "Antagonist of nucleolin, N6L, inhibits neovascularization in mouse models of retinopathies," *FASEB J.*, vol. 34, no. 4, pp. 5851–5862, Apr. 2020, doi: 10.1096/FJ.201901876R.

[27] A. K. Schuster, C. Erb, E. M. Hoffmann, T. Dietlein, and N. Pfeiffer, "The Diagnosis and Treatment of Glaucoma," *Dtsch. Arztebl. Int.*, vol. 117, no. 13, p. 225, Mar. 2020, doi: 10.3238/ARZTEBL.2020.0225.

[28] S. S. Hayreh, "Neovascular glaucoma," *Prog. Retin. Eye Res.*, vol. 26, no. 5, pp. 470–485, Sep. 2007, doi: 10.1016/J.PRETEYERES.2007.06.001.

[29] S. Senthil, T. Dada, T. Das, S. Kaushik, and G. V. Puthuran, "Neovascular glaucoma - A review," *BMC Ophthalmol.*, vol. 17, no. 1, p. 1, 2020, doi: 10.4103/ijo.IJO.

[30] I. L. Mcallister, "Central retinal vein occlusion: a review," *Clin. Experiment. Ophthalmol.*, vol. 40, no. 1, pp. 48–58, Jan. 2012, doi: 10.1111/J.1442-9071.2011.02713.X.

[31] F. J. Ascaso, R. Terao, R. Fujino, and T. Ahmed, “Risk Factors and Treatment Strategy for Retinal Vascular Occlusive Diseases,” *J. Clin. Med. 2022, Vol. 11, Page 6340*, vol. 11, no. 21, p. 6340, Oct. 2022, doi: 10.3390/JCM11216340.

[32] S. D. Schoenberger and S. J. Kim, “Nonsteroidal Anti-Inflammatory Drugs for Retinal Disease,” *Int. J. Inflam.*, vol. 2013, 2013, doi: 10.1155/2013/281981.

[33] E. A. Urias, G. A. Urias, F. Monickaraj, P. McGuire, and A. Das, “Novel therapeutic targets in diabetic macular edema: Beyond VEGF,” *Vision Res.*, vol. 139, no. March, pp. 221–227, 2017, doi: 10.1016/j.visres.2017.06.015.

[34] B. Lorenzo-Veiga, C. Alvarez-Lorenzo, T. Loftsson, and H. H. Sigurdsson, “Age-related ocular conditions: Current treatments and role of cyclodextrin-based nanotherapies,” *Int. J. Pharm.*, vol. 603, p. 120707, Jun. 2021, doi: 10.1016/J.IJPHARM.2021.120707.

[35] L. Zou, H. Lai, Q. Zhou, and F. Xiao, “Lasting Controversy on Ranibizumab and Bevacizumab,” *Theranostics*, vol. 1, pp. 395–402, Jan. 2012, doi: 10.7150/THNO/V01P0395.

[36] R. Anguita, A. Tasiopoulou, S. Shahid, J. Roth, S. Y. Sim, and P. J. Patel, “A Review of Aflibercept Treatment for Macular Disease,” *Ophthalmol. Ther.*, vol. 10, no. 3, pp. 413–428, Sep. 2021, doi: 10.1007/S40123-021-00354-1/FIGURES/2.

[37] J. S. Heier *et al.*, “Efficacy, durability, and safety of intravitreal faricimab up to every 16 weeks for neovascular age-related macular degeneration (TENAYA and LUCERNE): two randomised, double-masked, phase 3, non-inferiority trials,” *Lancet*, vol. 399, no. 10326, pp. 729–740, Feb. 2022, doi: 10.1016/S0140-6736(22)00010-1.

[38] A. Shoval *et al.*, “Anti-VEGF-Aptamer Modified C-Dots—A Hybrid Nanocomposite for Topical Treatment of Ocular Vascular Disorders,” *Small*, vol. 15, no. 40, pp. 1–10, 2019, doi: 10.1002/smll.201902776.

[39] E. Iturriaga-Goyon, B. Buentello-Volante, F. S. Magaña-Guerrero, and Y. Garfias, “Future Perspectives of Therapeutic, Diagnostic and Prognostic Aptamers in Eye Pathological Angiogenesis,” *Cells*, vol. 10, no. 6, p. 1455, 2021, doi: 10.3390/cells10061455.

[40] D. W. Drolet, L. S. Green, L. Gold, and N. Janjic, “Fit for the Eye: Aptamers in Ocular

Disorders," *Nucleic Acid Ther.*, vol. 26, no. 3, pp. 127–146, 2016, doi: 10.1089/nat.2015.0573.

[41] S. I. Ismail and W. Alshaer, "Therapeutic aptamers in discovery, preclinical and clinical stages," *Adv. Drug Deliv. Rev.*, vol. 134, pp. 51–64, 2018, doi: 10.1016/j.addr.2018.08.006.

[42] S. Burge, G. N. Parkinson, P. Hazel, A. K. Todd, and S. Neidle, "Quadruplex DNA: sequence, topology and structure," *Nucleic Acids Res.*, vol. 34, no. 19, p. 5402, Nov. 2006, doi: 10.1093/NAR/GKL655.

[43] D. Bhattacharyya, G. M. Arachchilage, and S. Basu, "Metal cations in G-quadruplex folding and stability," *Front. Chem.*, vol. 4, no. SEP, p. 38, 2016, doi: 10.3389/FCHEM.2016.00038/BIBTEX.

[44] J. Carvalho, J. A. Queiroz, and C. Cruz, "Circular dichroism of G-Quadruplex: A laboratory experiment for the study of topology and ligand binding," *J. Chem. Educ.*, vol. 94, no. 10, pp. 1547–1551, 2017, doi: 10.1021/acs.jchemed.7b00160.

[45] M. I. Umar, D. Ji, C. Y. Chan, and C. K. Kwok, "G-Quadruplex-Based Fluorescent Turn-On Ligands and Aptamers: From Development to Applications," *Mol. 2019, Vol. 24, Page 2416*, vol. 24, no. 13, p. 2416, Jun. 2019, doi: 10.3390/MOLECULES24132416.

[46] A. Miranda, T. Santos, E. Largy, and C. Cruz, "Locking up the AS1411 Aptamer with a Flanking Duplex: Towards an Improved Nucleolin-Targeting," *Pharm. 2021, Vol. 14, Page 121*, vol. 14, no. 2, p. 121, Feb. 2021, doi: 10.3390/PH14020121.

[47] T. Santos *et al.*, "Recognition of nucleolin through interaction with RNA G-quadruplex," *Biochem. Pharmacol.*, vol. 189, p. 114208, Jul. 2021, doi: 10.1016/J.BCP.2020.114208.

[48] B. Pagano *et al.*, "State-of-the-Art Methodologies for the Discovery and Characterization of DNA G-Quadruplex Binders," *Curr. Pharm. Des.*, vol. 18, no. 14, pp. 1880–1899, 2012, doi: 10.2174/138161212799958332.

[49] T. Santos, G. F. Salgado, E. J. Cabrita, and C. Cruz, "G-Quadruplexes and Their Ligands: Biophysical Methods to Unravel G-Quadruplex/Ligand Interactions," *Pharm. 2021, Vol. 14, Page 769*, vol. 14, no. 8, p. 769, Aug. 2021, doi: 10.3390/PH14080769.

[50] G. F. Salgado, C. Cazenave, A. Kerkour, and J. L. Mergny, "G-quadruplex DNA and ligand interaction in living cells using NMR spectroscopy," *Chem. Sci.*, vol. 6, no. 6, pp. 3314–3320, May 2015, doi: 10.1039/C4SC03853C.

[51] A. Tawani, S. K. Mishra, and A. Kumar, "Structural insight for the recognition of G-quadruplex structure at human c-myc promoter sequence by flavonoid Quercetin," *Sci. Rep.*, vol. 7, no. 1, pp. 1–13, Jun. 2017, doi: 10.1038/s41598-017-03906-3.

[52] A. Kerkour, J. L. Mergny, and G. F. Salgado, "NMR based model of human telomeric repeat G-quadruplex in complex with 2,4,6-triarylpyridine family ligand," *Biochim. Biophys. Acta - Gen. Subj.*, vol. 1861, no. 5, pp. 1293–1302, May 2017, doi: 10.1016/J.BBAGEN.2016.12.016.

[53] A. I. Karsisiotis, N. M. A. Hessari, E. Novellino, G. P. Spada, A. Randazzo, and M. Webba Da Silva, "Topological Characterization of Nucleic Acid G-Quadruplexes by UV Absorption and Circular Dichroism," *Angew. Chemie Int. Ed.*, vol. 50, no. 45, pp. 10645–10648, Nov. 2011, doi: 10.1002/ANIE.201105193.

[54] N. Tariq, T. Kume, L. Luo, Z. Cai, S. Dong, and R. B. Macgregor, "Dimethyl sulfoxide (DMSO) is a stabilizing co-solvent for G-quadruplex DNA," *Biophys. Chem.*, vol. 282, p. 106741, Mar. 2022, doi: 10.1016/J.BPC.2021.106741.

[55] S. Joshi, A. Singh, and S. Kukreti, "Porphyrin induced structural destabilization of a parallel DNA G-quadruplex in human MRP1 gene promoter," *J. Mol. Recognit.*, vol. 35, no. 3, p. e2950, Mar. 2022, doi: 10.1002/jmr.2950.

[56] A. Głuszyńska, B. Juskowiak, M. Kuta-Siejkowska, M. Hoffmann, and S. Haider, "Carbazole Derivatives' Binding to c-KIT G-Quadruplex DNA," *Mol. 2018, Vol. 23, Page 1134*, vol. 23, no. 5, p. 1134, May 2018, doi: 10.3390/MOLECULES23051134.

[57] Y. J. Lu *et al.*, "Benzothiazole-substituted benzofuroquinolinium dyes as new fluorescent probes for G-quadruplex DNA," *Dye. Pigment.*, vol. 122, pp. 94–102, Nov. 2015, doi: 10.1016/J.DYEPIG.2015.06.018.

[58] J. Carvalho *et al.*, "Aptamer-guided acridine derivatives for cervical cancer," *Org. Biomol. Chem.*, vol. 17, no. 11, pp. 2992–3002, Mar. 2019, doi: 10.1039/c90b00318e.

[59] J. Figueiredo *et al.*, "Screening of Scaffolds for the Design of G-Quadruplex Ligands," *Appl. Sci.*, vol. 12, no. 4, p. 2170, Feb. 2022, doi: 10.3390/APP12042170/S1.

[60] J. Carvalho and C. Cruz, "Forster resonance energy transfer for studying nucleic acids

denaturation: A chemical and biological sciences laboratory experiment," *Biochem. Mol. Biol. Educ.*, vol. 48, no. 4, pp. 329–336, Jul. 2020, doi: 10.1002/BMB.21353.

[61] E. W. M. Ng, D. T. Shima, P. Calias, E. T. Cunningham, D. R. Guyer, and A. P. Adamis, "Pegaptanib, a targeted anti-VEGF aptamer for ocular vascular disease," *Nat. Rev. Drug Discov.*, vol. 5, no. 2, pp. 123–132, 2006, doi: 10.1038/nrd1955.

[62] "Phase 2A Open Label Safety Study of Fovista® (Anti-PDGF BB) Regimen Administered in Combination With Anti-VEGF Therapy to Study Sub-Retinal Fibrosis in Neovascular AMD - Full Text View - ClinicalTrials.gov." https://clinicaltrials.gov/ct2/show/NCT02214628?term=Fovista&phase=01&draw=2&rank=1 (accessed Apr. 27, 2022).

[63] G. J. Jaffe, D. Eliott, J. A. Wells, J. L. Prenner, A. Papp, and S. Patel, "A Phase 1 Study of Intravitreous E10030 in Combination with Ranibizumab in Neovascular Age-Related Macular Degeneration," *Ophthalmology*, vol. 123, no. 1, pp. 78–85, Jan. 2016, doi: 10.1016/j.ophtha.2015.09.004.

[64] "A Phase 3 Safety and Efficacy Study of Fovista® (E10030) Intravitreous Administration in Combination With Lucentis® Compared to Lucentis® Monotherapy - Study Results - ClinicalTrials.gov." https://clinicaltrials.gov/ct2/show/results/NCT01940900 (accessed Apr. 27, 2022).

[65] H. Xu and M. Chen, "Targeting the complement system for the management of retinal inflammatory and degenerative diseases," *Eur. J. Pharmacol.*, vol. 787, p. 94, Sep. 2016, doi: 10.1016/J.EJPHAR.2016.03.001.

[66] J. V. Sarma and P. A. Ward, "The complement system," *Cell Tissue Res.*, vol. 343, no. 1, pp. 227–235, Jan. 2011, doi: 10.1007/S00441-010-1034-0/TABLES/1.

[67] A. Armento, M. Ueffing, and S. J. Clark, "The complement system in age-related macular degeneration," *Cell. Mol. Life Sci. 2021 7810*, vol. 78, no. 10, pp. 4487–4505, Mar. 2021, doi: 10.1007/S00018-021-03796-9.

[68] S. Romano, N. Fonseca, S. Simões, J. Gonçalves, and J. N. Moreira, "Nucleolin-based targeting strategies for cancer therapy: from targeted drug delivery to cytotoxic ligands," *Drug Discov. Today*, vol. 24, no. 10, pp. 1985–2001, Oct. 2019, doi: 10.1016/J.DRUDIS.2019.06.018.

[69] Y. Huang, H. Shi, H. Zhou, X. Song, S. Yuan, and Y. Luo, "The angiogenic function of

nucleolin is mediated by vascular endothelial growth factor and nonmuscle myosin," *Blood*, vol. 107, no. 9, pp. 3564–3571, May 2006, doi: 10.1182/BLOOD-2005-07-2961.

[70] W. Jia, Z. Yao, J. Zhao, Q. Guan, and L. Gao, "New perspectives of physiological and pathological functions of nucleolin (NCL)," *Life Sci.*, vol. 186, pp. 1–10, Oct. 2017, doi: 10.1016/J.LFS.2017.07.025.

[71] E. Iturriaga-Goyon *et al.*, "As1411 nucleolin-specific binding aptamers reduce pathological angiogenesis through inhibition of nucleolin phosphorylation," *Int. J. Mol. Sci.*, vol. 22, no. 23, 2021, doi: 10.3390/ijms222313150.

[72] D. Khiev *et al.*, "Emerging nano-formulations and nanomedicines applications for ocular drug delivery," *Nanomaterials*, vol. 11, no. 1, pp. 1–19, 2021, doi: 10.3390/nano11010173.

[73] J. Adijanto and M. I. Naash, "Nanoparticle-based technologies for retinal gene therapy," *Eur. J. Pharm. Biopharm.*, vol. 95, pp. 353–367, 2015, doi: 10.1016/j.ejpb.2014.12.028.

[74] D. Guimarães, A. Cavaco-Paulo, and E. Nogueira, "Design of liposomes as drug delivery system for therapeutic applications," *Int. J. Pharm.*, vol. 601, no. March, 2021, doi: 10.1016/j.ijpharm.2021.120571.

[75] C. Chen, S. Zhu, T. Huang, S. Wang, and X. Yan, "Analytical Techniques for Single-Liposome Characterization," doi: 10.1039/C3AY40219C.

[76] M. Kanásová and K. Nesměrák, "Systematic review of liposomes' characterization methods," *Monatshefte für Chemie - Chem. Mon. 2017 1489*, vol. 148, no. 9, pp. 1581–1593, Jul. 2017, doi: 10.1007/S00706-017-1994-9.

[77] Y. Yang, Y. Ma, and S. Wang, "A novel method to load topotecan into liposomes driven by a transmembrane NH4EDTA gradient," *Eur. J. Pharm. Biopharm.*, vol. 80, no. 2, pp. 332–339, Feb. 2012, doi: 10.1016/J.EJPB.2011.10.013.

[78] A. Fritze, F. Hens, A. Kimpfler, R. Schubert, and R. Peschka-Süss, "Remote loading of doxorubicin into liposomes driven by a transmembrane phosphate gradient," *Biochim. Biophys. Acta - Biomembr.*, vol. 1758, no. 10, pp. 1633–1640, Oct. 2006, doi: 10.1016/J.BBAMEM.2006.05.028.

[79] G. R. BARTLETT, "Phosphorus Assay in Column Chromatography," *J. Biol. Chem.*,

vol. 234, no. 3, pp. 466–468, Mar. 1959, doi: 10.1016/S0021-9258(18)70226-3.

[80] G. Rouser, S. Fleischer, and A. Yamamoto, "Two dimensional thin layer chromatographic separation of polar lipids and determination of phospholipids by phosphorus analysis of spots," *Lipids*, vol. 5, no. 5, pp. 494–496, 1970, doi: 10.1007/BF02531316.

[81] J. C. M. Stewart, "Colorimetric determination of phospholipids with ammonium ferrothiocyanate," *Anal. Biochem.*, vol. 104, no. 1, pp. 10–14, 1980, doi: 10.1016/0003-2697(80)90269-9.

[82] F. Szoka and D. Papahadjopoulos, "Procedure for preparation of liposomes with large internal aqueous space and high capture by reverse-phase evaporation," *Proc. Natl. Acad. Sci. U. S. A.*, vol. 75, no. 9, pp. 4194–4198, 1978, doi: 10.1073/PNAS.75.9.4194.

[83] C. Jaafar-Maalej, R. Diab, V. Andrieu, A. Elaissari, and H. Fessi, "Ethanol injection method for hydrophilic and lipophilic drug-loaded liposome preparation," *http://dx.doi.org/10.3109/08982100903347923*, vol. 20, no. 3, pp. 228–243, Sep. 2010, doi: 10.3109/08982100903347923.

[84] T. Li, D. Cipolla, T. Rades, and B. J. Boyd, "Drug nanocrystallisation within liposomes," *J. Control. Release*, vol. 288, pp. 96–110, Oct. 2018, doi: 10.1016/J.JCONREL.2018.09.001.

[85] J. J. López-Cano, M. A. González-Cela-Casamayor, V. Andrés-Guerrero, R. Herrero-Vanrell, and I. T. Molina-Martínez, "Liposomes as vehicles for topical ophthalmic drug delivery and ocular surface protection," *Expert Opin. Drug Deliv.*, vol. 18, no. 7, pp. 819–847, 2021, doi: 10.1080/17425247.2021.1872542.

[86] D. K. Karumanchi, Y. Skrypai, A. Thomas, and E. R. Gaillard, "Rational design of liposomes for sustained release drug delivery of bevacizumab to treat ocular angiogenesis," *J. Drug Deliv. Sci. Technol.*, vol. 47, pp. 275–282, Oct. 2018, doi: 10.1016/J.JDDST.2018.07.003.

[87] J. C. Altamirano-Vallejo *et al.*, "Characterization and pharmacokinetics of triamcinolone acetonide-loaded liposomes topical formulations for vitreoretinal drug delivery," *J. Ocul. Pharmacol. Ther.*, vol. 34, no. 5, pp. 416–425, 2018, doi: 10.1089/jop.2017.0099.

[88] M. Khalil, U. Hashmi, R. Riaz, and S. Rukh Abbas, "Chitosan coated liposomes (CCL)

containing triamcinolone acetonide for sustained delivery: A potential topical treatment for posterior segment diseases," *Int. J. Biol. Macromol.*, vol. 143, pp. 483–491, Jan. 2020, doi: 10.1016/J.IJBIOMAC.2019.10.256.

[89] S. Lai *et al.*, "Liposomes for effective drug delivery to the ocular posterior chamber," *J. Nanobiotechnology*, vol. 17, no. 1, pp. 1–12, May 2019, doi: 10.1186/S12951-019-0498-7/FIGURES/5.

[90] H. I. Chang and M. K. Yeh, "Clinical development of liposome-based drugs: formulation, characterization, and therapeutic efficacy," *Int. J. Nanomedicine*, vol. 7, p. 49, 2012, doi: 10.2147/IJN.S26766.

[91] V. De Matteis and L. Rizzello, "Noble Metals and Soft Bio-Inspired Nanoparticles in Retinal Diseases Treatment: A Perspective," *Cells 2020, Vol. 9, Page 679*, vol. 9, no. 3, p. 679, Mar. 2020, doi: 10.3390/CELLS9030679.

[92] I. Ielo *et al.*, "Synthesis, Chemical–Physical Characterization, and Biomedical Applications of Functional Gold Nanoparticles: A Review," *Mol. 2021, Vol. 26, Page 5823*, vol. 26, no. 19, p. 5823, Sep. 2021, doi: 10.3390/MOLECULES26195823.

[93] A. Irshad, M. Zahid, T. Husnain, A. Q. Rao, N. Sarwar, and I. Hussain, "A proactive model on innovative biomedical applications of gold nanoparticles," *Appl. Nanosci.*, vol. 10, no. 8, pp. 2453–2465, Aug. 2020, doi: 10.1007/S13204-019-01165-4/FIGURES/9.

[94] X. Gu, D. D. Li, G. H. Yeoh, R. A. Taylor, and V. Timchenko, "Heat Generation in Irradiated Gold Nanoparticle Solutions for Hyperthermia Applications," *Process. 2021, Vol. 9, Page 368*, vol. 9, no. 2, p. 368, Feb. 2021, doi: 10.3390/PR9020368.

[95] Y. Matsumura and H. Maeda, "A New Concept for Macromolecular Therapeutics in Cancer Chemotherapy: Mechanism of Tumoritropic Accumulation of Proteins and the Antitumor Agent Smancs1," *CANCER Res.*, vol. 46, 1986, Accessed: Apr. 13, 2022. [Online]. Available: http://aacrjournals.org/cancerres/article-pdf/46/12_Part_1/6387/2424185/cr0461 2p16387.pdf.

[96] H. Maeda, "Tumor-Selective Delivery of Macromolecular Drugs via the EPR Effect: Background and Future Prospects," *Bioconjug. Chem.*, vol. 21, no. 5, pp. 797–802, May 2010, doi: 10.1021/BC100070G.

[97] D. A. Giljohann, D. S. Seferos, W. L. Daniel, M. D. Massich, P. C. Patel, and C. A.

Mirkin, “Gold Nanoparticles for Biology and Medicine,” *Angew. Chemie Int. Ed.*, vol. 49, no. 19, pp. 3280–3294, Apr. 2010, doi: 10.1002/ANIE.200904359.

[98] R. Wang *et al.*, “Biomimetic Upconversion Nanoparticles and Gold Nanoparticles for Novel Simultaneous Dual-Modal Imaging-Guided Photothermal Therapy of Cancer,” *Cancers 2020, Vol. 12, Page 3136*, vol. 12, no. 11, p. 3136, Oct. 2020, doi: 10.3390/CANCERS12113136.

[99] Y. Zhang, H. Yang, Z. Zhou, K. Huang, S. Yang, and G. Han, “Recent Advances on Magnetic Relaxation Switching Assay-Based Nanosensors,” *Bioconjug. Chem.*, vol. 28, no. 4, pp. 869–879, Apr. 2017, doi: 10.1021/ACS.BIOCONJCHEM.7B00059/ASSET/IMAGES/ACS.BIOCONJCHEM.7B00059.SOCIAL.JPEG_V03.

[100] M. Shahid, “Water soluble gold nanoparticles based high relaxivity MRI contrast agents,” *Mater. Res. Express*, vol. 6, no. 12, p. 1250h1, Jan. 2020, doi: 10.1088/2053-1591/AB6B53.

[101] A. Dzimitrowicz, P. Jamróz, G. C. diCenzo, I. Sergiel, T. Kozlecki, and P. Pohl, “Preparation and characterization of gold nanoparticles prepared with aqueous extracts of Lamiaceae plants and the effect of follow-up treatment with atmospheric pressure glow microdischarge,” *Arab. J. Chem.*, vol. 12, no. 8, pp. 4118–4130, Dec. 2019, doi: 10.1016/J.ARABJC.2016.04.004.

[102] M. F. Zarabi, N. Arshadi, A. Farhangi, and A. Akbarzadeh, “Preparation and Characterization of Gold Nanoparticles with Amino Acids, Examination of Their Stability,” *Indian J. Clin. Biochem.*, vol. 29, no. 3, p. 306, 2014, doi: 10.1007/S12291-013-0358-4.

[103] H. Hinterwirth *et al.*, “Comparative method evaluation for size and size-distribution analysis of gold nanoparticles,” *J. Sep. Sci.*, vol. 36, no. 17, pp. 2952–2961, Sep. 2013, doi: 10.1002/JSSC.201300460.

[104] W. Haiss, N. T. K. Thanh, J. Aveyard, and D. G. Fernig, “Determination of size and concentration of gold nanoparticles from UV-Vis spectra,” *Anal. Chem.*, vol. 79, no. 11, pp. 4215–4221, Jun. 2007, doi: 10.1021/AC0702084/SUPPL_FILE/AC0702084SI20070321_014144.PDF.

[105] X. Xia *et al.*, “Quantifying the coverage density of poly(ethylene glycol) chains on the surface of gold nanostructures,” *ACS Nano*, vol. 6, no. 1, pp. 512–522, Jan. 2012, doi:

10.1021/NN2038516/SUPPL_FILE/NN2038516_SI_001.PDF.

[106] S. J. Bakri, J. S. Pulido, P. Mukherjee, R. J. Marler, and D. Mukhopadhyay, "Absence of histologic retinal toxicity of intravitreal nanogold in a rabbit model," *Retina*, vol. 28, no. 1, pp. 147–149, Jan. 2008, doi: 10.1097/IAE.0B013E3180DC9360.

[107] Y. Shi *et al.*, "Intravenously administered gold nanoparticles pass through the blood–retinal barrierdepending on the particle size, and induce no retinal toxicity," *Nanotechnology*, vol. 20, no. 50, p. 505101, Nov. 2009, doi: 10.1088/0957-4484/20/50/505101.

[108] Y. Dong, G. Wan, P. Yan, C. Qian, F. Li, and G. Peng, "Fabrication of resveratrol coated gold nanoparticles and investigation of their effect on diabetic retinopathy in streptozotocin induced diabetic rats," *J. Photochem. Photobiol. B Biol.*, vol. 195, pp. 51–57, Jun. 2019, doi: 10.1016/J.JPHOTOBIOL.2019.04.012.

[109] A. Laradji, B. B. Karakocak, A. V. Kolesnikov, V. J. Kefalov, and N. Ravi, "Hyaluronic Acid-Based Gold Nanoparticles for the Topical Delivery of Therapeutics to the Retina and the Retinal Pigment Epithelium," *Polym. 2021, Vol. 13, Page 3324*, vol. 13, no. 19, p. 3324, Sep. 2021, doi: 10.3390/POLYM13193324.

[110] E. Pereira *et al.*, "Evaluation of Acridine Orange Derivatives as DNA-Targeted Radiopharmaceuticals for Auger Therapy: Influence of the Radionuclide and Distance to DNA," *Sci. Reports 2017 71*, vol. 7, no. 1, pp. 1–16, Feb. 2017, doi: 10.1038/srep42544.

[111] L. Imbert *et al.*, "In Vitro Production of Perdeuterated Proteins in H2O for Biomolecular NMR Studies," *Methods Mol. Biol.*, vol. 2199, pp. 127–149, 2021, doi: 10.1007/978-1-0716-0892-0_8/COVER.

[112] T. Santos *et al.*, "Targeting a G-quadruplex from let-7e pre-miRNA with small molecules and nucleolin," *J. Pharm. Biomed. Anal.*, vol. 215, p. 114757, Jun. 2022, doi: 10.1016/J.JPBA.2022.114757.

[113] M. T. Malik *et al.*, "AS1411-conjugated gold nanospheres and their potential for breast cancer therapy," *Oncotarget*, vol. 6, no. 26, pp. 22270–22281, 2015, doi: 10.18632/ONCOTARGET.4207.

[114] C. A. Mirkin, R. L. Letsinger, R. C. Mucic, and J. J. Storhoff, "A DNA-based method for rationally assembling nanoparticles into macroscopic materials," *Nat. 1996*

3826592, vol. 382, no. 6592, pp. 607–609, Aug. 1996, doi: 10.1038/382607a0.

[115] H. Xing *et al.*, "Selective delivery of an anticancer drug with aptamer-functionalized liposomes to breast cancer cells in vitro and in vivo," *J. Mater. Chem. B*, vol. 1, no. 39, pp. 5288–5297, 2013, doi: 10.1039/c3tb20412j.

[116] N. Q. Do, W. J. Chung, T. H. A. Truong, B. Heddi, and A. T. Phan, "G-quadruplex structure of an anti-proliferative DNA sequence," *Nucleic Acids Res.*, vol. 45, no. 12, pp. 7487–7493, Jul. 2017, doi: 10.1093/NAR/GKX274.

[117] J. Carvalho *et al.*, "Phenanthroline polyazamacrocycles as G-quadruplex DNA binders," *Org. Biomol. Chem.*, vol. 16, no. 15, pp. 2776–2786, Apr. 2018, doi: 10.1039/C8OB00247A.

[118] S. Arumugam, M. Clarke Miller, J. Maliekal, P. J. Bates, J. O. Trent, and A. N. Lane, "Solution structure of the RBD1,2 domains from human nucleolin," *J. Biomol. NMR*, vol. 47, no. 1, pp. 79–83, May 2010, doi: 10.1007/S10858-010-9412-1/FIGURES/3.

[119] E. Poimenidi *et al.*, "Vascular endothelial growth factor A (VEGF-A) decreases expression and secretion of pleiotrophin in a VEGF receptor-independent manner," *Vascul. Pharmacol.*, vol. 80, pp. 11–19, May 2016, doi: 10.1016/J.VPH.2016.02.008.

[120] D. J. Uribe, K. Guo, Y. J. Shin, and D. Sun, "Heterogeneous nuclear ribonucleoprotein K and nucleolin as transcriptional activators of the vascular endothelial growth factor promoter through interaction with secondary DNA structures," *Biochemistry*, vol. 50, no. 18, pp. 3796–3806, May 2011, doi: 10.1021/BI101633B/SUPPL_FILE/BI101633B_SI_001.PDF.

[121] A. D. Bangham, J. De Gier, and G. D. Greville, "Osmotic properties and water permeability of phospholipid liquid crystals," *Chem. Phys. Lipids*, vol. 1, no. 3, pp. 225–246, May 1967, doi: 10.1016/0009-3084(67)90030-8.

[122] T. Santos *et al.*, "RNA G-quadruplex as supramolecular carrier for cancer-selective delivery," *Eur. J. Pharm. Biopharm.*, vol. 142, pp. 473–479, Sep. 2019, doi: 10.1016/J.EJPB.2019.07.017.

[123] J. Liu *et al.*, "Anti-angiogenic activity of bevacizumab-bearing dexamethasone-loaded PLGA nanoparticles for potential intravitreal applications," *Int. J. Nanomedicine*, vol. 14, pp. 8819–8834, 2019, doi: 10.2147/IJN.S217038.

Appendices

Appendix A

molecules

an Open Access Journal by MDPI

Indexed in: PubMed | CITESCORE 5.9 | IMPACT FACTOR 4.927

CERTIFICATE OF PUBLICATION

Certificate of publication for the article titled:

G-Quadruplex Aptamer-Ligand Characterization

Authored by:

David Moreira; Daniela Leitão; Jéssica Lopes-Nunes; Tiago Santos; Joana Figueiredo; André Miranda; Daniela Alexandre; Cândida Tomaz; Jean-Louis Mergny; Carla Cruz

Published in:

Molecules **2022**, Volume 27, Issue 20, 6781

MDPI Academic Open Access Publishing since 1996

Basel, October 2022

molecules

an Open Access Journal by MDPI

G-Quadruplex Aptamer-Ligand Characterization

David Moreira; Daniela Leitão; Jéssica Lopes-Nunes; Tiago Santos; Joana Figueiredo; André Miranda; Daniela Alexandre; Cândida Tomaz; Jean-Louis Mergny; Carla Cruz

Molecules **2022**, Volume 27, Issue 20, 6781

Appendix B

Development of aptamer nanoparticles for treatment of retinal diseases

D. Moreira[1(*)], J. Nunes[1], Fátima Santos[2], C. Cruz[1], C. Tomaz[1]
[1] CICS-UBI Centro de Investigação em Ciências da Saúde, Universidade da Beira Interior, Av. Infante D. Henrique, 6200-506 Covilhã, Portugal
[2] National Centre for Biotechnology (CNB-CSIC), Madrid, Spain.
(*)*Email:* david.moreira@ubi.pt

ABSTRACT

Retinal diseases, such as diabetic retinopathy or age-related macular degeneration, can lead to loss of vision, affecting the quality of life of the patients. Conventional therapies include corticosteroids or/and specific antibodies for anti-inflammatory and antiangiogenic effect. The administration can be made using intravitreal injections, ophthalmological implants, or topical formulations. DNA aptamers have emerged as a novel approach for retina treatment, since they exhibit affinity and specificity similar to antibodies. In addition, aptamers are easy to synthesize chemically, and show a good stability and a low immunogenicity. AS1411 is a guanine-rich aptamer with antineoplastic activity, that targets nucleolin, a cell-surface protein, highly expressed in some retinal diseases, acting as a co-receptor for several growth factors that are important in the proliferative process. AT11-L0 is a derivative of AS1411 aptamer that presents one more nucleotide and some differences in the sequence and also show interesting anti-proliferative properties. This study aimed to develop a nanoparticle formulation for intravitreal delivery of AT11-L0 in the eye to induce an anti-angiogenic effect. We conjugated AT11-L0 with two types of nanoparticles: liposomes and gold nanoparticles. The size of gold nanoparticles obtained using dynamic light scattering was 31.93 nm. The aptamer conjugation was verified by transmission electron microscopy. Liposomes have been made using three different lipids and the aptamer conjugation was verified using electrophoresis and a spectrophotometer method. The efficiency of the conjugation was 84.48%. These results show that these nanoparticles may be promising so they will be tested *in vitro* in a HUVEC model.

Acknowledgements: This work was supported by the European Regional Development Fund through the "Programa Operacional Regional do Centro (Centro 2020)—Sistema de Apoio à Investigação Científica e Tecnológica—Programas Integrados de IC&DT" (Project Centro-01-0145-FEDER-000019—C4—Centro de Competências em Cloud Computing) and by Bolsa de Inovação da SR Sul e Regiões Autónomas da Ordem dos Farmacêuticos 2021 (BInov)

Keywords: G-quadruplex Aptamers; retinal diseases; nanoparticles; nucleolin

Preference for communication: poster

CICS-UBI SYMPOSIUM 2020
UBI, Covilhã, Portugal

CICS-UBI Centro de Investigação em Ciências da Saúde
Health Sciences Research Centre

UBI Faculdade Ciências da Saúde

Development of aptamer nanoparticles for treatment of retinal diseases

D. Moreira[1(*)], J. Nunes[1], Fátima Santos[2], C. Cruz[1], C. Tomaz[1]

[1] CICS-UBI Centro de Investigação em Ciências da Saúde, Universidade da Beira Interior, Av. Infante D. Henrique, 6200-506 Covilhã, Portugal
[2] National Centre for Biotechnology (CNB-CSIC), Madrid, Spain
(*)Email: david.moreira@ubi.pt

Introduction

Retinal diseases, such as diabetic retinopathy or age-related macular degeneration, are generated by abnormal retinal blood vessels proliferation and are the leading cause of blindness [1]. Conventional therapies include corticosteroids or/ and specific antibodies for anti-inflammatory and antiangiogenic effects, respectively [2].

DNA aptamers are sequence-specific nucleic acids that have emerged as a novel approach for retina treatment, since they exhibit affinity and specificity similar to antibodies [3]. AS1411 is a guanine-rich aptamer with antineoplastic activity, that targets nucleolin, a cell-surface protein, highly expressed in some retinal diseases. AT11-L0 is a derivative of AS1411 aptamer that presents interesting anti-proliferative properties [4].

This study aimed to develop a nanoparticle formulation for intravitreal delivery of AT11-L0 in the eye to induce an anti-angiogenic effect.

Experimental setup

Gold nanoparticles

↓ AT11-L0 reduction with TCEP

↓ AT11-L0 and gold nanoparticles linkage by a disulphide bond

↓ Purification using lyophilization followed by dialysis

↓ Nanoparticles characterization

Liposomes

↓ Mixing of three different lipids and evaporation to form a thin layer

↓ Hydration with PBS

↓ "Freeze and Thaw"

↓ Extrusion

↓ Nanoparticles characterization

Results

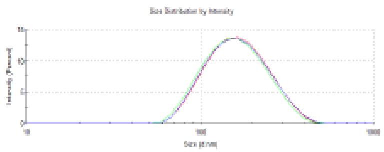

Fig.1 – Dynamic light scattering of gold nanoparticles conjugated with AT11-L0.

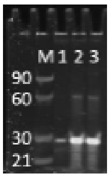

Fig.3 – Electrophoresis M – Molecular weight market, 1 – AT11-L0 aptamer, 2 – Liposomes conjugated with aptamer, 3 – Liposomes conjugated with aptamer after washing.

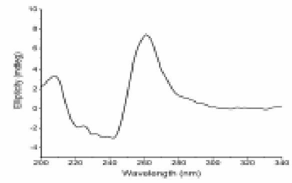

Fig.5 – CD spectra of G4 structures of AT11-L0 aptamer.

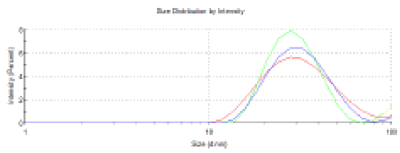

Fig.2 – Dynamic light scattering of liposomes conjugated with AT11-L0.

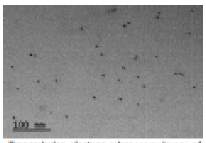

Fig.4 – Transmission electron microscopy image of gold nanoparticles.

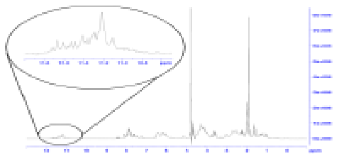

Fig.6 – NMR spectra of 80 µM AT11-L0 aptamer in 210 µL of 90% H_2O/10% D_2O, 20 mM KPi with zoom on the G-quadruplex signals.

Conclusion

- Nuclear magnetic resonance and circular dichroism spectra show that AT11-L0 aptamer form a parallel G4.
- Dynamic light scattering spectra show that the size of both types of nanoparticles is similar to the sizes recommended in the literature.
- The conjugation of the aptamer with the nanoparticles was confirmed by electrophoresis.
- These results show that these nanoparticles may be promising so they will be tested in vitro in a HUVEC model.

Bibliography

[1] [illegible]

[2] [illegible]

[3] [illegible]

[4] [illegible]

Acknowledgements

This work was supported by the European Regional Development Fund through the "Programa Operacional Regional do Centro (Centro 2020)—Sistema de Apoio à Investigação Científica e Tecnológica—Programas Integrados de IC&DT" (Project Centro-01-0145-FEDER-000019—C4—Centro de Competências em Cloud Computing) and by Bolsa de Inovação da Secção Regional Sul e Regiões Autónomas da Ordem dos Farmacêuticos 2021 (BInov)

Appendix C

Characterization of a nucleolin targeting aptamer to develop nanosystems against retinal diseases

D. Moreira[1*], J. Nunes[1], F. Santos[2], C. Cruz[1], C. Tomaz[1]

[1] CICS-UBI Centro de Investigação em Ciências da Saúde, Universidade da Beira Interior, Av. Infante D. Henrique, 6200-506 Covilhã, Portugal

[2] National Centre for Biotechnology (CNB-CSIC), Madrid, Spain.

[*] *Email:* david.moreira@ubi.pt

ABSTRACT

Retinal diseases, including diabetic retinopathy, age-related macular degeneration, retinopathy of prematurity and vessel occlusions may be originated by neovascularization usually triggered by a hypoxia episode leading to the overexpression of vascular endothelial growth factor (VEGF) and nucleolin. The treatments available are mainly corticosteroids or/and antibodies for some angiogenic molecules. Regarding the low efficacy of these therapies and their side effects, aptamers are an emerging tool that can like antibodies targeting these proteins with high specificity. Furthermore, aptamers are easier to synthesize and present higher stability and lower immunogenicity. AT11-L0 is an aptamer derivative of AS1411 composed by G-rich sequences which can adopt G-quadruplex structures and targeting nucleolin, a protein that can act as a co-receptor for several growth factors. Hence, this study aimed to characterize the AT11-L0 structure and its interaction with several ligands (stabilizing molecules or drugs) for the nucleolin targeting. This complex was then incorporated in a nanosystem to increase the bioavailability of the aptamer-based drug in the formulation. To achieve these objectives, we have performed biophysical studies, such as nuclear magnetic resonance, circular dichroism, and fluorescence experiments. Following biophysical characterization studies, we synthesised gold nanoparticles and liposomes containing AT11-L0 aptamer-drug complex. The results showed that AT11-L0 aptamer-drug complex has a high stability with melting temperatures reaching 45 °C to 60 °C allowing an efficiently targeting of nucleolin with a K_D in the order of micromolar. In future perspectives, these nanosystems will be tested in a HUVEC model.

Acknowledgements: This work was supported by the European Regional Development Fund through the "Programa Operacional Regional do Centro (Centro 2020)—Sistema de Apoio à Investigação Científica e Tecnológica—Programas Integrados de IC&DT" (Project Centro-01-0145-FEDER-000019—C4—Centro de Competências em Cloud Computing), CICS-UBI projects UIDB/00709/2020 and UIDP/00709/2020, financed by national funds through FCT/MCTES and by Bolsa de Inovação da SR Sul e Regiões Autónomas da Ordem dos Farmacêuticos 2021 (Blnov).

Keywords: G-quadruplex aptamers; retinal diseases; nanosystems; nucleolin.

Preference for communication: oral

Characterization of a nucleolin targeting aptamer to develop nanosystems against retinal diseases

D. Moreira[1(*)], J. Nunes[1], F. Santos[2], C. Cruz[1], C. Tomaz[1]

[1] CICS-UBI Centro de Investigação em Ciências da Saúde, Universidade da Beira Interior, Av. Infante D. Henrique, 6200-506 Covilhã, Portugal

[2] National Centre for Biotechnology (CNB-CSIC), Madrid, Spain

(*) *Email:* david.moreira@ubi.pt

XVII International CICSUBI Symposium

Appendix D

VIII Ciclo de Conferências
da Faculdade de Ciências
Escola e Universidade

23 e 24 setembro 2022

APTAMERO ANTI-NUCLEOLINA NO TRATAMENTO DE DOENÇAS NEOVASCULARES DA RETINA

D. Moreira[1(*)], J. Lopes-Nunes[1], F. Santos[2], C. Cruz[1], C. Tomaz[1]

[1] CICS-UBI Centro de Investigação em Ciências da Saúde, Universidade da Beira Interior, Av. Infante D. Henrique, 6200-506 Covilhã, Portugal; [2] National Centre for Biotechnology (CNB-CSIC), Madrid, Spain.

Resumo

As doenças neovasculares da retina resultam da sobre-expressão de moléculas, como o fator de crescimento endotelial vascular (VEGF) ou a nucleolina (NCL). Estas moléculas originam um processo inflamatório e angiogénico que pode desencadear doenças como a retinopatia diabética. Os tratamentos atuais incluem cirurgia, corticosteroides e anticorpos monoclonais (AM) anti-VEGF. No entanto, estas terapias apresentam algumas desvantagens, nomeadamente a diminuição de eficácia ao longo do tempo e alguns efeitos secundários graves. Assim, os aptameros de ácidos nucleicos surgem como uma alternativa aos AM devido à sua elevada especificidade, a produção por síntese química, e ainda menor imunogenicidade e maior estabilidade. O AT11-Lo é um derivado do AS1411 composto por uma sequência rica em guaninas formando uma estrutura G-quadruplex que se liga à NCL. Este estudo pretendeu caraterizar a estrutura do AT11-Lo e estudar a sua interação com ligandos (moléculas estabilizadoras) e com moléculas terapêuticas para inibição da angiogénese desencadeada pela NCL. Finalmente, os complexos aptamero/ligando foram incorporados em nanossistemas de modo a melhorar a sua biodisponibilidade. Este estudo teve uma primeira abordagem biofísica com estudos de caraterização como dicroísmo circular, ressonância magnética nuclear e estudos de fluorescência. De seguida, realizou-se a síntese química de lipossomas e nanopartículas de ouro. Os resultados obtidos mostram que o AT11-Lo forma uma estrutura G-quadruplex paralela, estabilizada por ligandos como o C_8 ou o PhenDC3, e que interage com elevada afinidade com a NCL. O trabalho será finalizado com a avaliação da capacidade de inibição da angiogénese em células HUVEC.

Acknowledgements: This work was supported by the European Regional Development Fund through the "Programa Operacional Regional do Centro (Centro 2020)—Sistema de Apoio à Investigação Científica e Tecnológica—Programas Integrados de IC&DT" (Project Centro-01-0145-FEDER-000019—C4—Centro de Competências em Cloud Computing), CICS-UBI projects UIDB/00709/2020 and UIDP/00709/2020, financed by national funds through FCT/MCTES and by Bolsa de Inovação da SR Sul e Regiões Autónomas da Ordem dos Farmacêuticos 2021 (BInov).

Palavras-chave: Aptameros G-qudruplex, Nucleolina, Doenças da retina, Nanopartículas.

Aptamero anti-nucleolina no tratamento de doenças neovasculares da retina

D. Moreira[1(*)], J. Lopes-Nunes[1], F. Santos[2], C. Cruz[1,3], C. Tomaz[1,3]

[1] CICS-UBI Centro de Investigação em Ciências da Saúde, Universidade da Beira Interior, 6200-506 Covilhã, Portugal;
[2] National Centre for Biotechnology (CNB-CSIC), Madrid, Spain.
[3] Departamento de Química- Faculdade de Ciências, Universidade da Beira Interior 6200-001 Covilhã, Portugal.

Introdução

- As doenças neovasculares da retina são originadas por hipoxia que leva à sobre expressão de moléculas como o fator de crescimento endotelial vascular (VEGF) ou a nucleolina (NCL).
- Estas moléculas originam um processo inflamatório e angiogénico que pode desencadear doenças como a retinopatia diabética ou a degeneração macular associada à idade.
- Os tratamentos atuais incluem cirurgia, corticosteroides e ainda aptameros anti-VEGF. No entanto, estas terapias têm baixa eficácia e alguns efeitos secundários graves.
- Alguns aptameros de DNA que formam estruturas de G-quadruplex (G4) ligam especificamente à NCL, podendo bloquear a sua atividade.
- As estruturas G4 podem ser estabilizadas por ligandos de G4, como o PhenDC3 ou o C_8. Os aptameros G4 podem ainda ser usados na formulação de sistemas de entrega de fármacos anti-inflamatórios como a dexametasona.
- **Objetivo: caracterizar o aptamero AT11-L0, derivado do AS1411, e produzir nanopartículas para inibir a ação da NCL no retinoblastoma.**

Desenho experimental

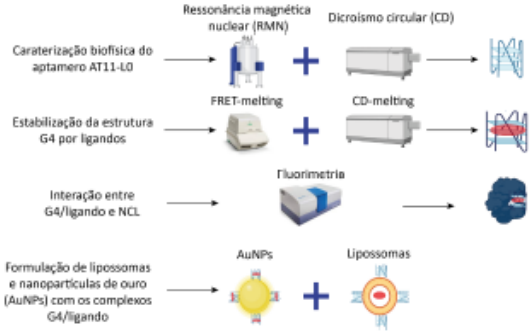

Resultados

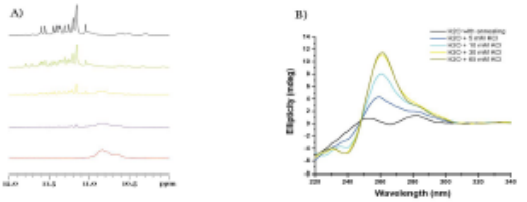

Fig.1 – Espetros mostrando a formação do G4 no AT11-L0 com adições de KCl (0,5,10,30 e 65 mM) em A) RMN e B) CD.

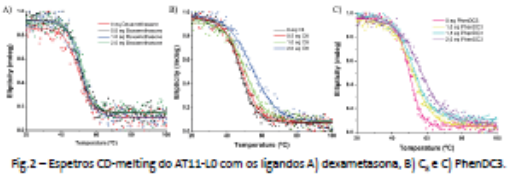

Fig.2 – Espetros CD-melting do AT11-L0 com os ligandos A) dexametasona, B) C_8 e C) PhenDC3.

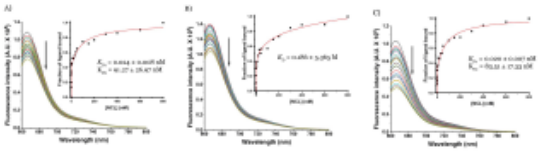

Fig.3 – Titulações de fluorescência com os complexos AT11-L0/ A) dexametasona, B) C_8 e C) PhenDC3.

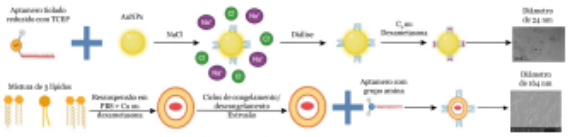

Fig.4– Representação esquemática da síntese dos lipossomas e das AuNPs.

Conclusões

- O AT11-L0 forma uma estrutura de G4 paralela, estabilizada pelos ligandos C8 ou PhenDC3 e possui elevada afinidade para a NCL.
- A dexametasona não promove a estabilização da estrutura G4 e apresenta baixa afinidade para a NCL.
- Foi possível conjugar o aptamero com as nanopartículas de ouro e com os lipossomas.
- Serão realizados ensaios de viabilidade celular e de inibição da angiogénese em células HUVEC.

Agradecimentos

This work was supported by the European Regional Development Fund through the "Programa Operacional Regional do Centro (Centro 2020)—Sistema de Apoio à Investigação Científica e Tecnológica—Programas Integrados de IC&DT" (Project Centro-01-0145-FEDER-000019—C4—Centro de Competências em Cloud Computing), CICS-UBI projects UIDB/00709/2020 and UIDP/00709/2020, financed by national funds through FCT/MCTES and by Bolsa de Inovação da SR Sul e Regiões Autónomas da Ordem dos Farmacêuticos 2021 (Binov).

Appendix E

Aptamero anti-nucleolina para o desenvolvimento de nanopartículas para terapia do retinoblastoma

D. Moreira[1(*)], J. Lopes-Nunes[1], F. Santos[2], C. Cruz[1], C. Tomaz[1]

[1] CICS-UBI Centro de Investigação em Ciências da Saúde, Universidade da Beira Interior, Av. Infante D. Henrique, 6200-506 Covilhã, Portugal

[2] National Centre for Biotechnology (CNB-CSIC), Madrid, Spain.

* David Nabais Moreira, Rua da Saudade Nº7, Aldeia Velha, 6320-069 Sabugal, 969122581, david.moreira@ubi.pt

Abstract

a) Introdução: O retinoblastoma é um cancro ocular que afeta a retina de crianças representando cerca de 3% dos cancros infantis no mundo. Este tumor se não for tratado pode levar à perda de visão e, em estadios mais avançados, levar à morte.
Os tratamentos existentes são inespecíficos e consistem em cirurgias, radio- ou quimioterapia e uso do laser. Assim, têm-se desenvolvido terapias que focam alvos moleculares como a nucleolina. Esta proteína está sobre-expressa à superfície de células do retinoblastoma e potencia a angiogénese e a proliferação celular descontrolada.
Deste modo, os aptameros de DNA, que se ligam de forma específica à nucleolina, surgem como alternativa para inibição desta proteína no retinoblastoma. Os aptameros apresentam elevada afinidade e especificidade como os anticorpos, mas têm a vantagem de serem mais fáceis de produzir e exibirem baixa imunogenicidade e alta estabilidade. O AS1411, um dos aptameros mais estudados, apresenta uma sequência rica em guaninas formando uma estrutura em G-quadruplex (G4) que interage com a nucleolina, inibindo o crescimento de células tumorais em alguns tipos de cancro.

b) Objetivos: Este estudo pretende caraterizar o aptamero AT11-L0, derivado do AS1411, e produzir nanopartículas que visem inibir a ação da nucleolina no retinoblastoma.

c) Materiais e métodos: Para a caraterização biofísica do aptamero, realizaram-se ensaios de dicroísmo circular (DC) e de ressonância magnética nuclear (RMN). Seguidamente, estudou-se a estabilização da estrutura do G4 no aptamero AT11-L0 utilizando moléculas de baixo peso molecular (ligandos PM<850 Da) usando as técnicas de FRET- e de CD-melting. Realizaram-se titulações de fluorescência para obter informação acerca da interação entre o complexo AT11-L0 G4/ligando e a nucleolina. Finalmente, estes complexos foram associados a nanopartículas de ouro e lipossomas.

d) Resultados: Os resultados de DC e de RMN indicam que o AT11-L0 forma uma estrutura em G4 estável (Temperatura de melting ≈ 50ºC) para concentrações de KCl superiores a 30 mM. Os resultados de CD-melting mostram que a dexametasona tem uma fraca estabilização da estrutura (1,70ºC) enquanto que os ligandos PhenDC3 e C8 apresentam estabilizações da ordem 6,67ºC e 6,68ºC, respetivamente. A titulação de fluorescência indica constantes de dissociação (K_D) na ordem do nanomolar. As nanopartículas de ouro e os lipossomas produzidos apresentam tamanhos de, aproximadamente, 20 nm e 180 nm, respetivamente.

e) Conclusões: O AT11-L0 forma uma estrutura de G4 estabilizada pela adição dos ligandos C8 ou PhenDC3. Os complexos G4/ligando apresentam uma afinidade elevada para a nucleolina, com K_D na ordem do nanomolar. Finalmente, foi possível conjugar o aptamero, tanto com as nanopartículas de ouro, como com os lipossomas. Para testar a eficiência destas nanopartículas, irão ser realizados ensaios de viabilidade celular e de inibição da angiogénese.

CICS-UBI Centro de Investigação em Ciências da Saúde

E-POSTER 14

FACULDADE CIÊNCIAS DA SAÚDE

Aptamero anti-nucleolina para o desenvolvimento de nanopartículas para terapia do retinoblastoma

D. Moreira[1(*)], J. Lopes-Nunes[1], F. Santos[2], C. Cruz[1], C. Tomaz[1]

[1] CICS-UBI Centro de Investigação em Ciências da Saúde, Universidade da Beira Interior, Av. Infante D. Henrique, 6200-506 Covilhã, Portugal. 2 National Centre for Biotechnology (CNB-CSIC), Madrid, Spain. *david.moreira@ubi.pt

Introdução

O Retinoblastoma tem, em Portugal, uma incidência anual de 4,04 casos por cada 100.000 nados-vivos. Os tratamentos atuais são pouco específicos: cirurgia, radio- ou quimioterapia e uso de laser.

No entanto, verificou-se que a proteína nucleolina (NCL) está sobre-expressa nesta patologia, podendo funcionar como potencial alvo terapêutico. Os aptameros de DNA que formam estruturas de G-quadruplex (G4) ligam especificamente à NCL, podendo bloquear a sua atividade. As estruturas G4 podem ser estabilizadas por ligandos de G4, como o PhenDC3 ou o C_8. Os aptameros G4 podem ainda ser usados na formulação de sistemas de entrega de fármacos anti-inflamatórios como a dexametasona.

Este estudo pretende caracterizar o aptamero AT11-L0, derivado do AS1411, e produzir nanopartículas que visem inibir a ação da NCL no retinoblastoma.

Desenho experimental

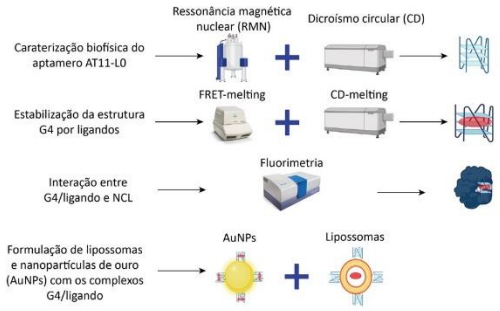

Resultados

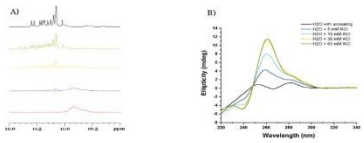

Fig.1 – Espetros mostrando a formação do G4 no AT11-L0 com adições de KCl (0,5,10,30 e 65 mM) em A) RMN e B) CD.

Tabela 1 – ΔT_m da estrutura G4 do aptamero AT11-L0 promovida pela adição de dexametasona, C_8 e PhenDC3.

Ligando	Dexametasona	C_8	PhenDC3
ΔT_m (°C)	1,71	6,68	6,67

Tabela 2 – K_D dos complexos AT11-L0/dexametasona, AT11-L0/C_8, e AT11-L0/PhenDC3 para a NCL.

AT11-L0/Dexametasona	AT11-L0/C_8		AT11-L0/PhenDC3	
K_D = 0,186 M	K_{D1} = 0,024 nM	K_{D2} = 91,27 nM	K_{D1} = 0,020 nM	K_{D2} = 83,51 nM

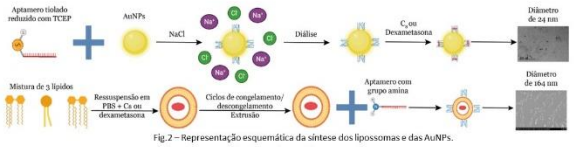

Fig.2 – Representação esquemática da síntese dos lipossomas e das AuNPs.

Conclusões

O AT11-L0 forma uma estrutura de G4 paralela, estabilizada pelos ligandos C8 ou PhenDC3, e possui elevada afinidade para a NCL. Já a dexametasona não promove a estabilização da estrutura G4 e apresenta baixa afinidade para a NCL.

Foi possível conjugar o aptamero com as nanopartículas de ouro e com os lipossomas.

Finalmente, irão ser realizados ensaios de viabilidade celular e de inibição da angiogénese em células HUVEC.

FCT COMPETE 2020 PORTUGAL 2020